AD-A037 185 MINNESOTA UNIV MINNEAPOLIS DEPT OF ELECTRICAL ENGIN--ETC F/G 17/5
LOW-FREQUENCY NOISE IN (HG, CD) TE DETECTORS.(U)
OCT 76 H I HANAFI, A VAN DER ZIEL F33615-74-C-5104
UNCLASSIFIED AFML-TR-76-175 NL

1 OF 2
ADA037185

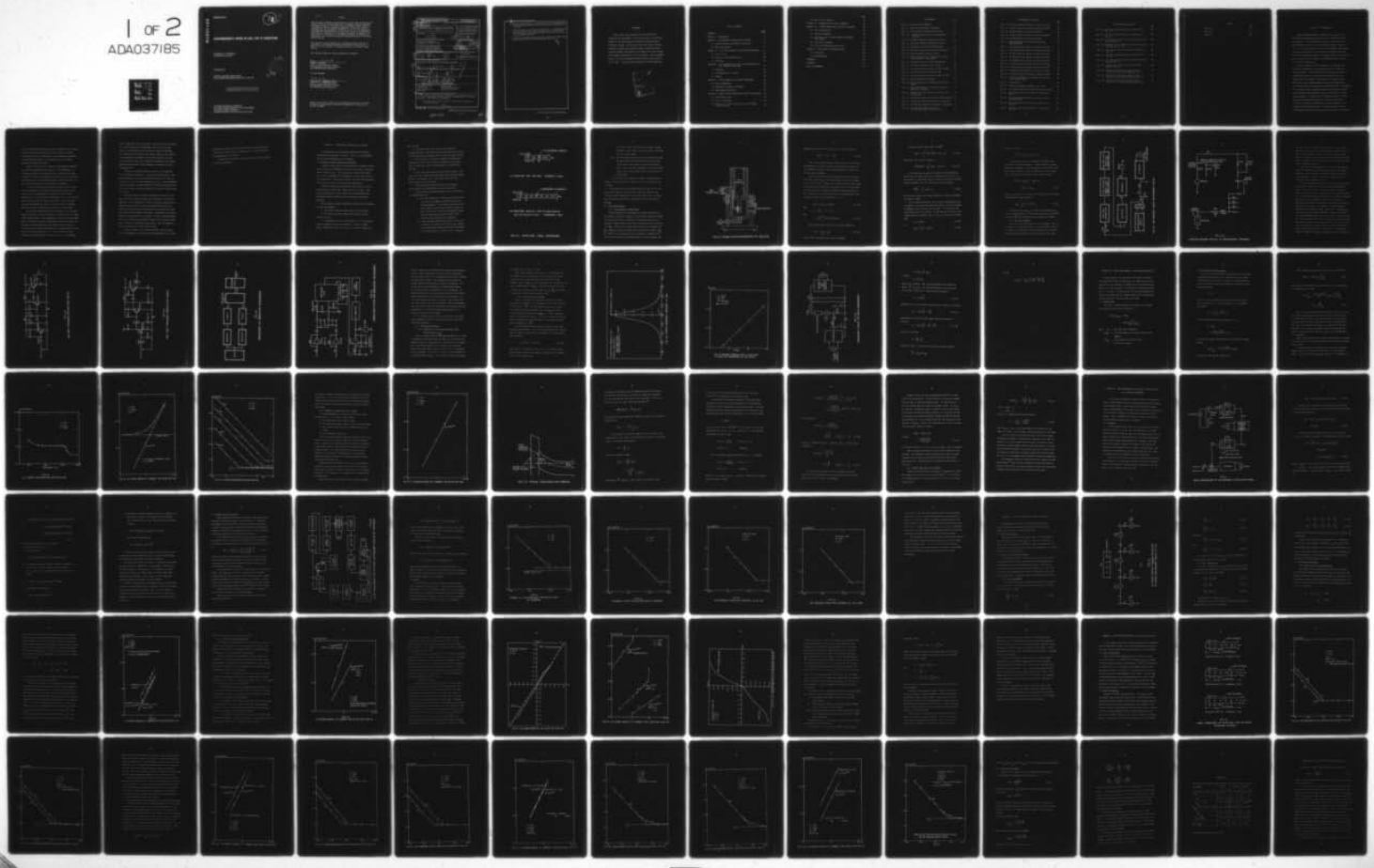

ADA037185

AFML-TR-76-175

LOW-FREQUENCY NOISE IN (HG, CD) TE DETECTORS

UNIVERSITY OF MINNESOTA
MINNEAPOLIS, MN 55455

D D C
REPRODUCED
MAR 22 1977
C

OCTOBER 1976

TECHNICAL REPORT AFML-TR-76-175
FINAL REPORT FOR PERIOD APRIL 1974 - JUNE 1976

Approved for public release; distribution unlimited

AIR FORCE MATERIALS LABORATORY
AIR FORCE WRIGHT AERONAUTICAL LABORATORIES
AIR FORCE SYSTEMS COMMAND
WRIGHT-PATTERSON AIR FORCE BASE, OHIO 45433

NOTICE

When Government drawings, specifications, or other data are used for any purpose other than in connection with a definitely related Government procurement operation, the United States Government thereby incurs no responsibility nor any obligation whatsoever; and the fact that the government may have formulated, furnished, or in any way supplied the said drawings, specifications, or other data, is not to be regarded by implication or otherwise as in any manner licensing the holder or any other person or corporation, or conveying any rights or permission to manufacture, use, or sell any patented invention that may in any way be related thereto.

This report has been reviewed by the Information Office (OI) and is releasable to the National Technical Information Service (NTIS). At NTIS, it will be available to the general public, including foreign nations.

This Technical Report has been reviewed and is approved.

Robert L. Hickmott

ROBERT L. HICKMOTT
Laser & Optical Materials Branch
Electromagnetic Materials Division
Air Force Materials Laboratory

FOR THE COMMANDER

W G D Frederick

WILLIAM G. D. FREDERICK, Chief
Laser & Optical Materials Branch
Electromagnetic Materials Division
Air Force Materials Laboratory

Copies of this report should not be returned unless return is required by security considerations, contractual obligations, or notice on a specific document.

AIR FORCE - 21 FEBRUARY 77 - 150

SECURITY CLASSIFICATION OF THIS PAGE (When Data Entered)

(19) **REPORT DOCUMENTATION PAGE**

READ INSTRUCTIONS BEFORE COMPLETING FORM

(18) REPORT NUMBER: AFML-TR-76-175

2. GOVT ACCESSION NO.

3. RECIPIENT'S CATALOG NUMBER

(6) 4. TITLE (and Subtitle): LOW-FREQUENCY NOISE IN (HG,CD) TE DETECTORS

5. TYPE OF REPORT & PERIOD COVERED: Final Report April 1, 1974- June 30, 1976

6. PERFORMING ORG. REPORT NUMBER

7. AUTHOR(s): H. I. Hanafi; A. van der Ziel

(15) 8. CONTRACT OR GRANT NUMBER(s): F33615-74-C-5104 new

9. PERFORMING ORGANIZATION NAME AND ADDRESS: University of Minnesota, Minneapolis, Minnesota 55455

10. PROGRAM ELEMENT, PROJECT, TASK AREA & WORK UNIT NUMBERS: 62102F; 7371; 73710230

(12) 146 p.

11. CONTROLLING OFFICE NAME AND ADDRESS: Air Force Materials Laboratory, Mr. R. L. Hickmott, AFML/LPO, Wright Patterson AFB, Ohio 45433

(11) 12. REPORT DATE: Oct[illegible]76

13. NUMBER OF PAGES: 135

14. MONITORING AGENCY NAME & ADDRESS (if different from Controlling Office)

(9) Final rept. 1 Apr 74 - 30 June 76

15. SECURITY CLASS. (of this report): Unclassified

15a. DECLASSIFICATION/DOWNGRADING SCHEDULE

16. DISTRIBUTION STATEMENT (of this Report)

Approved for public release; distribution unlimited.

(10) Hussein Ibrahim Hanafi

17. DISTRIBUTION STATEMENT (of the abstract entered in Block 20, if different from Report)

Aldert van der Ziel

18. SUPPLEMENTARY NOTES

None

(16) 7371 (17) 02

19. KEY WORDS (Continue on reverse side if necessary and identify by block number)

low-frequency noise
contact noise
grain boundary noise
bulk noise
surface noise
Photoconductive detectors
Modulation technique

20. ABSTRACT (Continue on reverse side if necessary and identify by block number)

The purpose of this study was to identify and understand the sources of 1/f noise in n-type HgCd Te detectors and to recommend methods for reducing this noise. Four items were investigated:

a) Noise generated at noisy contacts. This could be interpreted as injection 1/f noise.

DD FORM 1 JAN 73 1473 EDITION OF 1 NOV 65 IS OBSOLETE

SECURITY CLASSIFICATION OF THIS PAGE (When Data Entered)

over

233 520

HB

b) Noise at grain boundaries. We found devices with grain boundaries to be noisier than those without it; in our geometry the difference was a factor 4.

c) Noise generated at the surface versus bulk noise. We found the noise to be more variable from sample to sample than bulk noise permits. We also showed by a direct experiment (MIS devices) that the flicker noise was surface generated.

d) A modulation technique was developed for discriminating between noise sources, but was not used in the experiments under (c).

FOREWORD

This report was prepared by the Electrical Engineering Department of the University of Minnesota based on the PhD thesis of Hussein Ibrahim Hanafi. Professor Aldert van der Ziel was the thesis advisor. Honeywell Corporate Research Center provided single crystal HgCdTe selected by Joe Schmit who also helped with sample preparation and contacting. The equipment was set up and preliminary measurements were made by H. M. Choe. Figures were prepared by John Humphreys.

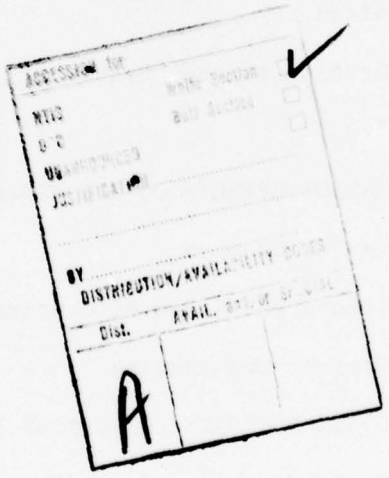

TABLE OF CONTENTS

ILLUSTRATIONS

ILLUSTRATIONS (continued)

ILLUSTRATIONS (continued)

TABLES

CHAPTER I. INTRODUCTION

Mercury Cadmium Telluride, denoted by $Hg_{1-x}\ Cd_x\ Te$, is a Zinc-blende semiconductor whose band gap is a function of alloy composition x. The band gap varies from the "negative gap" of HgTe($\simeq$-0.03eV) for x=0 to the wide band gap of CdTe($\simeq$ 1.5eV) for x=1. This system is attractive for infrared detector applications because the composition can be adjusted to yield detectors with the desired wavelength response. The compositions used in this work are x$\simeq$0.2 and x$\simeq$0.4 corresponding to wavelength limits at 77°K of 14μ and 3μ respectively.

The main objective of this research was to identify the mechanisms responsible for low frequency noise (1/f noise) in n-type (Hg,Cd)Te. McWhorter[1] developed a model for 1/f noise in semiconductors based on the existence of surface traps. He proposed that fluctuations in the capture and release of bulk electrons at these surface traps will produce fluctuations in the bulk electron concentration and consequently in the conductivity. When a steady current is passed through the semiconductor sample, the conductivity fluctuations will appear as voltage across the sample terminals. To obtain the 1/f frequency dependence of the noise power from these fluctuations, McWhorter assumed that electron tunneling is the mechanism by which bulk electrons are released from the surface traps. He further assumed that the semiconductor surface layer has some finite thickness and that the

traps are uniformly distributed over this thickness. The tunneling probability depends exponentially on the distance over which tunneling must occur. Consequently, a distribution of lifetimes is obtained which leads to the characteristic 1/f frequency dependence for the noise power.

Based on 1/f data for a variety of semiconductors, Hooge[2,3] has recently proposed that 1/f noise is a bulk phenomenon. By studying 1/f noise of concentration cells, thermocells and Hall voltage[4,5], he and his co-workers have shown that what is actually fluctuating is the carrier mobility rather than their number. No model has been proposed for such mobility fluctuations.

Van der Ziel[6] has shown in detail, what was already implied earlier by Klaassen[7], that Hooge's experimental formula for the flicker noise in semiconductors could also be derived from a surface model. Verifying Hooge's experimental formula is therefore not a sound criterion for bulk flicker noise; rather some more detailed measurements are needed to settle the question whether the flicker noise in (Hg,Cd)Te is a surface or a bulk effect.

The specific problem addressed in this work was to determine whether 1/f noise in n-type (Hg,Cd)Te is a surface effect or a bulk effect (Chapter VIII). The experimental devices used to accomplish this task were Metal-Insulator-Semiconductor (MIS) structures. By applying a voltage between the metal (gate) electrode and the semiconductor, the surface condition can be changed between accumulation, depletion and inversion. It was felt that this will modulate any surface generated noise and so one can discriminate

between bulk noise and surface noise. Noise measurements performed on several MIS devices indicated that the 1/f noise in these devices is independent of the field plate (gate) voltage while the thermal noise increased as the surface condition was changed from accumulated to depleted. We concluded from this that 1/f noise in these devices, and in (Hg,Cd)Te in general, is a surface phenomenon rather than a bulk phenomenon as explained in detail in Chapter VIII.

The effect of grain boundaries on 1/f noise in (Hg,Cd)Te was also studied (Chapter VI). It was found experimentally, that grain boundaries in the tested devices increase the 1/f noise by a factor of 4 over 1/f noise measured in case of no grain boundaries. This was explained in terms of Bess's[8,9] findings that dislocations give rise to excess noise over and above the "normal" flicker noise (1/f noise).

The third study we carried out (Chapter V) was that of the effect of "poor" contacts (excess noise contacts) on 1/f noise in (Hg,Cd)Te. It was found that a "poor" non-current carrying noise measuring contact will not affect the device 1/f noise while a current carrying poor contact will generate excess noise over and above normal flicker noise of the device. The amount of this noise depends on the polarity of the current. A carrier injection model for the poor contact was proposed to explain our experimental data. This study was not performed in great detail since the making of "good" contacts is not a very difficult task.

Finally, a method to discriminate between different noise sources by modulation techniques was discussed (Chapter IV). This

technique was shown to be very useful at high frequencies and low current where thermal noise is dominant over 1/f noise and generation-recombination (g-r) noise.

A detailed description of all detectors used in this research is shown in Appendix A.

CHAPTER II. EXPERIMENTAL TECHNIQUES AND EQUIPMENT

In this chapter the experimental procedures of detector fabrication are considered in detail. The d.c. noise measurement principle and technique are also described.

2.1 Crystal Processing and Sample Preparation

Crystals of Hg_{1-x} Cd_x Te were obtained from Honeywell Research Center, Bloomington, Minnesota as slices of about 2mm in thickness and 10 x 10 mm in area. The crystals were n-type with x either $\simeq$0.2 or $\simeq$0.4 corresponding to a band gap of 0.09 eV and 0.41 eV at 77°K respectively. Some of the crystals contained grain boundaries and were used to study 1/f noise at grain boundaries.

Different samples were prepared to study contact 1/f noise, grain boundary 1/f noise and, surface and bulk 1/f noise. The detailed preparation of these samples will be described in the appropriate chapter, while here we will describe the general technique.

The technique of sample preparation consisted of the following step by step procedure:

1. The crystal slice was lapped with 12μ grit on glass.

2. The slice was then polished with 0.3μ grit on micro cloth (10-15 min.).

3. The polished slice was etched repeatedly in a solution of 5 parts by volume of bromine and 95 parts by volume of methyl alcohol (etching rate was 2μ per 3 sec.). The total etching time

was ≈15 sec.

4. The etched slice was epoxied to a well polished germanium substrate. (The epoxy used was Scotch Cast 504 electrical resin manufactured by 3M Company which was cured overnight at 65°C.)

5. The top side of the slice was prepared by lapping and polishing as in steps 1 and 2 until the thickness of the crystal slice was about 30μ. Then it was etched down to a thickness of about 20μ.

6. The crystal was coated with watch crystals cement. (The cement used was G-S Hypo-Tube Cement manufactured by Germanow Simon Machine Co., Rochester, N.Y.). The detectors were then cut in proper shapes by a 5 mil wire saw.

7. The individual detectors were cleaned thoroughly in methyl alcohol, then etched down to the desired thickness.

8. Three different methods were used to make ohmic contacts to (Hg,Cd)Te detectors:

i) The first method was by soldering gold leads directly to the top of the sample using Indium (In) as the soldering material. A very fine In soldering iron was used so that the contact had a diameter of about 10 mils. (Fig. 2.1a). This method consistently showed very low contact noise and was used when a well defined contact geometry was not required.

ii) In the case when a well defined contact geometry was necessary, e.g. contact noise study or grain boundary noise study, ohmic contacts were made by evaporating In on the detector (e.g. see Fig. 2.1b); then gold

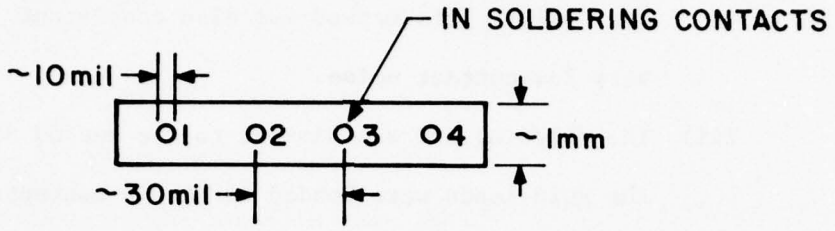

(a) DETECTORS 5661 AND 5663 (THICKNESS $\simeq 3.5\mu$)

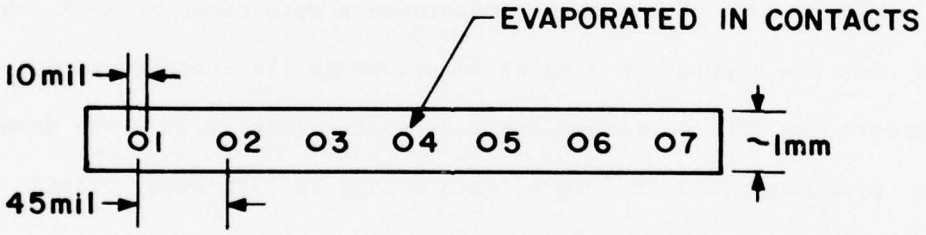

(b) DETECTORS 9746-P5, 9747-P5 AND 9748-P5
USED FOR CONTACTS STUDY (THICKNESS $\simeq 23\mu$)

FIG 2.1 DETECTORS FINAL DIMENSIONS

leads were bonded using silver epoxy (Acme, E-Solder No. 3021). This method was also consistent in showing very low contact noise.

iii) The third method was similar to the second except that the gold leads were bonded to the In contacts using silver paste. Such contacts always gave excessive noise. They were used to demonstrate the effect which excess noise contacts might have on the 1/f noise of the detector.

9. Each detector was mounted on a "TO8" IC header using G.E. varnish. The gold leads were soldered to the IC header pins using In solder.

Since most of the noise measurements were taken at 77°K, the detector was mounted in a metal dewar, while its contacts were connected to BNC connectors for easy access (Fig. 2.2). The dewar was evacuated to 2×10^{-4} Torr, then cooled to 77°K using liquid nitrogen.

2.2 Noise Measurements

2.2.1 The Principle of Measurement

We are interested in evaluating the random fluctuations in the value of a physical variable X; X may be the voltage or current in an electronic device, temperature of the device or any other variable. Random variables X(t) can be characterized on a statistical basis. One way is to characterize them by their averages, the most important being the average value $\bar{X}$ and the mean square value $\overline{X^2}$. Often $\bar{X}$ is zero and then the most significant quantity is $\overline{X^2}$. If $\bar{X}$ is not zero then one introduces $(X-\bar{X})$ as a new variable; the

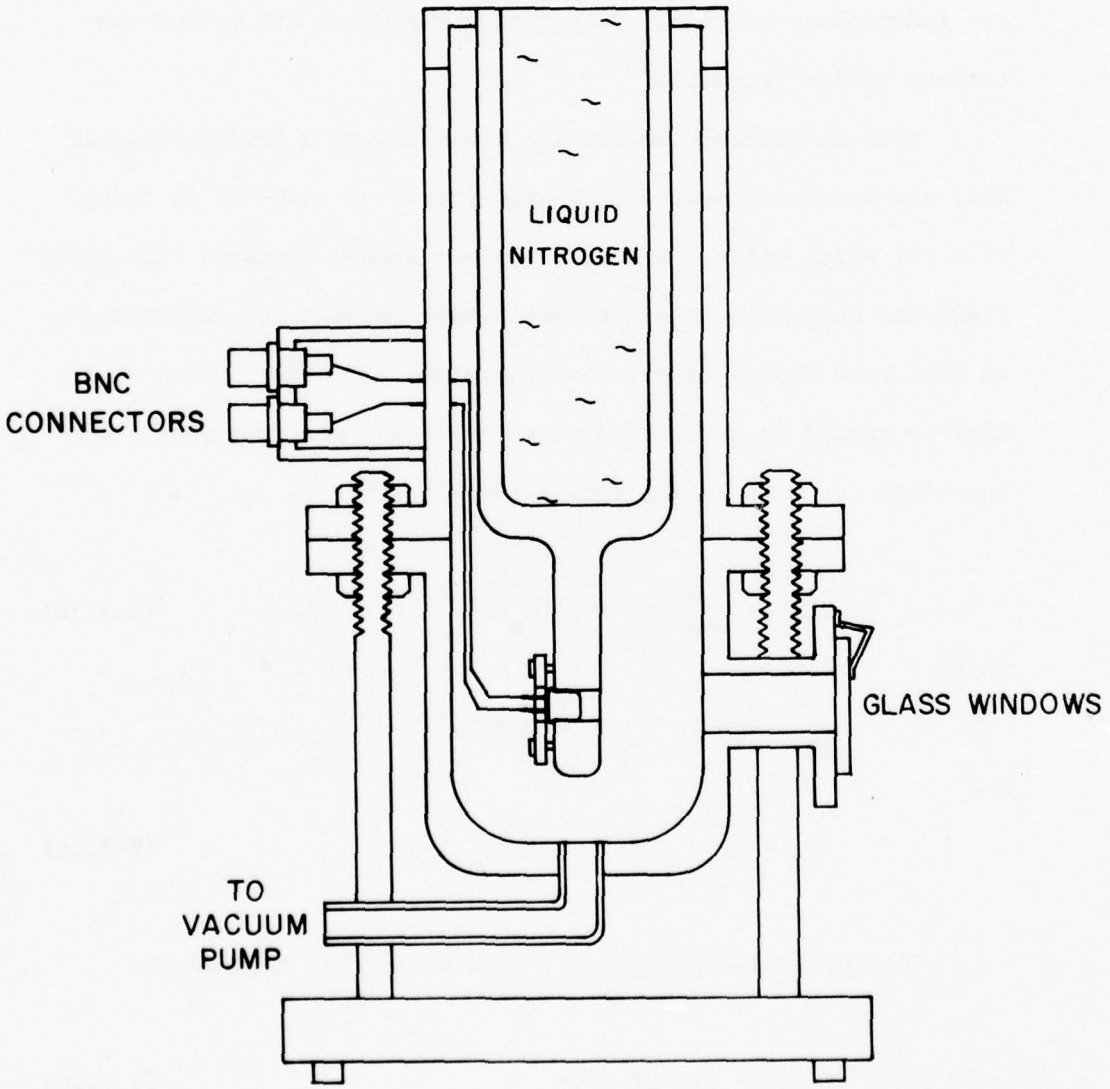

FIG 2.2 DEWAR FOR MEASUREMENTS ON (Hg, Cd) Te

significant average is then the variance of X(t), defined as

$$\overline{(X-\bar{X})^2} = \overline{X^2} - (\bar{X})^2 \qquad (2.2.1a)$$

Most of the significant noise sources give rise to fluctuating quantities that have averages and mean square averages that are independent of time. Such random variables are called stationary random variables.

Now, in general the Fourier transform of a random variable X(t) may be spread over a very high frequency range as is indeed true for white noise. However, the electronic circuits like amplifiers and quadratic detectors which must be used for measurements on X(t) have finite bandwidths. Therefore a Fourier analysis of X(t) is needed to understand what really is being measured. One can write for X(t) in the interval $0 \leq t \leq T$,

$$X(t) = \sum_{n=-\infty}^{\infty} a_n \exp(j\omega_n t) \qquad (2.2.1b)$$

where

$$\omega_n = \frac{2\pi n}{T}, \quad n = 0, \pm 1, \pm 2. \ .$$

and

$$a_n = \frac{1}{T}\int_0^T X(t) \exp(-j\omega_n t)\, dt \qquad (2.2.1c)$$

The spectral density $S_X(f)$ of X(t) is then defined as

$$S_X(f) = \lim_{T\to\infty} 2T\, a_n a_n^* \qquad (2.2.1d)$$

where the asterisk denotes the complex conjugate.

According to Wiener-Khintchine theorem[10]

$$S_X(f) = 4 \int_o^\infty \overline{X(t)\ X(t+s)}\ \cos \omega s\ \ ds \qquad (2.2.1e)$$

By inversion, Eq. (2.2.1e) reduces to

$$\overline{X(t)\ X(t+s)}\ = \int_o^\infty S_X(f)\ \ \cos \omega s\ df \qquad (2.2.1f)$$

In calculations one usually evaluates the autocorrelation function and determines $S_X(f)$ with the help of Eq. (2.2.1e). In measurements one determines $S_X(f)$ and evaluates the autocorrelation function using Eq. (2.2.1f). Putting S=0 in this equation

$$\overline{X^2(t)} = \int_o^\infty S_X(f)\ \ df \qquad (2.2.1g)$$

thus the mean square value can be obtained by a simple integration once $S_X(f)$ is known.

In the actual measurement, the stationary random signal X(t) is applied to the input of an arbitrary linear system (an amplifier, for example) with a transfer function g(f). Let Y(t) denote the signal coming out of the system. If $S_X(f)$ and $S_Y(f)$ are the corresponding spectral densities and x_n and y_n the Fourier coefficients, then

$$y_n = x_n\ g(f) \qquad (2.2.1h)$$

or

$$S_y(f) = S_x(f)\ \ |g(f)|^2 \qquad (2.2.1i)$$

Using Eq. (2.2.1g)

$$\overline{Y^2(t)} = \int_0^\infty S_x(f) \, |g(f)|^2 \, df$$

If the linear system is an amplifier, then $\overline{Y^2(t)}$ can be measured with a quadratic detector. If the amplifier is sharply tuned at the frequency f_o, then the measured value of $\overline{Y^2(t)}$ yields $S_x(f)$ almost immediately. Since the amplifier is sharply tuned, $S_x(f) \approx S_x(f_o)$ over the pass band of the amplifier so that

$$\overline{Y^2(t)} = S_x(f_o) \int_0^\infty |g(f)|^2 \, df$$

$$= S_x(f_o) \; g_o^2 \; B_{eff} \qquad (2.2.1j)$$

where $g_o = g(f_o)$ is the midband response and B_{eff} is the effective bandwidth of the system, defined as

$$B_{eff} = \frac{1}{g_o^2} \int_0^\infty |g(f)|^2 \, df \qquad (2.2.1k)$$

The value of g_o and B_{eff} can easily be determined with the help of a signal generator. Consequently, $S_x(f_o)$ can be evaluated as soon as $\overline{Y^2(t)}$ has been measured and g_o and B_{eff} determined.

2.2.2 Measuring Equipment

The experimental setup used for the low frequency (10 Hz to 100 KHz) noise measurments is shown in a block diagram in Fig. 2.3. It consists of a wide band preamplifier made with low noise PNP silicon transistors and shows a very low equivalent input noise

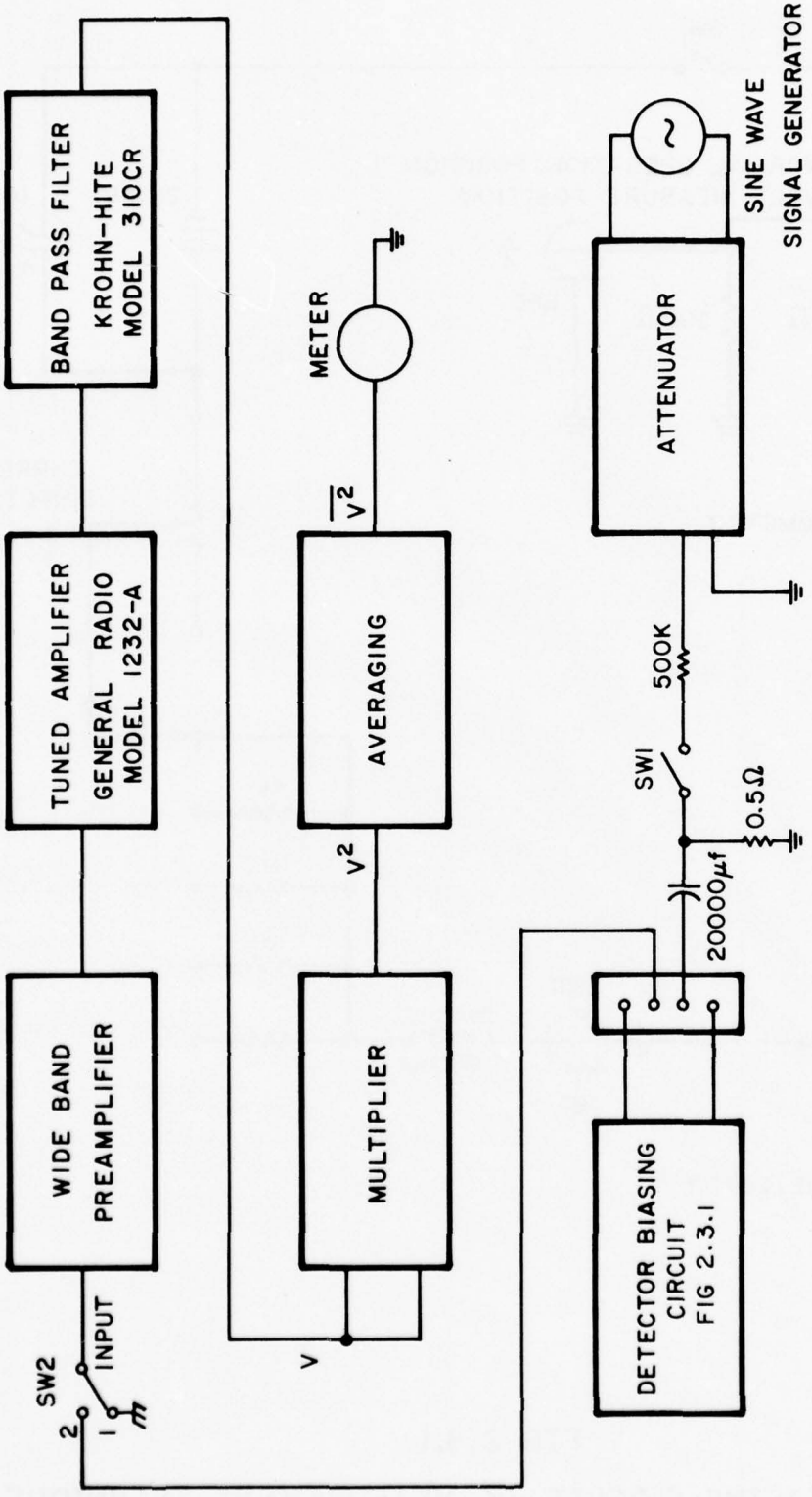

FIG 2.3 LOW FREQUENCY NOISE MEASUREMENT SYSTEM

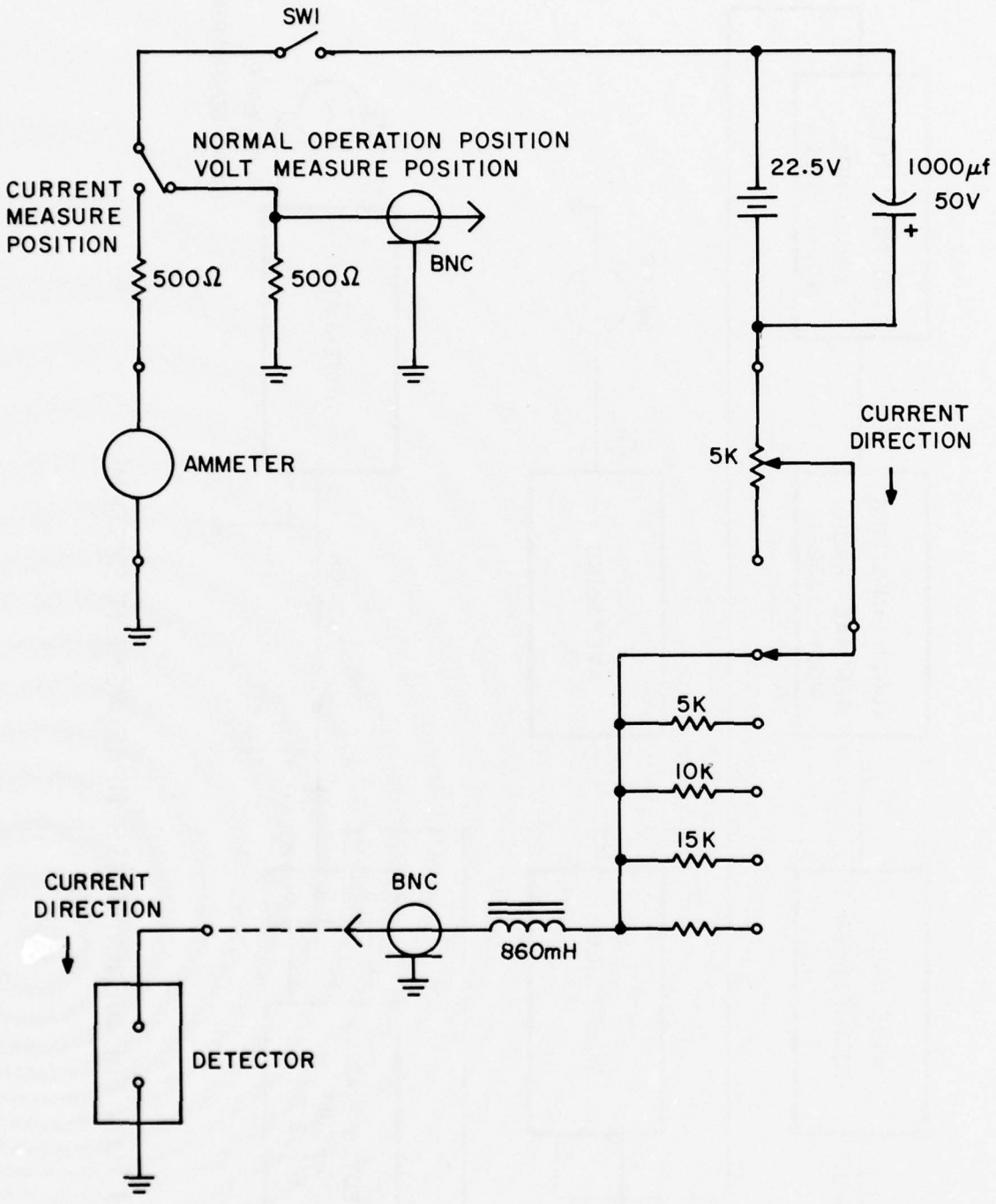

FIG 2.3.1

DETECTOR BIASING CIRCUIT. DC MEASUREMENT TECHNIQUE

resistance (about 20 ohms at 10 Hz and above). It has an input impedance of about 2 KΩ (Fig. 2.4). Another preamplifier (Fig. 2.5) with an input impedance of about 2 MΩ was made using low noise JFETS. Its equivalent input resistance is about 600 ohms at 100 Hz. These two preamplifiers were enough to cover any practical impedance level of (Hg,Cd)Te detectors.

The output of the preamplifier was fed into a tuned amplifier which is a modified version of General Radio model 1232-A tuned amplifier. This was followed by a bandpass filter model 310 CR, made by Krohn-Hite, which was followed by a squaring and then averaging circuits (Quadratic detector).

A cross-correlator circuit was used as the quadratic detector in our system. Figure 2.6 describes a correlation measurement setup; it is generally used in noise measurements to avoid the problem of amplifier noise. The noise signal from the device under test is fed into two parallel channels where the signal is amplified and filtered. The two signals v_1 and v_2 are then fed into a multiplier whose output is proportional to the product of instantaneous values of v_1 and v_2. This product is passed through an averaging circuit which gives $\overline{v_1 v_2}$. During the averaging process the noises associated with two amplifiers disappear because they are uncorrelated whereas the noise signal to be measured is retained. This cross-correlator can be used as a quadratic detector by feeding the signal into both inputs of the multiplier; to do so the switch S_1 is put in position 1 as shown in Fig. 2.7 which describes the actual cross-correlator system. In this system the amplifiers consist of Signetics μA709 operational amplifiers with a gain of 10.

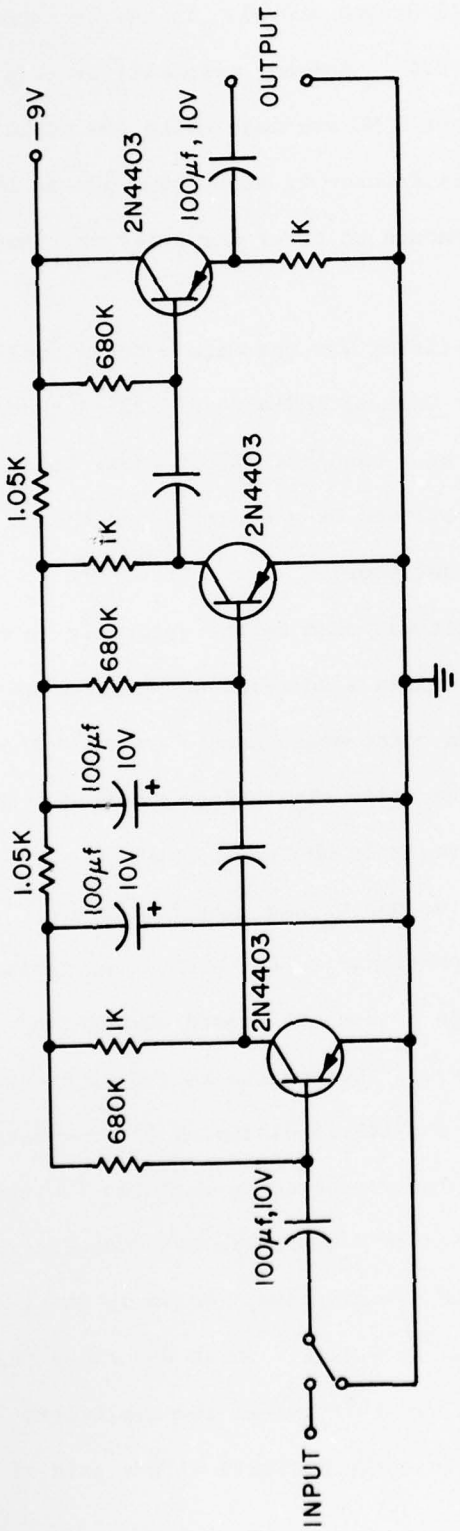

FIG 2.4

LOW INPUT IMPEDANCE PREAMPLIFIER CIRCUIT

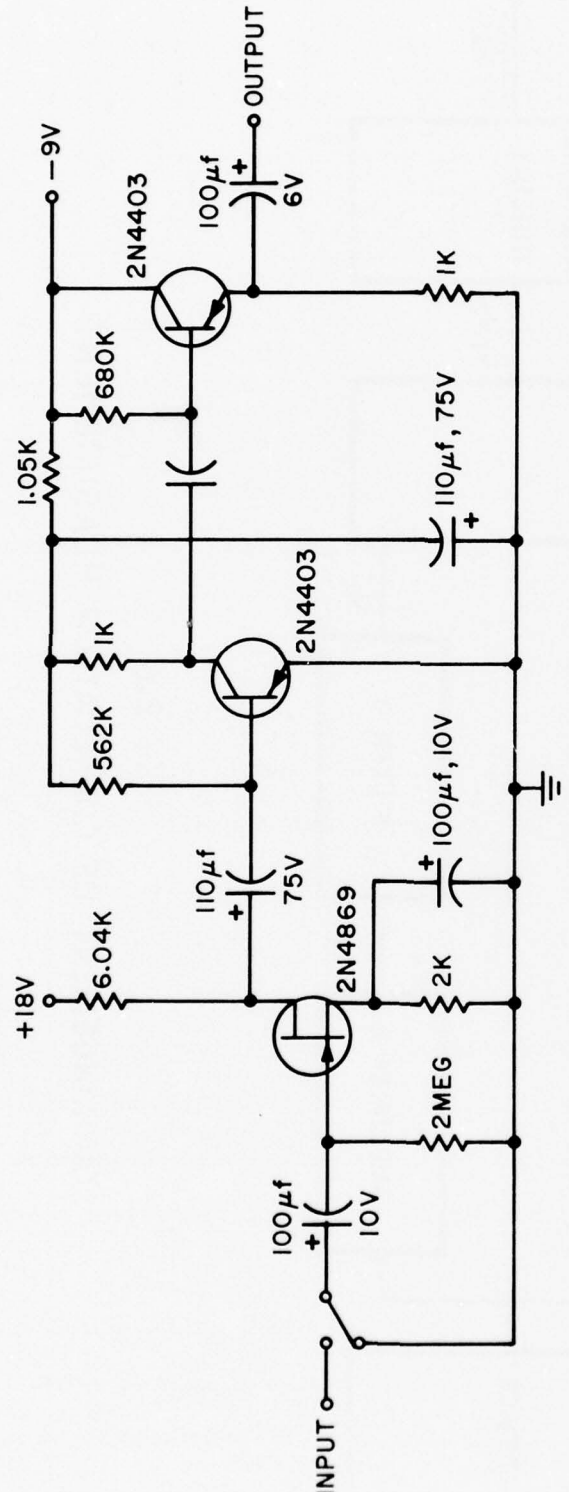

FIG 2.5

HIGH INPUT IMPEDANCE PREAMPLIFIER CIRCUIT

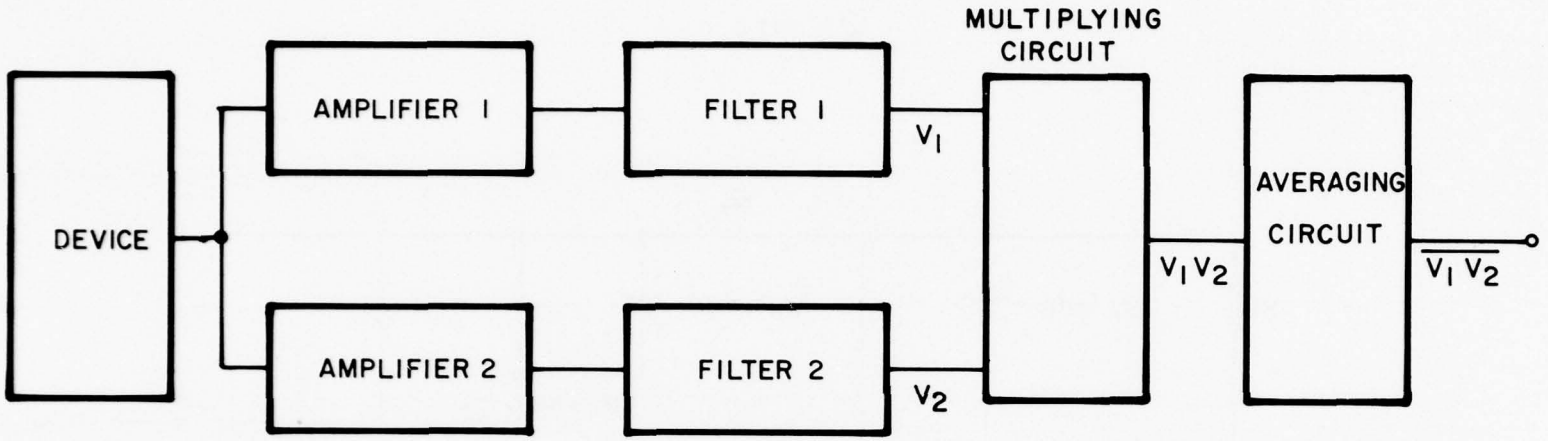

FIG 2.6

ARRANGEMENT OF CORRELATION MEASUREMENT

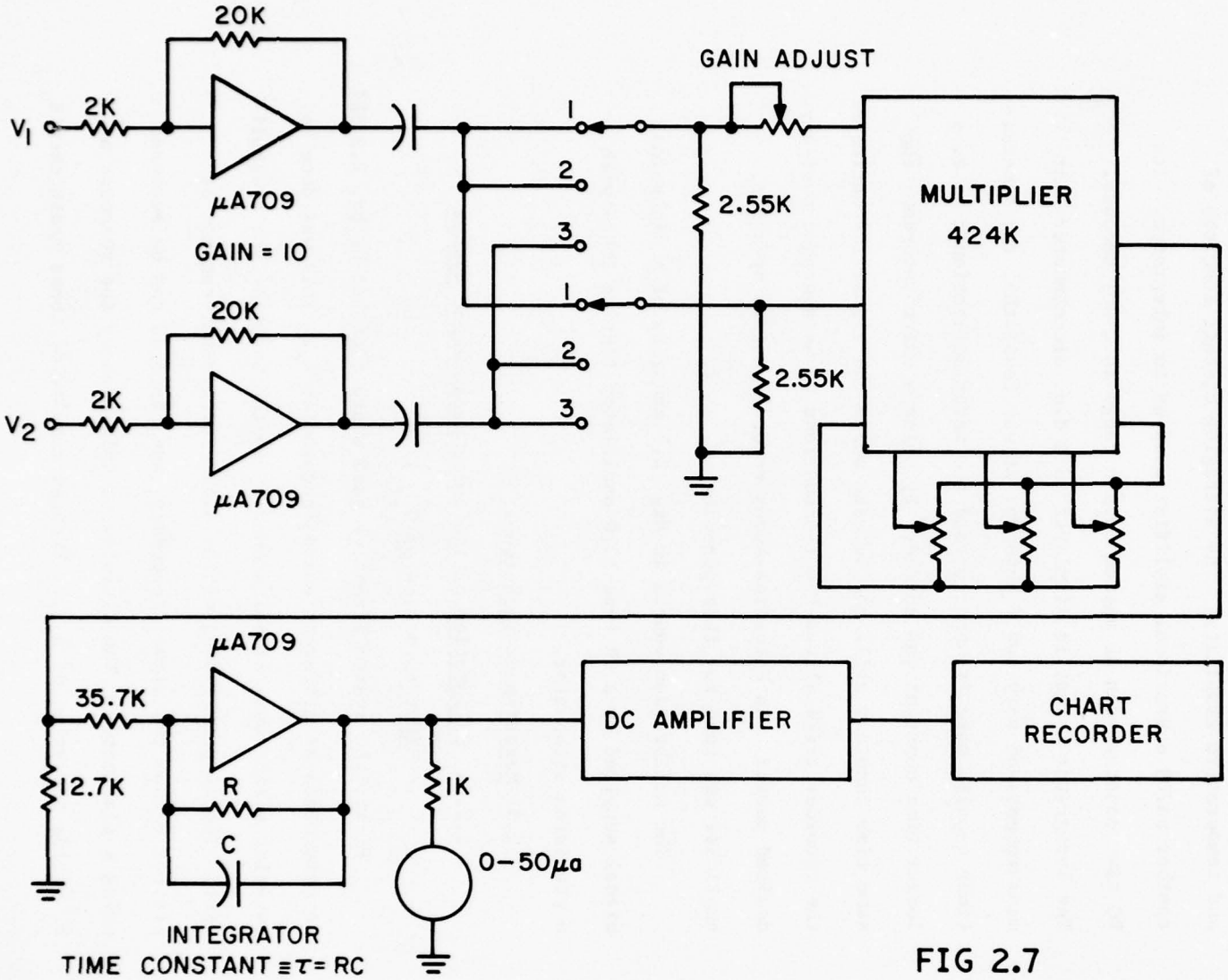

FIG 2.7
CORRELATOR SYSTEM AND INDICATING INSTRUMENTS

424K is a high accuracy wideband multiplier made by Analog Devices. It uses a pulse-width/height technique to develop the multiply function, which results in a very high accuracy, excellent linearity and temperature stability. The averaging circuit consists of another μA709 operational amplifier used as an integrator. Its RC time constant can be varied over a range (0.2-20) seconds. The integrator output is displayed on a d.c. microammeter. At measurements of very low frequency, it was found that the fluctuations usually make it hard to read the meter deflections; i.e. a longer time constant was needed. By using a chart recorder, the same time constant still can be used while the visual inspection of the recorder trace allows the fluctuations to be averaged over any desired period. An Esterline-Angus recorder driven by a d.c. amplifier was used for this purpose.

The calibration source in Fig. 2.3 consists of a sinusoidal signal supplied by a GR type 1310 oscillator (2Hz to 2MHz) with a precision attenuator.

2.2.3 Measurement Techniques

2.2.3a Calibration of the noise measurement system (Determination of B_{eff})

First, the system effective band width (defined by Eq. 2.2.1k) is determined at different tuned frequencies f_o. This was done by sweeping a sine wave signal around f_o to the input of the preamplifier. The output reading of the d.c. microammeter can now be plotted versus the signal frequency, and its area can be measured using a planimeter. The division of this area by the response at f_o yields the value of B_{eff}. Typical results of these measurements

are shown in Fig. 2.8 for f_o = 1KHz.

Next, the performance of the system is tested by measuring the thermal noise of wirewound resistors, which have white noise, at different frequencies through the range of interest (10Hz - 100KHz). Typical results of these measurements are shown in Fig. 2.9 at f_o = 1KHz, where $\overline{V^2} = 4KTRB_{eff}$ is plotted versus R. The curve is linear and its slope gives the value of $B_{eff} (= \frac{\overline{V^2}}{4KTR})$ which shows a good agreement with the value measured above.

2.2.3b Noise measurement procedure

Figure 2.10 describes the equivalent circuit for the noise measurement of the device. The preamplifier noise is represented by a series e.m.f. $\sqrt{\overline{V_n^2}}$. The main amplifier and the rest of the measuring system have been assumed to be noiseless since their noise contribution is negligible compared to $\sqrt{\overline{V_n^2}}$. The device noise is represented by an e.m.f. $\sqrt{\overline{V_d^2}}$. R is a wirewound resistor and it is assumed to be noiseless since its contribution is negligible as compared to $\sqrt{\overline{V_d^2}}$.

Let the measuring system be tuned at frequency f_o with bandwidth B_{eff} and gain g(f). For every noise measurement, the quadratic detector output M, read by the d.c. microammeter, indicates a noise power such that

$$M \alpha \int S_v(f) \; |g(f)|^2 \, df \qquad (2.2.3a)$$

where $S_v(f)$ is the spectral density of the noise voltage V across the two input terminals of the system. Assuming a small bandwidth, (2.2.3a) can be rewritten as

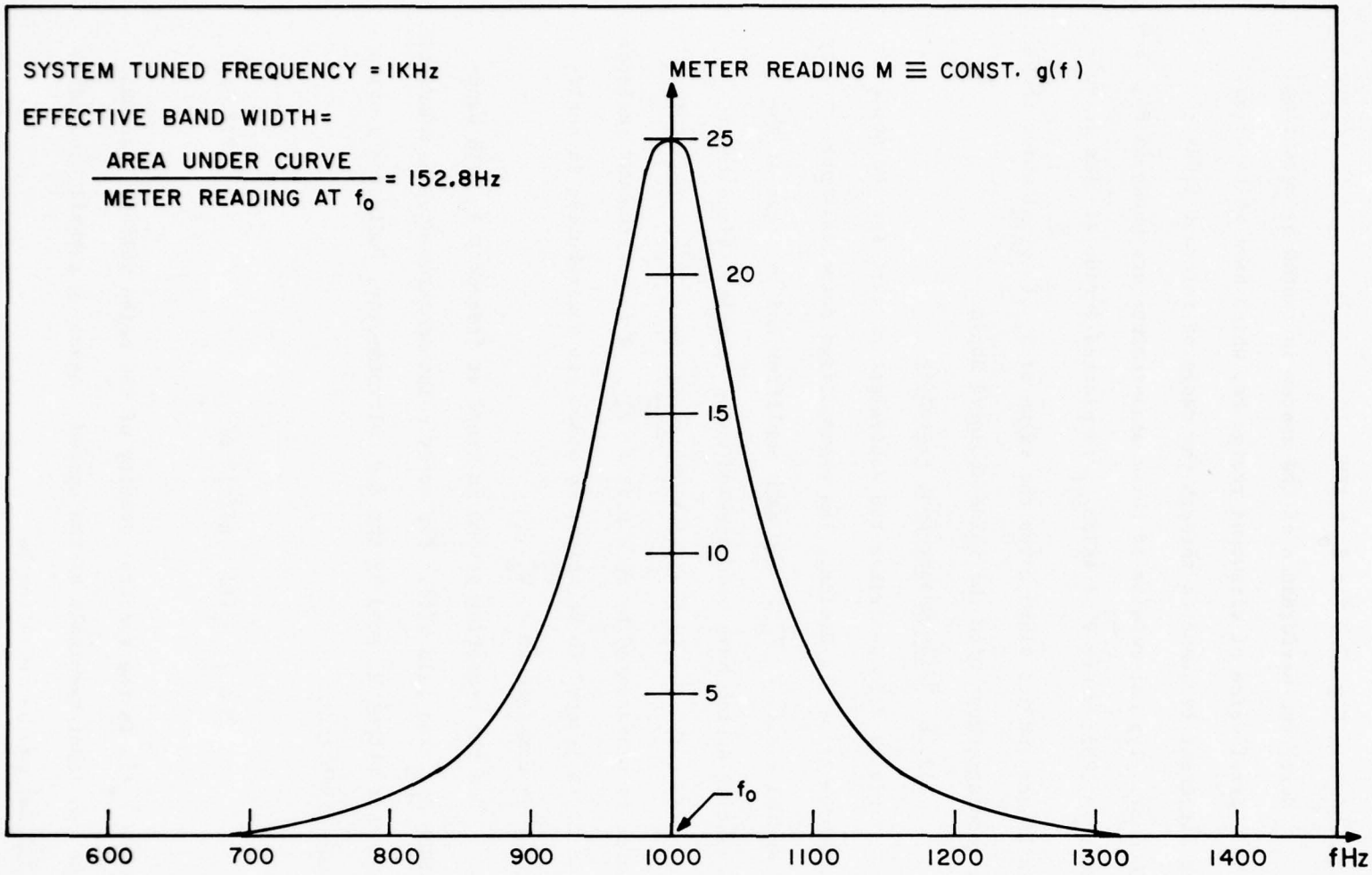

FIG 2.8 SYSTEM FREQUENCY RESPONSE AT 1KHz

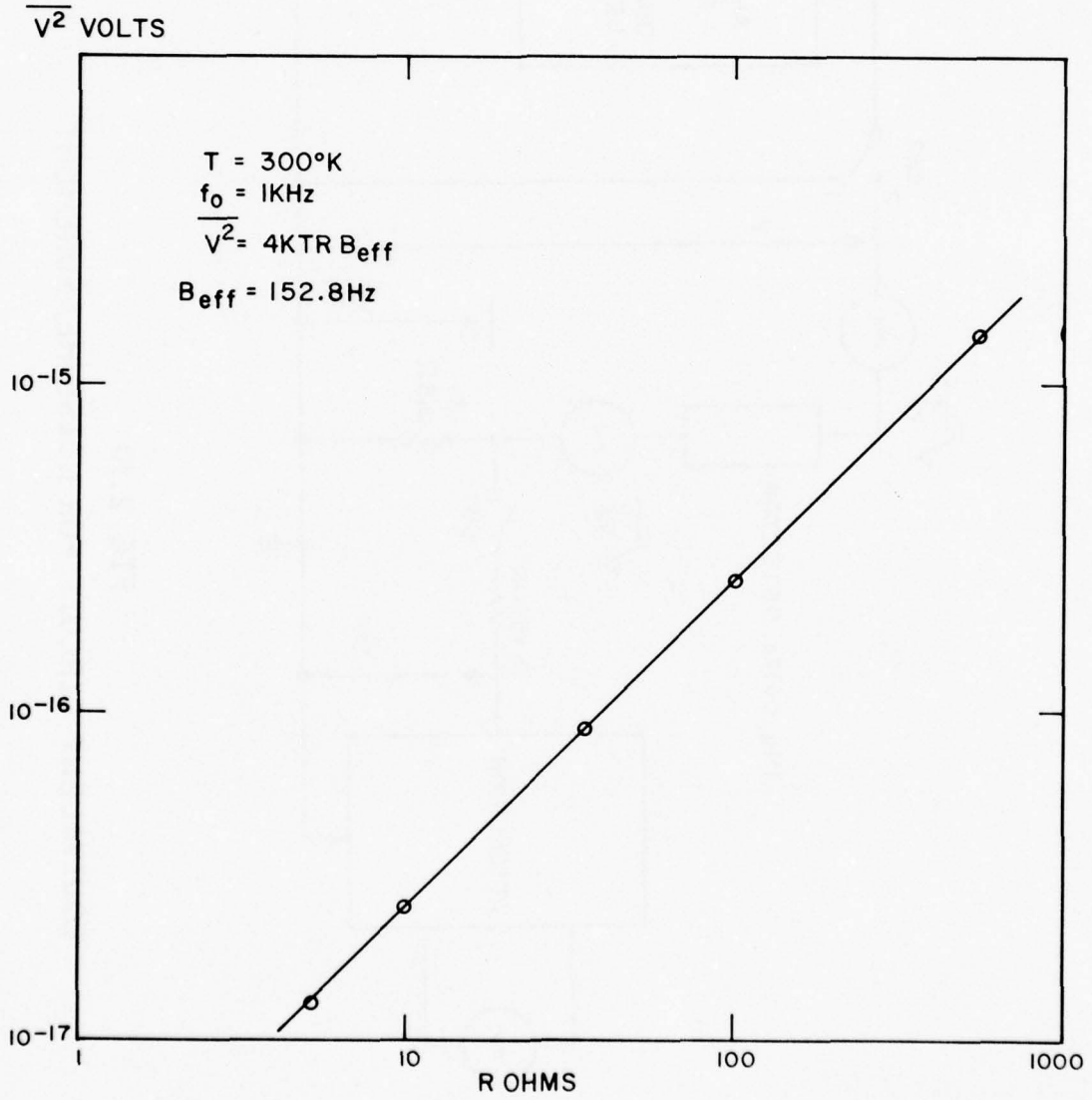

FIG 2.9 MEASURED THERMAL NOISE OF RESISTORS
TO CHECK THE PERFORMANCE OF THE SYSTEM

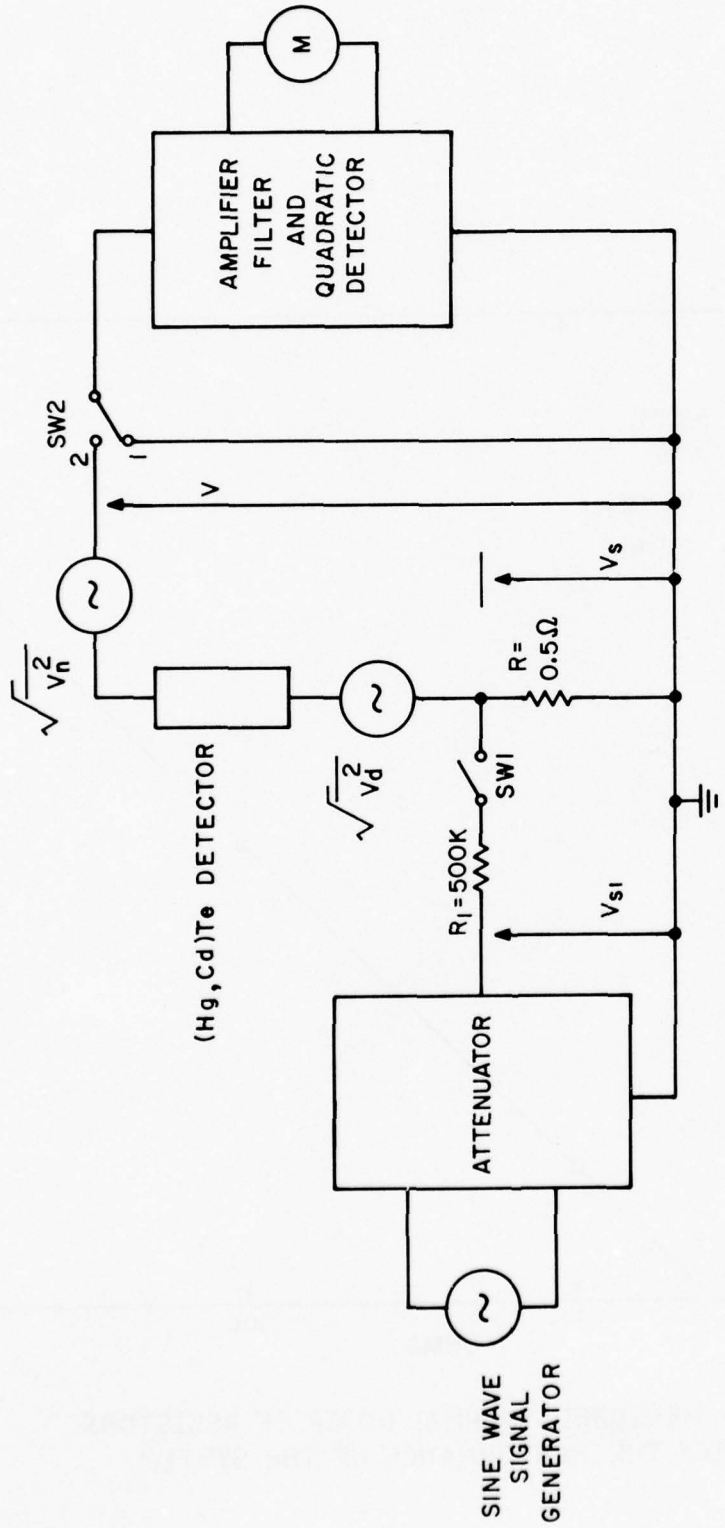

FIG 2.10

EQUIVALENT CIRCUIT FOR NOISE MEASUREMENT

$$M \alpha S_v(f_o)\, g_o^2\, B_{eff}$$

therefore

$$M = K\, \overline{V^2}\, g_o^2$$

where K is a constant. Now, three measurements are required to obtain $\overline{V_D^2}$ or $S_{V_D}(f)$. The first measurement is taken with SW1 open and SW2 in position 1. Then the meter reading is

$$M_1 = K\, g_o^2\, \overline{V_n^2} \qquad (2.2.3b)$$

Measurement 2 is taken with SW1 open and SW2 in position 2, therefore

$$M_2 = K\, g_o^2\, (\overline{V_n^2} + \overline{V_D^2}) \qquad (2.2.3c)$$

Measurement 3 is taken with SW1 closed and SW2 in position 2, yielding

$$M_3 = K\, g_o^2\, (\overline{V_n^2} + \overline{V_D^2} + \overline{V_S^2}) \qquad (2.2.3d)$$

where V_s is given by,

$$V_S = \frac{R}{R_1}\, V_{S_1}$$

Solving (2.2.3b), (2.2.3c) and (2.2.3d) and using the relation

$$\overline{V_D^2} = S_{V_D}(f_o)\, B_{eff}$$

we get

$$S_{V_D}(f_o) = \frac{1}{B_{eff}} V_{S_1}^2 \left(\frac{R}{R_1}\right)^2 \frac{M_2 - M_1}{M_3 - M_2}$$

CHAPTER III. BASIC NOISE SOURCES IN PHOTOCONDUCTIVE DEVICES

In this chapter, the three basic noise sources in photoconductive devices that are operated at low light levels, and to which a d.c. bias current I_o is applied will be discussed briefly. They are: 1) Thermal noise; 2) Generation-recombination noise; and, 3) 1/f noise. We consider here an n-type photoconductor of length L and assume that the thermal generation and recombination processes give rise to band to band transitions.

3.1 Thermal noise

It is due to thermal agitation of carriers in the sample. Its voltage spectral density is given by,

$$[S_v(f)]_{thermal} = 4KTR_o$$

$$= 4KT \frac{L^2}{e(N_o\mu_n + P_o\mu_p)}$$

where R_o = the sample dark resistance,

$N_o(P_o)$ = the total number of electrons (holes) in the sample,

$\mu_n(\mu_p)$ = the electron (hole) mobility and

L = the detector length.

3.2 Generation-recombination noise

This is caused by spontaneous fluctuations in the generation, recombination and trapping rates of the carriers, thus causing fluctuations in the free carrier densities. Since electrons and holes are assumed to appear and disappear in pairs (band to band transitions), hence

$$\Delta N = \Delta P$$

where ΔN and ΔP are fluctuations around the equilibrium values N_o and P_o respectively. The fluctuation ΔR, in the resistance is therefore

$$\Delta R = -\left[\frac{e(\mu_n + \mu_p)R_o^2}{L^2}\right] \Delta N$$

The corresponding fluctuation in voltage, ΔV, is

$$\Delta V = \Delta R I_o$$

$$= -\left[\frac{e(\mu_n + \mu_p)R_o^2}{L^2}\right] I_o \Delta N$$

and hence the voltage fluctuation due to g-r noise has a spectral density

$$[S_v(f)]_{g-r} = \left[\frac{e(\mu_n + \mu_p)R_o^2}{L^2}\right]^2 I_o^2 S_N(f)$$

where $S_N(f)$ is the spectral density of ΔN.

Now it follows easily from the theory of g-r noise[11] that

$$S_N(f) = 4g(N_o) \frac{\tau_o^2}{1 + \omega^2 \tau_o^2} \qquad (3.2a)$$

where $g(N_o)$ is the thermal generation rate and τ_o is the lifetime of added carriers, so that

$$[S_v(f)]_{g-r} = \left[\frac{e(\mu_n + \mu_p)R_o^2}{L^2}\right]^2 4g(N_o) \frac{\tau_o^2 I_o^2}{1 + \omega^2 \tau_o^2}$$

$$= K_1 \frac{I_o^2}{1 + \omega^2 \tau_o^2} \qquad (3.2b)$$

The g-r noise spectrum of detector #5661 is shown in Fig. 3.1. The figure indicates that the carrier lifetime for this detector is approximately 10^{-8} sec. One can see from Eq. (3.2b) that the g-r noise for these devices is expected to vary proportionally to I_o^2. Fig. 3.2 is a plot of g-r noise vs. current I_o for the same detector. It is obtained from high frequency measurements and shows a very good agreement with Eq. (3.2a) i.e. an I_o^2 dependence.

3.3 1/f Noise

When a direct current passes through a photoconductor material, an excess noise is observed over and above the previously mentioned noise sources.

The basic feature of this noise is its frequency spectrum, shown in Fig. 3.3 for detector #5661, which is of the form $1/f^{\alpha}$ where α is close to unity (hence the name 1/f). Its dependence on

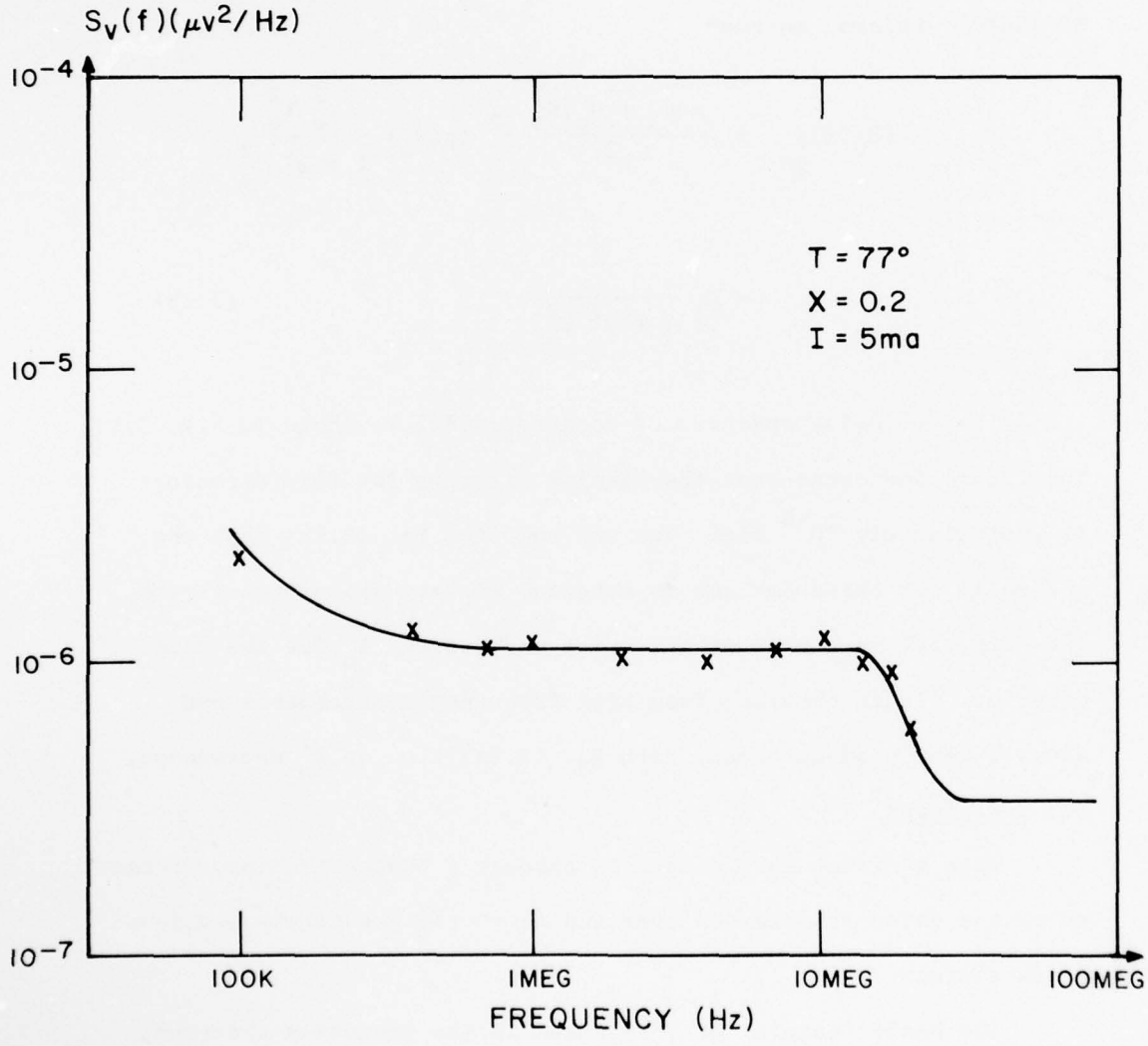

FIG 3.1
g-r NOISE SPECTRUM FOR DETECTOR 5661

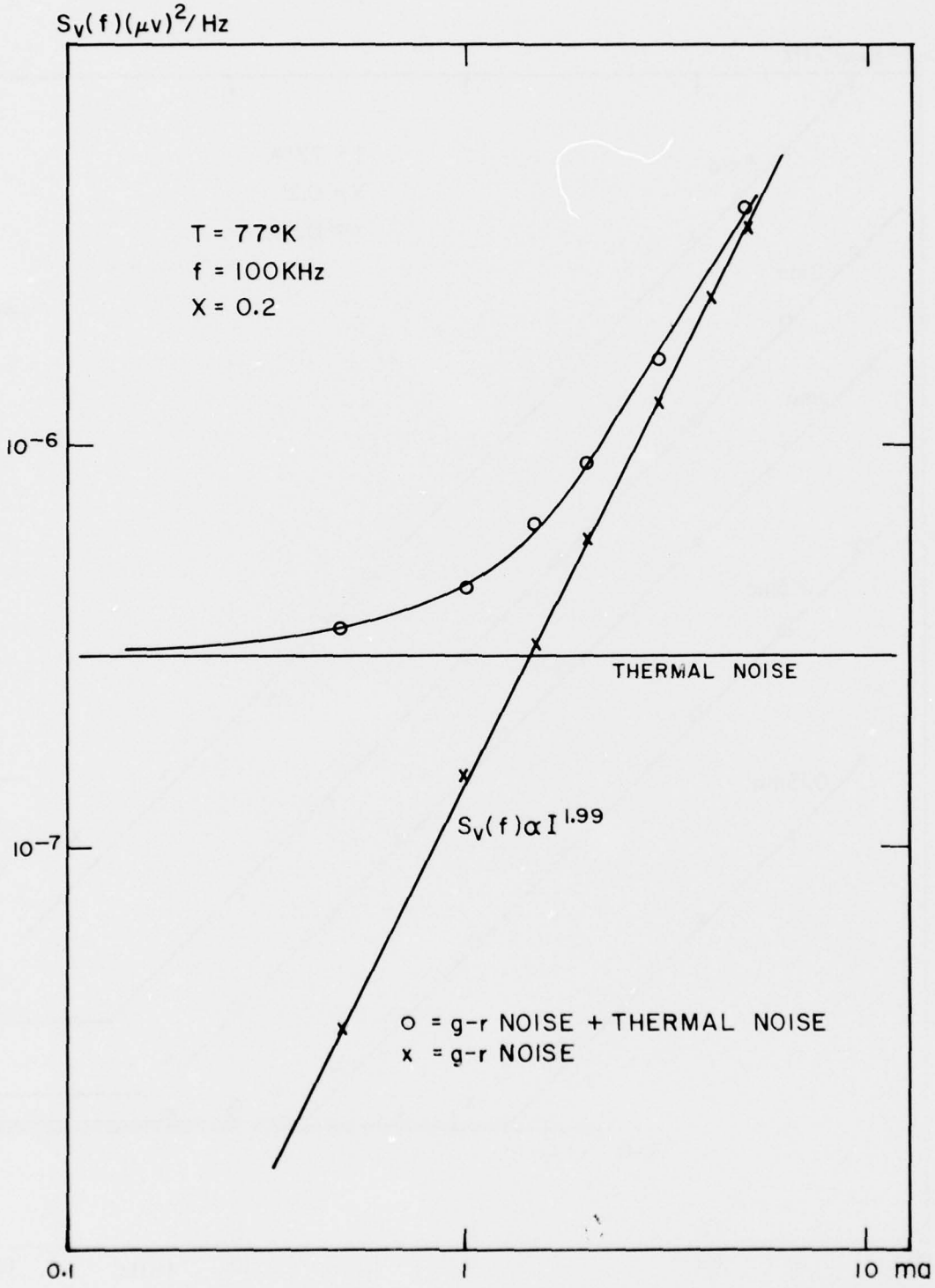

FIG 3.2 g-r NOISE VERSUS DC CURRENT FOR DETECTOR 5661

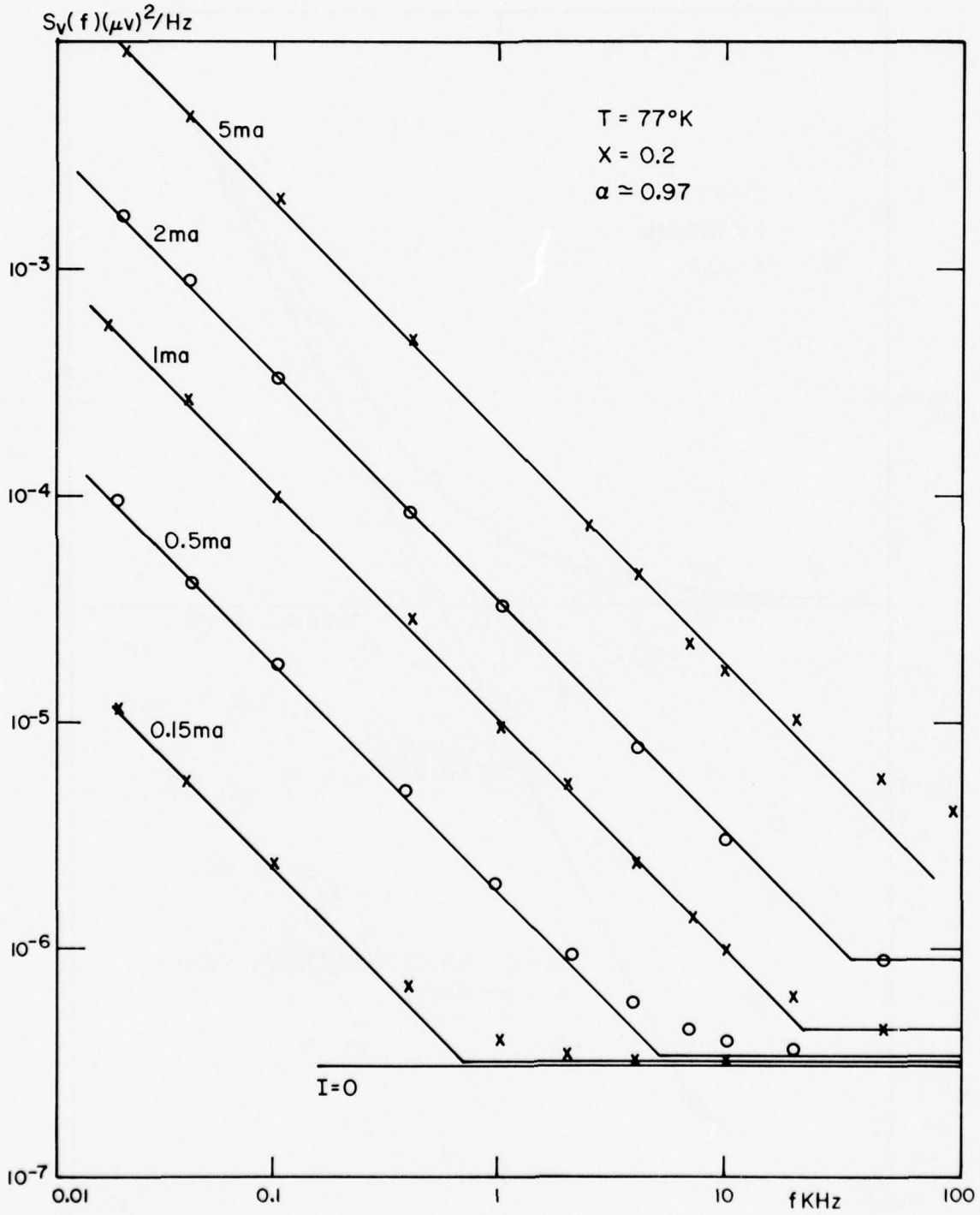

FIG 3.3 I/F NOISE SPECTRUM FOR DETECTOR 5661

the current is found to be proportional to the square of the steady current (Fig. 3.4); then 1/f noise may be considered to be due to conductivity fluctuations, which in turn are caused by the fluctuation in the number of carriers (surface model) or their mobilities (bulk model).

3.3.1 McWhorter's surface model for 1/f noise

The simplified model for a semiconductor surface is illustrated in Fig. 3.5. It consists of four regions.

a) The semiconductor bulk, shown as n-type.

b) The surface space charge region, shown as depletion region.

c) The interface region between the semiconductor and its oxide.

d) The semiconductor oxide film.

There are surface states associated with regions c and d. The states that occur at the interface proper are referred to as fast states, in that they can communicate with the semiconductor bulk in a rapid manner and must reside within a few angstroms of the semiconductor surface. The states occuring in the oxide layer are referred to as slow states. They communicate with the bulk by tunneling through the insulation or by thermal emission over the barrier indicated in Fig. 3.5.

McWhorter[1] developed a model for 1/f noise in semiconductors based on the existence of the slow surface states. Fluctuations in the capture and release of bulk electrons by these states produce fluctuations in the bulk electron concentration and consequently in the conductivity.

Suppose the number N of carriers in the semiconductor sample

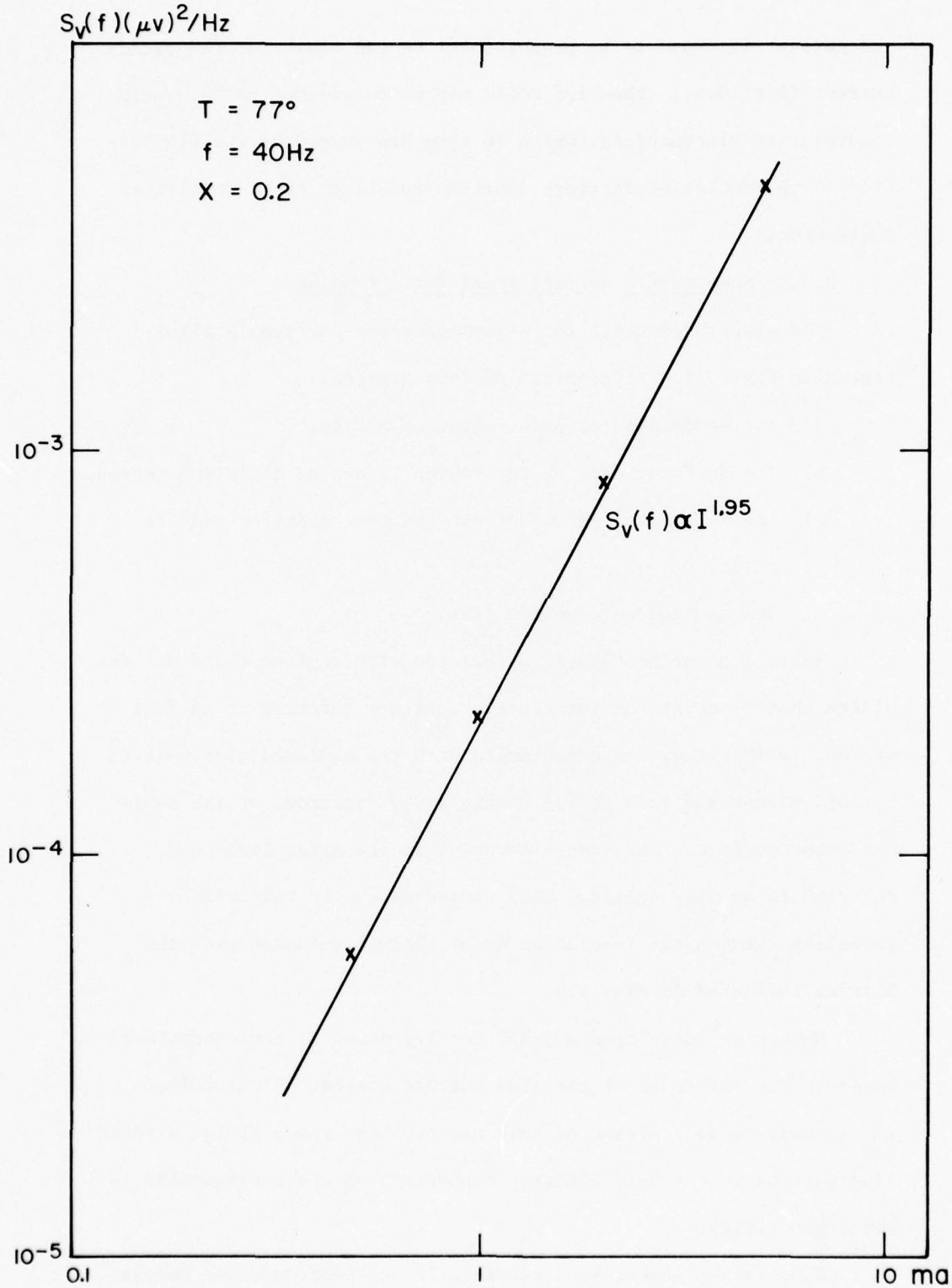

FIG 3.4 I/F NOISE VERSUS DC CURRENT FOR DETECTOR 5661

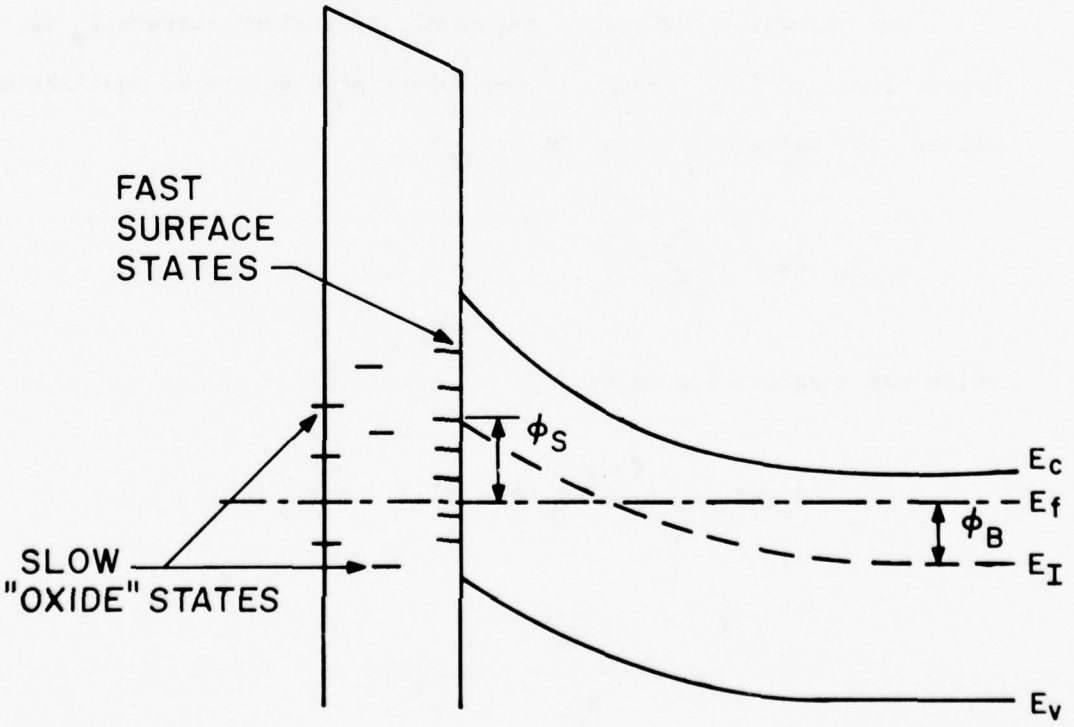

FIG 3.5 TYPICAL SEMICONDUCTOR SURFACE

fluctuates by an amount ΔN due to communication with these states and that this fluctuation is governed by a single time constant τ i.e. only one type of slow surface states is present. Then, it is easily seen that the auto correlation function is[12]

$$\overline{\Delta N(t)\Delta N(t+s)} = \overline{\Delta N^2} \exp(-\frac{s}{\tau})$$

By applying the Wiener-Khintchine theorem we obtain for the spectral density of ΔN

$$S_N(f) = 4\,\overline{\Delta N^2}\,\frac{\tau}{1+\omega^2\tau^2}$$

Now the voltage V across the sample at a given current I_o is proportional to 1/N. Hence, if the subscript o refers to equilibrium values, the voltage fluctuation is

$$\Delta V = -\frac{V_o}{N_o}\,\Delta N$$

which has a spectral density

$$S_V(f) = (\frac{V_o}{N_o})^2\, S_N(f)$$

$$= 4\,\frac{V_o^2\,\overline{\Delta N^2}}{N_o^2}\,\frac{\tau}{1+\omega^2\tau^2}$$

Next we put $\overline{\Delta N^2} = \beta(N_o)\,N_o$, where $\beta(N_o)$ is a measure for the

efficiency of the interaction between oxide states and free carriers[7,6]; $\beta(N_o)$ may be a slow function of N_o.

To obtain the 1/f frequency dependence of the noise power spectrum, we assume that electron tunneling is the mechanism by which bulk electrons communicate with the oxide states. Since the tunneling probability depends exponentially on the distance x over which tunneling must occur, the dependence of τ on x may be written

$$\tau = \tau_o \exp(\alpha x)$$

where α is of the order of 10^8 cm^{-1}. We now assume a uniform trap distribution in x for $x_1 < x < x_2$; usually $x_1 = 0$. The normalized distribution function is then

$$g(x)\, dx = \frac{dx}{x_2 - x_1} \qquad \text{for } x_1 < x < x_2$$

$$g(x)\, dx = 0 \qquad \text{otherwise.}$$

The corresponding normalized distribution in τ is therefore

$$g(\tau)\, d\tau = \frac{d\tau/\tau}{\ln(\tau_2/\tau_1)} \qquad \text{for } \tau_1 < \tau < \tau_2$$

$$g(\tau)\, d\tau = 0 \qquad \text{otherwise.}$$

where $\tau_1 = \tau_o \exp(\alpha x_1)$ and $\tau_2 = \tau_o \exp(\alpha x_2)$. Therefore by averaging $S_v(f)$ over all τ's yields

$$[S_v(f)]_{1/f} = \frac{4\,\beta(N_o)\,V_o^2}{N_o \ln(\tau_2/\tau_1)} \int_{\tau_1}^{\tau_2} \frac{\tau}{1+\omega^2\tau^2}\,\frac{d\tau}{\tau}$$

$$= \frac{4\,\beta(N_o)\,V_o^2}{\omega N_o \ln(\tau_2/\tau_1)} [\tan^{-1}\omega\tau_2 - \tan^{-1}\omega\tau_1]$$

which reduces to

$$[S_v(f)]_{1/f} = \frac{\beta(N_o)\,V_o^2}{f\,N_o \ln(\tau_2/\tau_1)}$$

$$= \frac{C_1}{N_o}\frac{V_o^2}{f} \qquad \text{for } \frac{1}{\tau_2} < \omega < \frac{1}{\tau_1} \qquad (3.3.1a)$$

where $C_1 = \beta(N_o)/[\ln(\tau_2/\tau_1)]$. Since $V_o = I_o R_o$, (3.3.1a) can be written as

$$[S_v(f)]_{1/f} = \frac{C_1 R_o^2}{N_o}\frac{I_o^2}{f}$$

$$= K_2 \frac{I_o^2}{f} \qquad \text{for } \frac{1}{\tau_2} < \omega < \frac{1}{\tau_1} \qquad (3.3.1b)$$

It should be noted that Eq. (3.3.1a) contains the factor $\beta(N_o)$, which is proportional to the trap density, which in turn is proportional to the surface state density.

Formula (3.3.1a) has been interpreted by Hooge[2,3] as a bulk effect (see next section). We see, however, that under our assumptions it also can come from surface effect. The derivations of (3.3.1a) assumes that the surface is uniformly active. If that is not the case, the factor C_1 must be slightly altered because $\beta(N_o)$ will differ for different surface elements. Let us assume that the active part of the surface has $\beta(N_o) = \beta'(N_o)$ and that the inactive part has $\beta(N_o) = 0$. Let us further assume that the fraction S of the surface is inactive. Since in the derivation of (3.3.1a) we average over all surface elements, we have

$$\overline{\beta(N_o)} = \beta'(N_o)\ (1-S),$$

so that

$$C = \frac{\beta'(N_o)\ (1-S)}{\ln(\tau_2/\tau_1)} \qquad (3.3.1c)$$

For S=0 this reduces to (3.3.1a), since now $\beta(N_o) = \beta'(N_o)$ throughout.

Such a situation could occur if part of the surface was fully depleted. The electrons of the bulk would then be unable to reach that part of the surface, and for this reason, that part would become inactive. This effect will be considered in more detail in Sec. 8.4.

3.3.2 Hooge's Bulk Model for 1/f Noise

Based on 1/f noise data for a variety of semiconductors, Hooge has proposed that 1/f noise is a bulk phenomenon[2,3]. He arrived at the following empirical expression for the 1/f noise power spectral density $S_v(f)$,

$$[S_v(f)]_{1/f} = \frac{K_2 V_o^{\beta}}{f^{\alpha}} = \frac{K_2}{f^{\alpha}} (I_o R_o)^{\beta} \qquad (3.3.2a)$$

with $\beta \equiv$ const. $\simeq 2$

$\alpha \equiv$ const. $\simeq 1$

and K_2 is an empirical coefficient given by

$$K_2 = \frac{C_2}{N_{total}} = \frac{2x10^{-3}}{N_{total}} \qquad (3.3.2b)$$

where $N_{total} = n_o Lwt$ is the total number of the carriers in the sample, L, w and t are the length, width and thickness of the sample.

The fact that the experimental results of 1/f noise studies on homogeneous samples can generally be expressed by the simple relations (3.3.2a and b) shows that 1/f noise is essentially a bulk effect and excludes surface effects as the main source of 1/f noise. In other words, relations (3.3.2a and b) show that 1/f noise is not some spurious effect due to accidental impurities or imperfections, but that it is a systematic effect inherent in electrical conduction.

By studying 1/f noise of concentration cells, thermo cells and Hall voltage,[4,5] Hooge and his co-workers have shown that what is actually fluctuating is the carrier mobility rather than their number. No model has been proposed for such mobility fluctuations.

CHAPTER IV. NOISE MEASUREMENTS OF (Hg,Cd)Te DECTECTORS BY AN A.C. MODULATION TECHNIQUE

It was shown in Chapter III that both the g-r noise and 1/f noise in photoconductive devices vary proportionally to the square of the steady current. This, along with the fact that thermal noise is independent of the current, made it possible to develop an a.c. modulation technique to discriminate between these noise sources. This technique is very useful at high frequencies and low current where thermal noise is dominant.

4.1 Technique

In the proposed scheme, Fig. 4.1, the detector bias is modulated by a signal $I_o + I_m \cos \omega_m t$ of low frequency f_m, say 5Hz. The flicker noise and the g-r noise are then modulated by this l.f. signal, whereas the thermal noise is not. By first amplifying the noise using a sharply tuned amplifier at a frequency $f_1 (f_1 >> f_m)$ and then detecting it normally, the output of the detector is modulated in the rhythm of the l.f. signal of frequency f_m. This modulation is detected by a phase sensitive detector, but, since the thermal noise is not modulated, it is not detected.

Let the g-r noise and the 1/f noise of the (Hg,Cd)Te detector be represented by a fluctuating resistance δR and let the thermal noise of this detector be represented by a fluctuating e.m.f. $\delta v'$. Hence, $v_1(t)$ is given by (see Fig. 4.1).

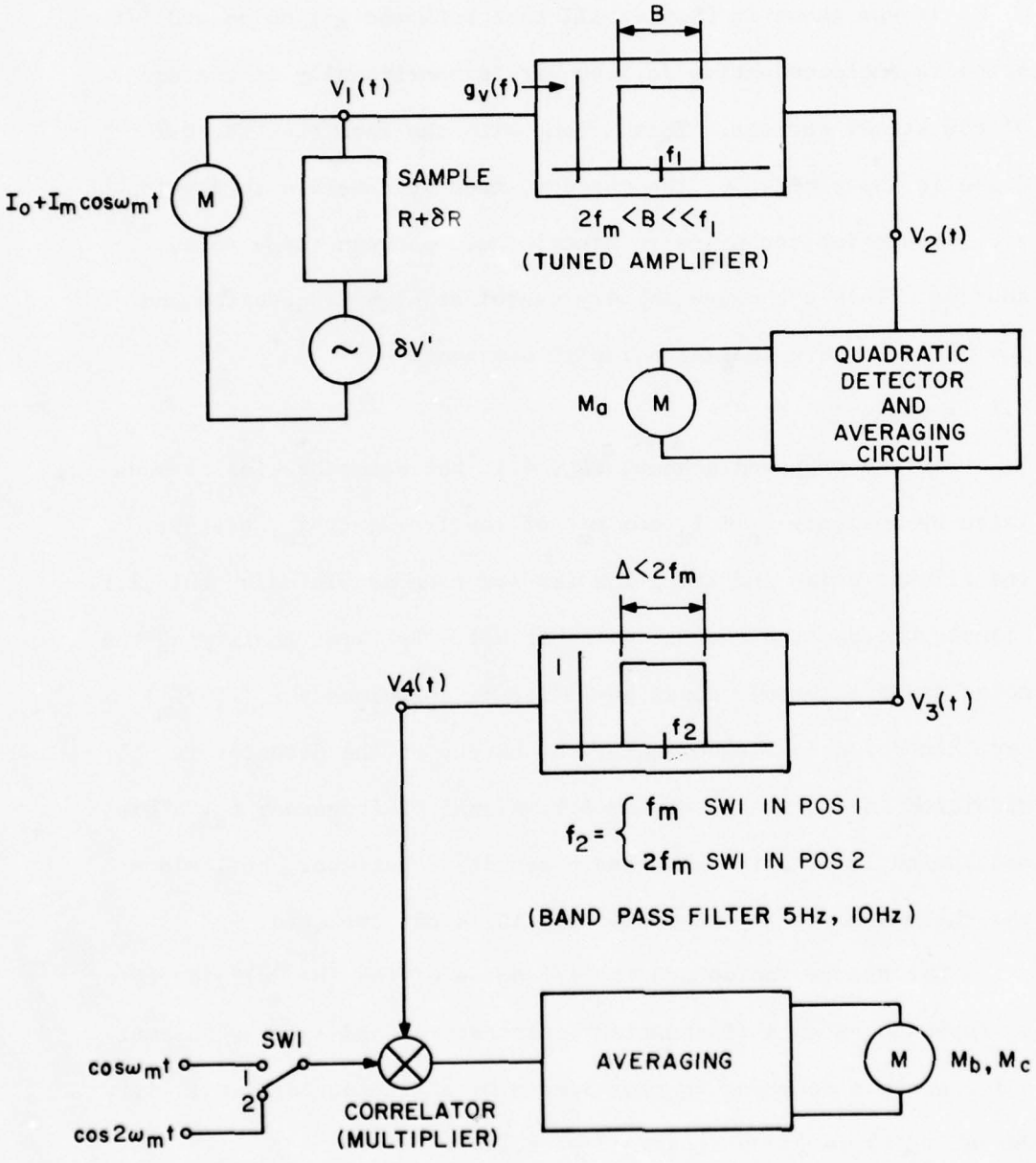

FIG 4.1

NOISE MEASUREMENT BY LOW FREQUENCY MODULATION SCHEME

$$v_1(t) = (I_o + I_m \cos\omega_m t)\ (R + \delta R) + \delta v' \qquad (4.1a)$$

If $g_v(f)$ is the voltage gain of the amplifier and B is its effective bandwidth, where $f_1 >> B > 2f_m$, then the noise $v_2(t)$ at the output of the amplifier is

$$v_2(t) = (I_o + I_m \cos\omega_m t)\ \delta R(f_1)\ g_v(f_1)$$

$$+ \delta v' g_v(f_1) \qquad (4.1b)$$

If the amplifier is sharply tuned at f_1, *i.e.* $B << f_1$, the output of the quadratic detector and averaging circuit $v_3(t)$ is then

$$v_3(t) \propto \overline{v_2^2(t)} = (I_o + I_m \cos\omega_m t)^2\ S_R(f_1)$$

$$\cdot\ B\,|g_v(f_1)|^2$$

$$+ S_{v'}(f_1) \cdot B\,|g_v(f_1)|^2 \qquad (4.1c)$$

where $S_R(f_1)$ = the spectral density of fluctuation δR at f_1 and

$S_{v'}(f_1)$ = the spectral density of the device thermal noise.

Using the identity $\cos^2\omega_m t = \frac{1}{2}[1 + \cos 2\omega_m t]$ we can rewrite (4.1c) as

$$v_3(t)\alpha[I_o^2\, S_R\,(f_1) + S_{v'}\,(f_1) + \tfrac{1}{2}\, I_m^2\, S_R(f_1)]|g_v(f_1)|^2.B$$

$$+ 2\, I_o I_m\, S_R(f_1)|g_v(f_1)|^2\, B\, \cos\omega_m t$$

$$+ \tfrac{1}{2}\, I_m^2\, S_R(f_1)|g_v(f_1)|^2\, B\, \cos 2\omega_m t$$

(4.1d)

We now have three methods of measurements,

a) Direct measurement, $I_m = 0$:

Eq.(4.1d) gives

$$M_a \alpha\, I_o^2\, S_R(f_1)|g_v(f_1)|^2\, B + S_{v'}(f_1)|g_v(f_1)|^2\, B$$

b) Measurement with phase-sensitive detector at frequency ω_m:

In this case the bandpass filter will be tuned at $f_2 = f_m = 5$Hz (Fig. 4.1) while SW1 will be in position 1, hence

$$v_4(t)\ \alpha\ 2\, I_o I_m\, S_R(f_1)|g_v(f_1)|^2\, B\, \cos\omega_m t$$

and the meter reading M_b is

$$M_b\ \alpha\ I_o I_m\, S_R(f_1)|g_v(f_1)|^2 B$$

c) Measurement with phase-sensitive detector at frequency $2\omega_m$: This case is similar to (b) except that the band pass filter is tuned at $f_2 = 2f_m = 10\text{Hz}$ and SW1 is in position 2, hence

$$V_4(t) \propto \frac{1}{2} I_m^2 S_R(f_1) \left|g_v(f_1)\right|^2 B \cos 2\omega_m t$$

and the meter reading M_c is

$$M_c \propto \frac{1}{4} I_m^2 S_R(f_1) \left|g_v(f_1)\right|^2 B$$

At high frequencies and low current, where thermal noise may be dominant, the measurements (b) and (c) eliminate thermal noise. This modulation scheme thus has distinct advantages.

The above discussion is still valid if a parameter other than the device current is modulated. A good example is modulation of the noise by means of a field plate. If we apply an a.c. bias voltage to the plate, the surface noise but not the other noise sources will be modulated. Here (b) and (c) measure only the modulation effect but eliminate all other effects.

We were intending to use this method to separate bulk flicker noise from surface flicker noise in (Hg,Cd)Te detectors using metal-insulator-semiconductor structures. But, as will be shown in Chapter VII, the 1/f noise in the tested devices was found to be independent of the field-plate voltage, so that the method will not work here.

4.2 Calibration of the system

A block diagram of the noise measurement setup using the low frequency modulation technique is shown in Fig. 4.2. The direct measurement and the measurement with phase sensitive detector at frequencies ω_m and $2\omega_m$ have involved three different system gains, therefore we needed a common calibration source. Here we employed an LED light source and a sinusoidal signal source.

If the LED emits radiant power $P_{lo} + P_1 \sin\omega_1 t$, it is shown in Appendix B that the spectral density $S_R'(f)$ of the resistance fluctuations of the detector due to the modulating light $P_1 \sin\omega_1 t$ is

$$S_R'(f) = \frac{1}{2} \frac{K^2 L^4}{(h\nu)^2 e^2} \frac{(u_n\tau_n + \mu_p\tau_p)^2}{(N_o\mu_n + P_o\mu_p)^4} \frac{P_1^2}{B} \qquad (4.2a)$$

where K is a light coupling constant between the source and the detector which includes reflection coefficient and quantum efficiency; N_o, P_o are the "dark" numbers of carriers and τ_n, τ_p are the lifetimes of the added carriers.

To demonstrate the feasibility of the method, we used detector #5663. The change ΔR_o in its d.c. resistance due to incident radiant power P_{lo} is in the order of 10^{-5} ohms, which may be safely neglected compared to its dark resistance R_o = 180 ohms. We also found a good linear relationship between $S_R'(f)$ and P_1 in Eq. (4.2a) in the interesting $S_R(f)$ range, from 10^{-10} ohm^2/Hz to 10^{-13} ohm^2/Hz.

This enabled us to calibrate the system by the LED light source without introducing a considerable error.

First I_m was set to zero, hence the output reading of the quadratic detector is

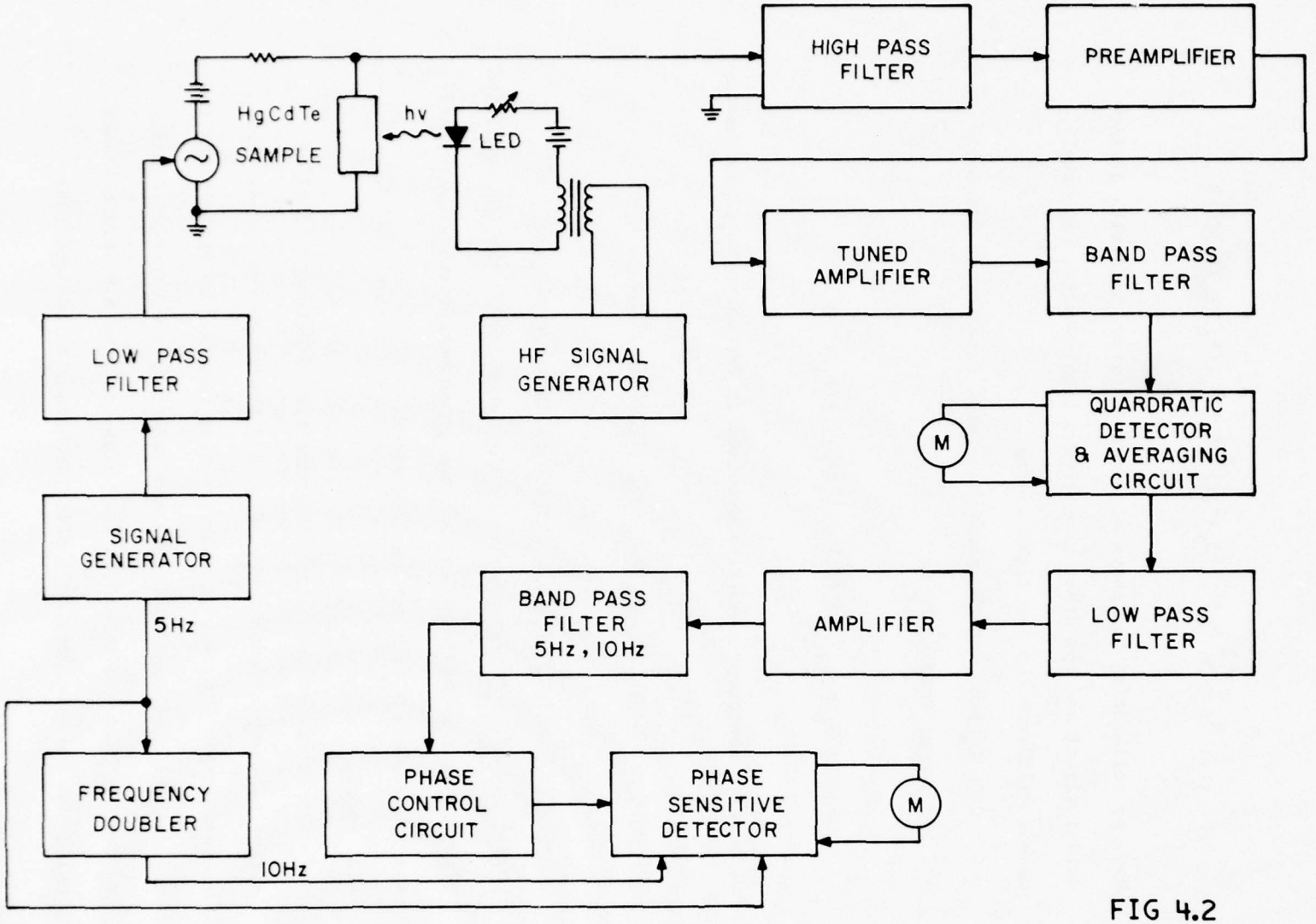

FIG 4.2

NOISE MEASUREMENT SET UP USING LOW FREQUENCY MODULATION TECHNIQUE

$$M_a \alpha I_o^2 S_R(f_1)|g_v(f_1)|^2 B + S_{v'}(f_1)|g_v(f_1)|^2 B$$

Now, by calibrating the above measurement twice, once with a sinusoidal signal and the other time with a light source, separately, we can calibrate the LED light source.

With $I_m \neq 0$, and the phase sensitive detector at frequency ω_m, the output reading M_b is

$$M_b \alpha I_o I_m [S_R(f_1) + S_R''(f_1)]|g(f_1)|^2 B$$

while with the phase sensitive detector at frequency $2\omega_m$, the reading is

$$M_c \alpha \frac{1}{2} I_m^2 [S_R(f_1) + S_R'''(f_1)]|g(f_1)|^2 B$$

where $S_R''(f_1)$ and $S_R'''(f_1)$ are the LED calibration signals. If $S_R''(f_1)$ and $S_R'''(f_1)$ are adjusted by the intensity of the LED modulated light in each measurement so that the phase sensitive detector reading is doubled, $S_R(f_1)$ can be determined.

4.3 Results

First we measured the noise spectrum of detector #5663 by direct measurement with I_m=0. Fig. 4.3 shows the results of these measurements. Fig. 4.4 is obtained from Fig. 4.3 by subtracting the thermal noise, then dividing by the square of the detector biasing current (I_o=1mA) to obtain $S_R(f)$. Figs. 4.5 and 4.6 were obtained using the low frequency modulation technique at 5Hz and 10Hz

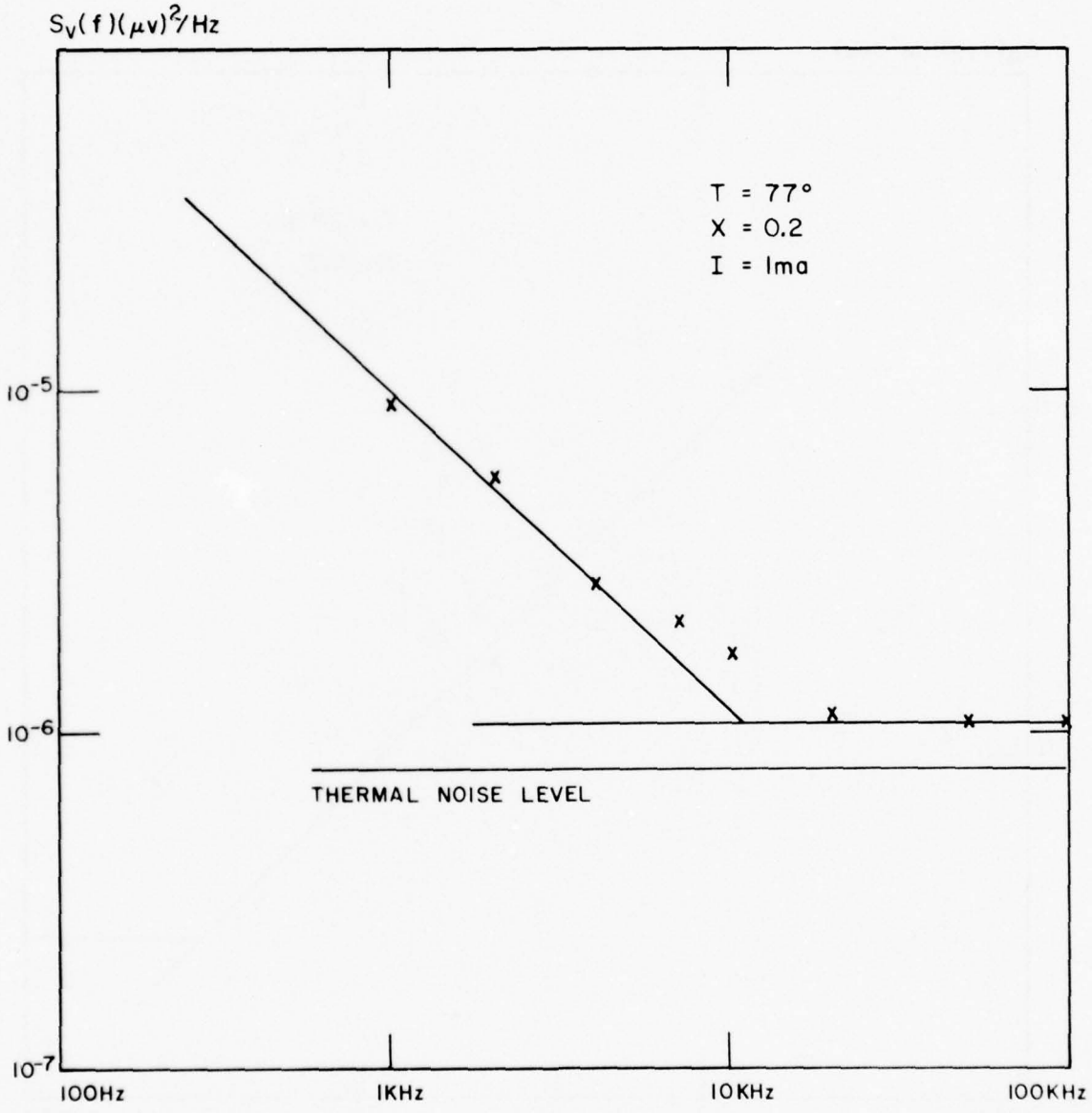

FIG 4.3
THERMAL +g-r+ FLICKER NOISE FOR DETECTOR 5663
DC TECHNIQUE

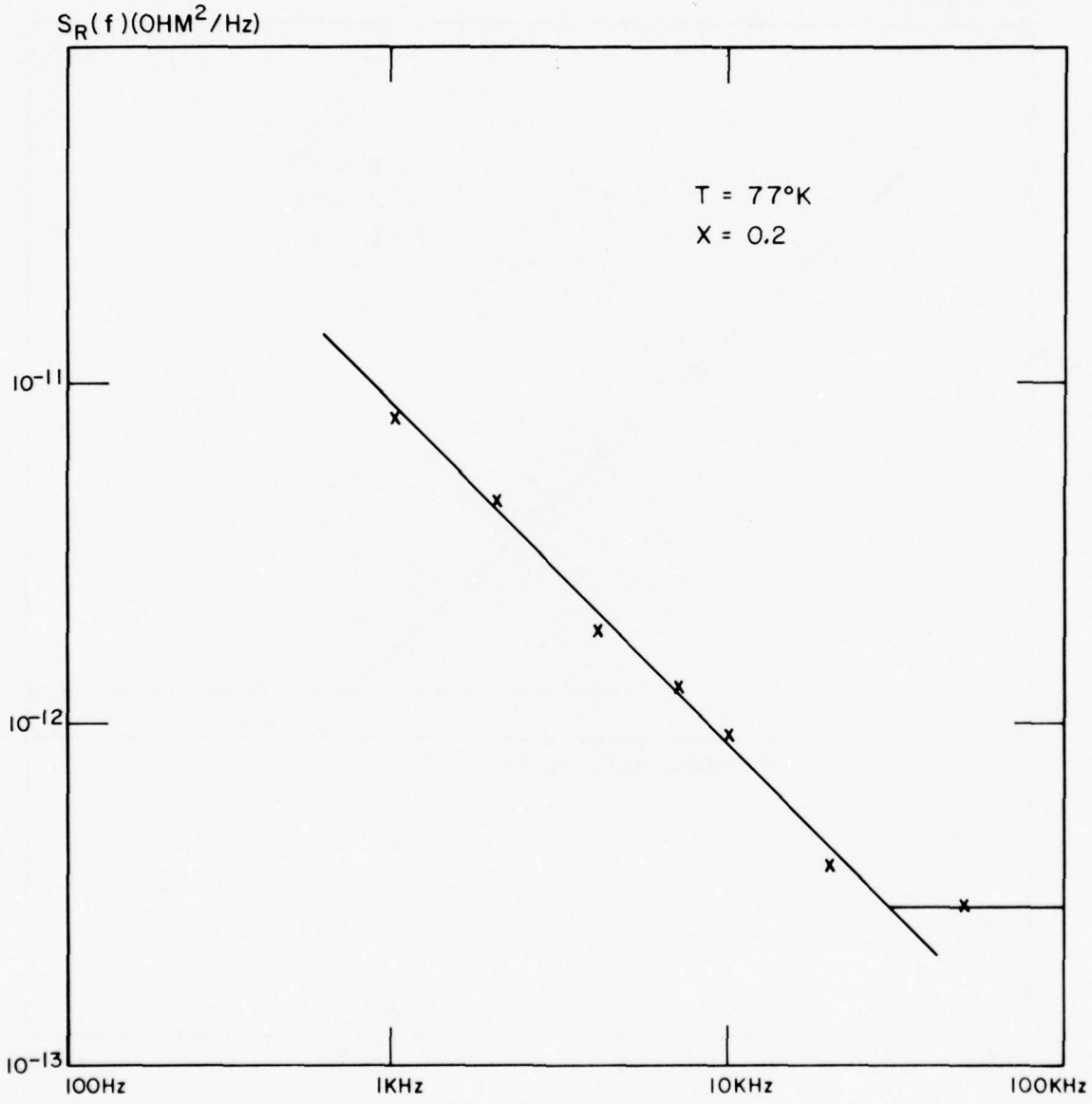

FIG 4.4
FLICKER+g-r NOISE FOR DETECTOR 5663.DC TECHNIQUE

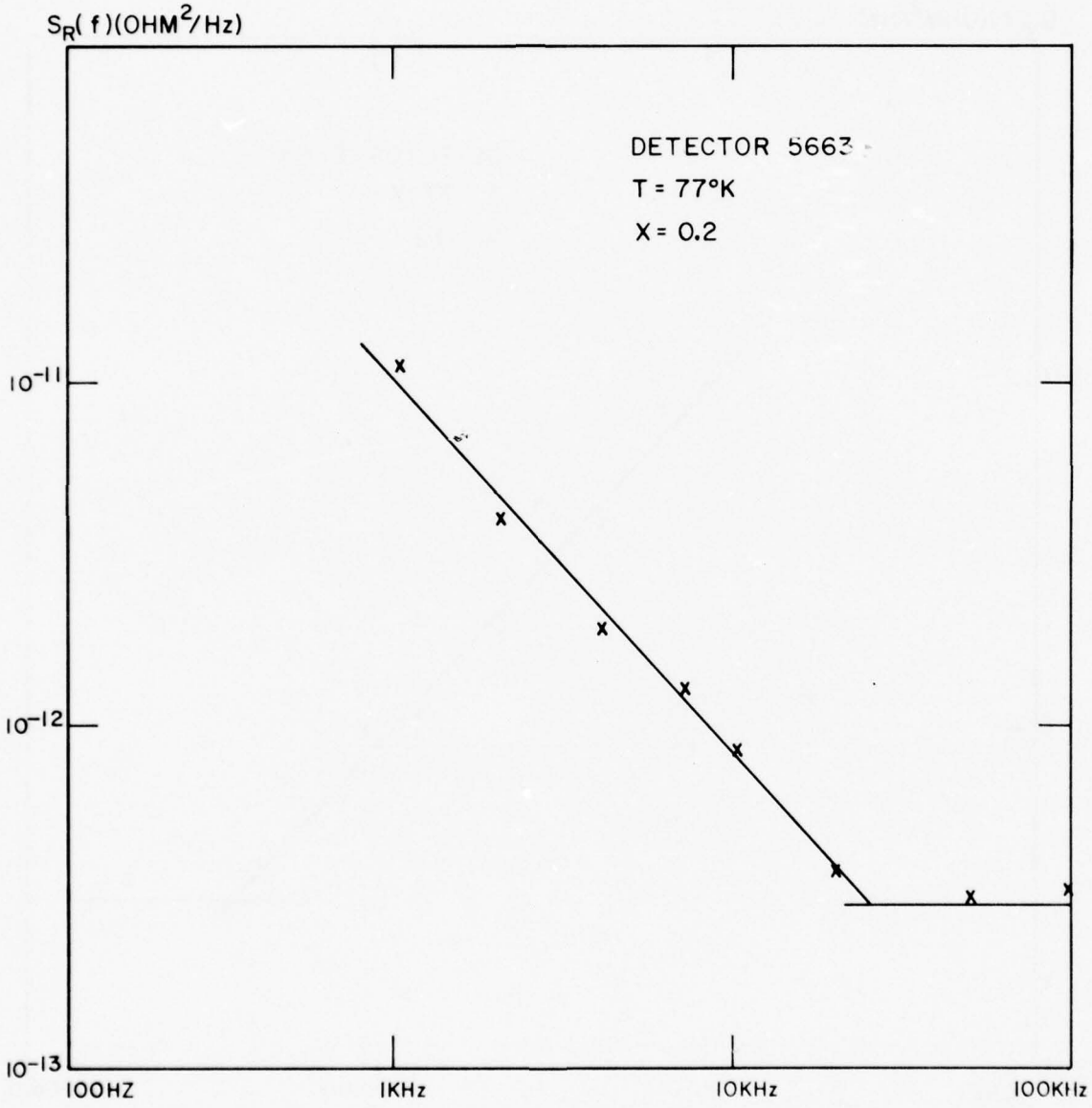

FIG 4.5
LOW FREQUENCY MODULATION TECHNIQUE ($f_2 = f_m = 5Hz$)

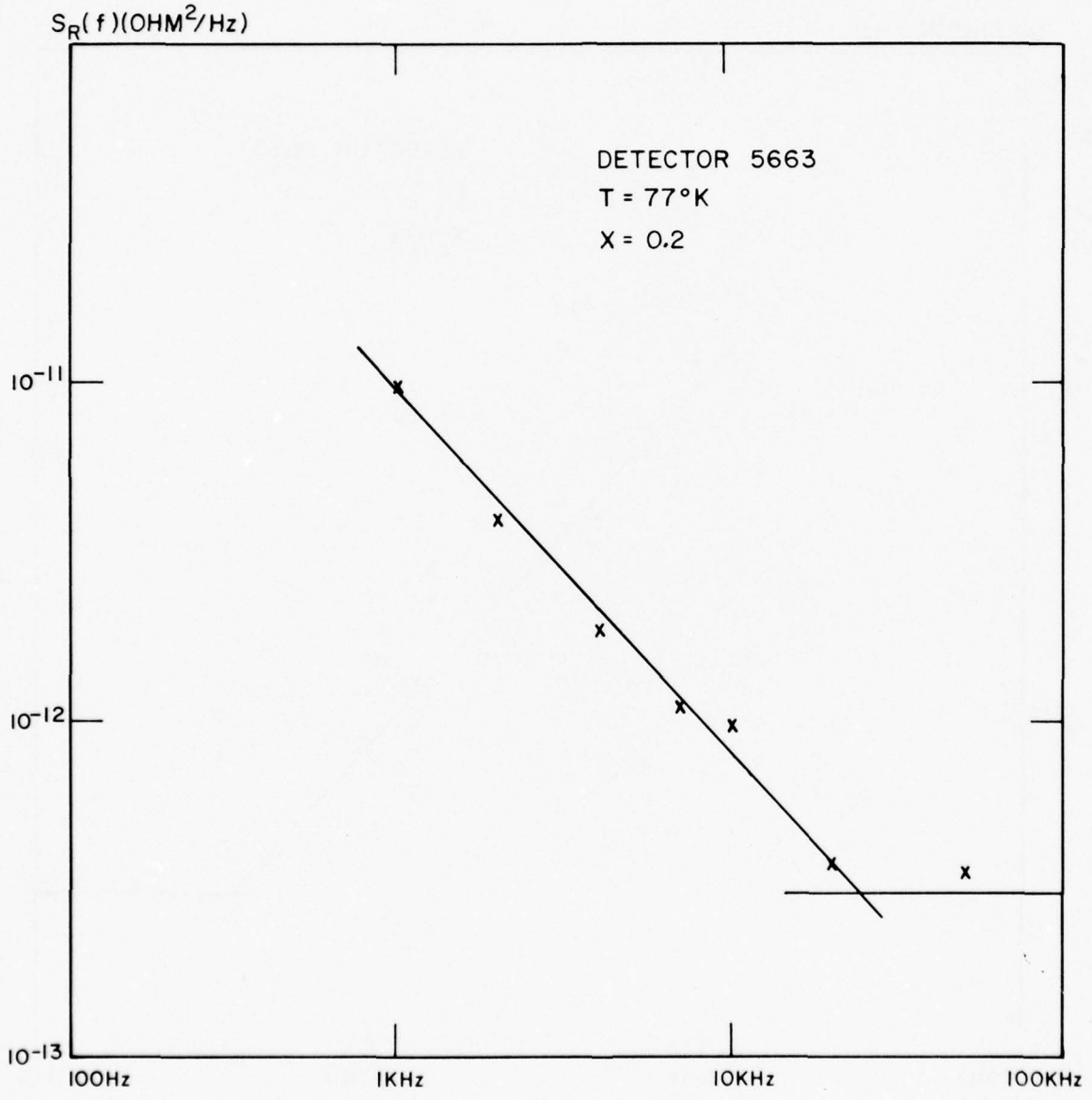

FIG 4.6

LOW FREQUENCY MODULATION TECHNIQUE ($f_2 = 2f_m = 10Hz$)

respectively. Since the noise modulated signal and the reference signal at the input of the phase sensitive detector should be in phase, the reference signal at $2f_m$=10Hz was obtained using a frequency doubler circuit instead of another signal generator as shown in Fig. 4.2. A comparison between Figs. 4.4, 4.5 and 4.6 indicates that each of the three methods gives reliable results, and that the discrimination between the noise sources should be feasible.

We conclude here that this low frequency modulation method has a big advantage to measure the high frequency noise without interference by thermal noise. In Figs. 4.5 and 4.6 the g-r noise, which is smaller than the thermal noise at frequencies above 20KHz, is measured with much smaller error than that in the direct measurement.

CHAPTER V. CONTACT EFFECTS ON 1/f NOISE IN (Hg,Cd)Te

The purpose of this chapter is to study the effect of excess noise (poor) non-current carrying and current carrying contacts on 1/f noise in (Hg,Cd)Te detectors.

5.1 Device Fabrication

The detectors used for this study (Fig. 2.1b) were prepared by the procedures described in Sec. 2.1. They were fabricated from n-type (ρ=0.05Ωcm,n≈1.1x10^{16}cm^{-3}) (Hg,Cd)Te crystal #91174-P5 with x≈0.39. The poor contacts were made using method (iii) indicated in Step #8 of the same section.

5.2 Resistance and Noise of Contacts

In devices having four or more contacts, some of the contact resistances and their noise contributions may be determined by d.c. measurements and noise measurements respectively. This will be illustrated using a four contact detector shown in Fig. 5.1a. Fig. 5.1b shows the equivalent noise circuit of the detector indicating the bulk and contact resistances, and the equivalent noise sources.

5.2.1 D.C. Measurements

If a steady current $I_{1,4}$ is passed between contacts #1 and #4 and, using a VTVM, the voltage drop between contacts 1-2, 2-3 and 3-4 are measured, we get

$$\frac{V_{1,2}}{I_{1,4}} = r_{c_1} + r_1 \qquad (5.2.1a)$$

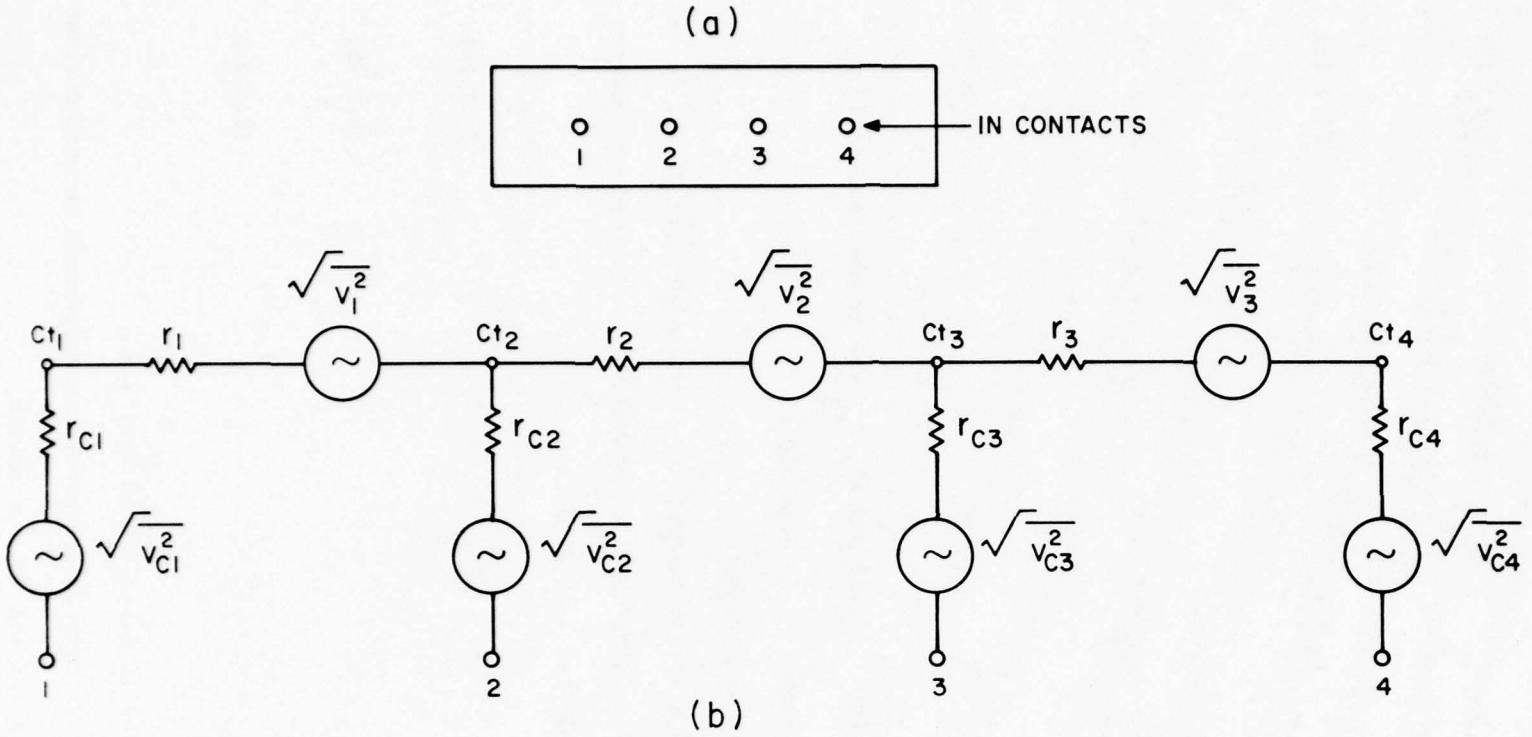

FIG 5.1

(a) FOUR CONTACT (Hg,Cd)Te DETECTOR

(b) NOISE EQUIVALENT CIRCUIT OF (a)

$$\frac{V_{2,3}}{I_{1,4}} = r_2 \tag{5.2.1b}$$

$$\frac{V_{3,4}}{I_{1,4}} = r_3 + r_{c_4} \tag{5.2.1c}$$

Similarly

$$\frac{V_{1,2}}{I_{1,2}} = r_{c_1} + r_1 + r_{c_2} \tag{5.2.1d}$$

and

$$\frac{V_{3,4}}{I_{3,4}} = r_{c_3} + r_3 + r_{c_4} \tag{5.2.1e}$$

Now, from Eqs. (5.2.1a and d), r_{c_2} can be obtained while r_{c_3} can be obtained from Eqs. (5.2.1c and e).

5.2.2 Noise Measurements

If we pass a steady current $I_{1,4}$ betwen contacts #1 and #4 and noise measurements using the d.c. technique are carried out between contacts 1-2, 2-3 and 3-4, we obtain

$$\overline{v^2_{1,2}} = \overline{v^2_{c_1}} + \overline{v^2_1} \tag{5.2.2a}$$

$$\overline{v^2_{2,3}} = \overline{v^2_2} \tag{5.2.2b}$$

$$\overline{v^2_{3,4}} = \overline{v^2_3} + \overline{v^2_{c_4}} \tag{5.2.2c}$$

Eq. (5.2.2b) is justified in Sec. 5.3.

Similarly, if noise measurements are performed between current-carrying contacts 1-2 and 3-4, we obtain

$$I_{1,2} : \overline{v_{1,2}^2} = \overline{v_{c_1}^2} + \overline{v_1^2} + \overline{v_{c_2}^2} \qquad (5.2.2d)$$

$$I_{3,4} : \overline{v_{3,4}^2} = \overline{v_{c_3}^2} + \overline{v_3^2} + \overline{v_{c_4}^2} \qquad (5.2.2e)$$

from Eqs. (5.2.2a and d) and (5.2.2c and e) we obtain $\overline{v_{c_2}^2}$ and $\overline{v_{c_3}^2}$ respectively.

Hence, in detectors with four contacts, it is possible to separate the "inner contact" resistances, r_{c_2} and r_{c_3} and noise contributions, $\overline{v_{c_2}^2}$ and $\overline{v_{c_3}^2}$, by the procedures mentioned above. In fact, for detectors with more than four contacts, resistances and noise contributions of all contacts except the end ones can be separated by following similar procedures.

5.3 Experiments and Results

5.3.1 Non-Current Carrying Bad Contacts

The purpose of this experiment is to determine the effect of "poor" noise measuring contacts on the detector 1/f noise. The detector (#9747-P5) fabricated for this purpose is shown in Fig. 2.1. It had seven contacts; all but contact #4 were good contacts. The contact resistances were determined by d.c. measurements (Sec. 5.2.1) and were found to be

$$r_{c_2}, r_{c_3}, r_{c_5}, r_{c_6} < 2 \text{ ohms}$$

$$r_{c_4} > 15 \text{ ohms}$$

Contact #4 was shown to be of poor property from d.c. measurements; later noise measurents indicated an excess noise from this contact. We have found this result to be true with several other contacts, a high resistance contact always contributes an excess amount of noise; in fact, these contacts were the cause of some non-linear behavior in the d.c. characteristics of the device as will be shown in the next section. From noise measurements at 40Hz (bandwidth = 6.184Hz) and at 5mA, we get

$$\overline{v_{c_2}^2}\ ,\ \overline{v_{c_3}^2}\ ,\ \overline{v_{c_5}^2}\ ,\ \overline{v_{c_6}^2} < 3.6\times10^{-6} \quad (\mu V)^2$$

$$\overline{v_{c_4}^2} \approx 3\times10^{-4} \quad (\mu V)^2$$

which indicates that contact #4 contributes noise two orders of magnitude higher than any of the other contacts.

To determine the effect of this contact on the low frequency noise of the device, the device was d.c. biased between contacts 2-6 and the noise measurements using d.c. technique were performed between contacts 3-4, 4-5 then 3-5. The results are shown in Fig. 5.2 (here and in the following, the notation $I_{a,b}$ used in the figures is understood to imply a bias polarity such that the current flows from a to b. In the case under consideration, therefore, the bias is indicated as $I_{2,6}$). By adding the two noise spectra $S_{v_{3,4}}(f)$ and $S_{v_{4,5}}(f)$ we obtained the circles shown in the same figure which corresponded very well to the measured values of $S_{v_{3,5}}(f)$. This indeed shows that a "poor" non-current carrying noise measuring

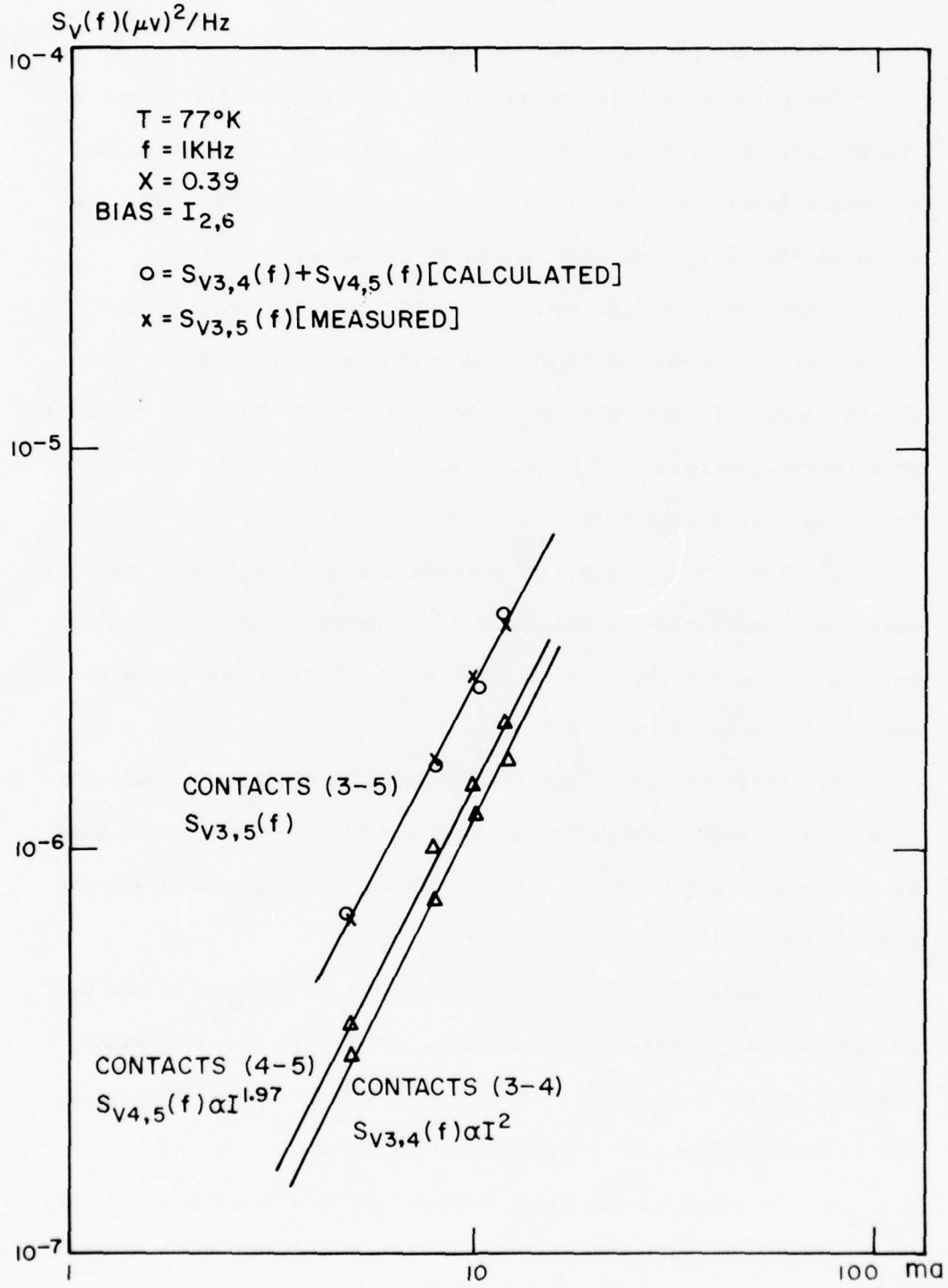

FIG 5.2
I/F NOISE VERSUS DC CURRENT FOR DETECTOR 9747-P5

contact does not affect the device 1/f noise.

5.3.2 Current Carrying Bad Contacts

The purpose of this experiment is to determine the effect of "poor" current carrying contacts on the detector 1/f noise. The detectors fabricated for this purpose (#9748-P5 and #9746-P5) are shown in Fig. 2.1; and each has seven contacts.

First, we tested detector #9748-P5. All its contacts but contact #2 were found to be of good performance and did not show excess noise. To determine the effect of contact #2 (poor contact) when carrying current on the low frequency noise of the device, the following experiments were carried out:

1. The device was biased between two good contacts (3 and 6) while noise measurements using the d.c. technique were performed between contacts 4 and 5. A plot of $S_{V_{4,5}}$ (1KHz) versus I was obtained and is indicated by curve A in Fig. 5.3.

2. While keeping the noise measuring contacts the same, the device was biased between contacts #2 and #6. Contact #2 was used as the anode. A plot of $S_{V_{4,5}}$ (1KHz) versus I was obtained and was similar to that obtained in experiment 1.

3. Experiment 2 was repeated except that contact #2 was used as the cathode in this case. Again, 4 and 5 were the measuring contacts. Fig. 5.3, curve B shows the results of this experiment. The results indicate a large increase in noise.

4. We measured the noise between contacts 4 and 5 while they were carrying current. There was no difference with curve A, Fig.5.3, as expected, since contacts 4 and 5 were good contacts.

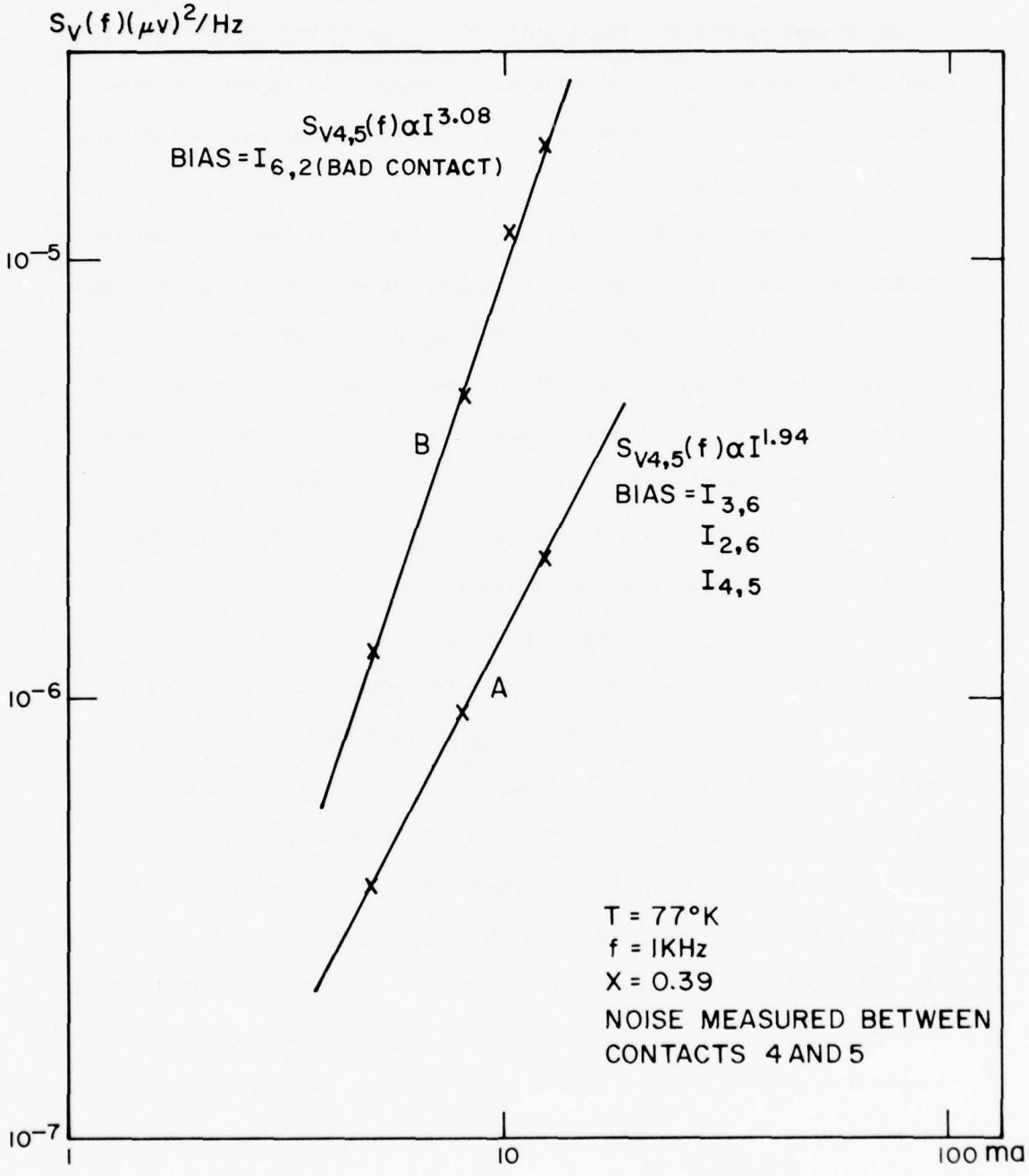

FIG 5.3
I/F NOISE VERSUS DC CURRENT FOR DETECTOR 9748-P5

Finally, the device d.c. characteristics between contacts 2 and 6 were measured; the results are shown in Fig. 5.4. As would be expected from the noise measurements, the characteristics show a dependence on the polarity of the biasing current as indicated by the asymmetry of the curve.

Detector #9746-P5 was tested next. D.C. and noise measurements indicated that all its contacts were good except for contact #6 which showed "very" high resistance and 1/f noise. The effect of the current carrying bad contact (#6) on the device 1/f noise, measured between contacts #3-4, was determined in the same manner as in the case of detector #9748-P5, and the results are shown in Fig. 5.5. Fig. 5.6 shows the d.c. characteristics of detector #9746-P5 which were measured between contacts 2 and 6.

Discussion of Results

As would be expected from the non-linearity and asymmetry of the d.c. characteristics of detectors #9748-P5 and 9746-P5, the polarity of the biasing current will have an effect on the noise. This indeed was found to be true. In the first case, detector #9748-P5, the non-linearity was found only when using contact #2 as the cathode (we were dealing with n-typematerial). This manifested itself in that the noise when measured between the non-current carrying contacts 4-5 was larger when using "bad" contact #2 as the cathode (curve B, Fig. 5.3) than when using the same contact as the anode (curve A, Fig. 5.3). We notice also that $S_{V_{4,5}}(f)$ varies faster than I^2 ($\sim I^3$) in the former case, (curve B, Fig. 5.3). In the second case, detector #9746-P5, the non-linearity was found when using contact #6 either as an anode or as a cathode, indicating

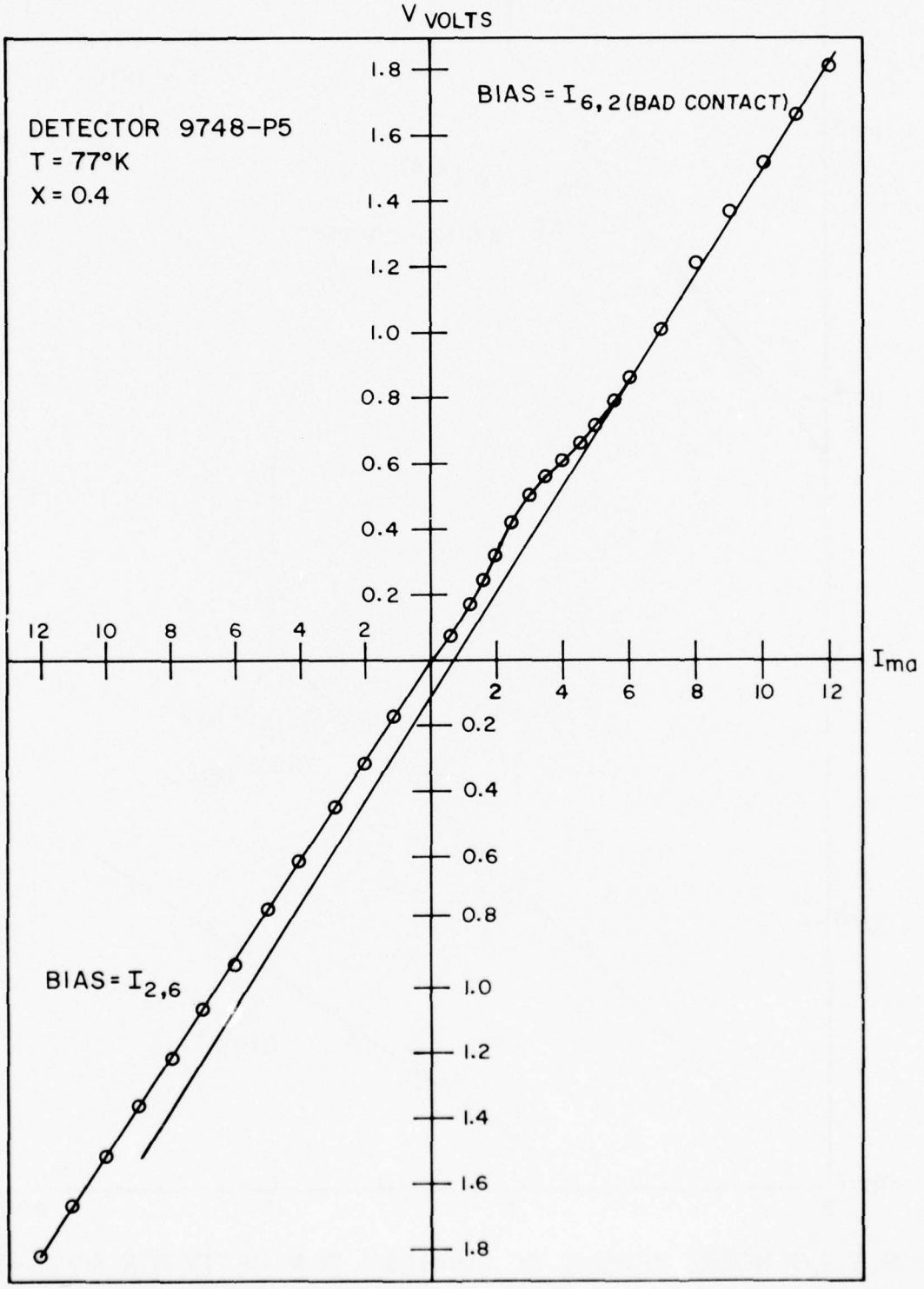

FIG 5.4 DC CHARACTERISTICS OF DETECTOR 9748-P5

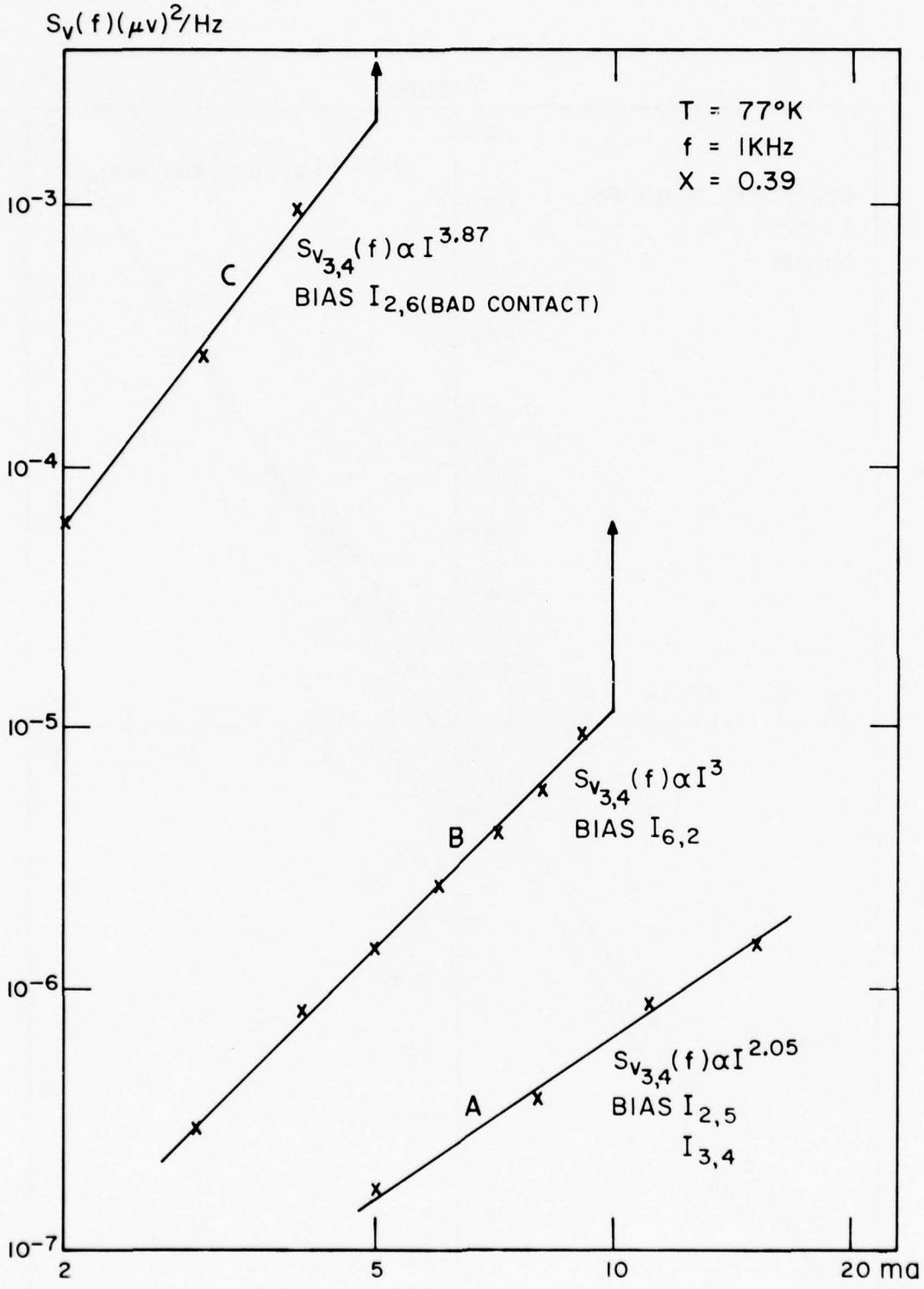

FIG 5.5 I/F NOISE VERSUS DC CURRENT FOR DETECTOR 9746-P5

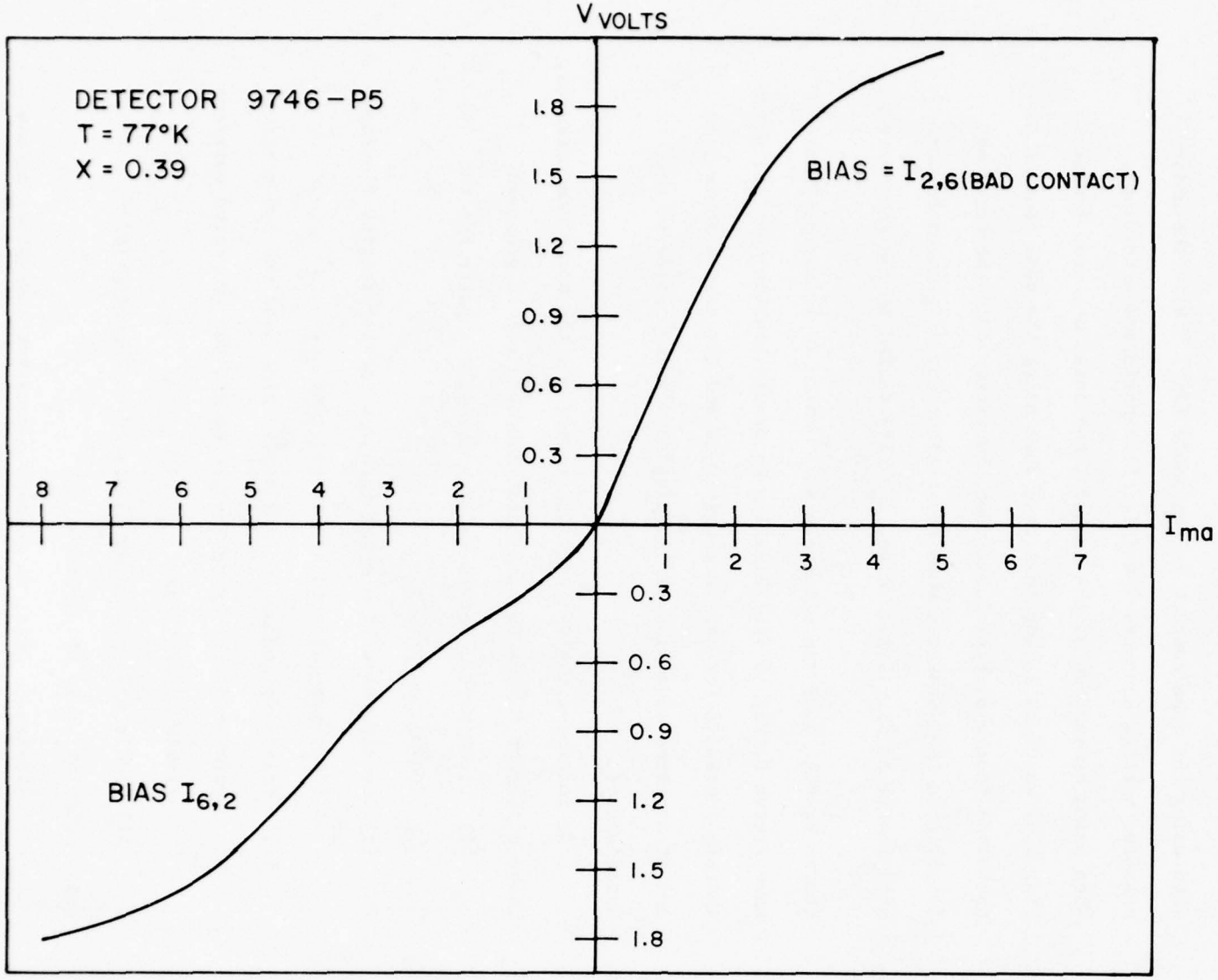

FIG 5.6 DC CHARACTERISTICS OF DETECTOR 9746-P5

a "very" poor contact. The d.c. characteristics were asymmetrical with much steeper characteristics when using contact #6 as the cathode (we are dealing with n-type material) than that obtained when using the same contact as the anode (Fig. 5.6). The noise measured between contacts 3-4 (Fig. 5.5) performed accordingly. When using contact #6 as the cathode, the noise measured (curve C, Fig. 5.5) was much larger than that when using the same contact as the anode (curve B, Fig. 5.5). But, in either case the noise was larger than that measured when the current carrying contacts were good (curve A, Fig. 5.5). Also, $S_{V_{3,4}}(f)$ varied in the former case, (curve C, Fig. 5.5) approximately as I^4 while as I^3 in the latter case (curve B, Fig. 5.5). Finally, we should mention that the noise sharply increased for case B above 10 ma and for case C above 5 ma and it appeared as a kind of "popping" or "spiky" noise on the oscilloscope.

To interpret the V-I characteristics and the noise measurements, three different models for the "bad" contacts may be proposed.

i) Diode model, formed between the silver paste and the indium contact.

ii) Carrier injection model in which carrier density fluctuations are injected by the bad contact.

iii) Collision ionization and avalanching, near the bad contact, between deeper lying impurities and the generated carriers flowing downstream.

All models will give a non-linear d.c. characteristic, but the noise behavior would be different.

To illustrate this, we connect a constant current I_o across

the sample. Then

$$I_o = e\mu nEA \quad \text{and} \quad V = -\int_a^b Edx$$

where n is the carrier density in the sample, E the field strength, V the voltage between contacts a and b, and A the cross-sectional area of the sample. Hence,

$$\Delta I = e\mu(n_o \Delta E + E_o \Delta n)A = 0$$

and

$$\Delta E = -\frac{E_o}{n_o} \Delta n$$

so

$$\Delta V = -\int_a^b \Delta E dx = \int_a^b \frac{E_o}{n_o} \Delta n \, dx$$

Here Δn and ΔE are flucuations around the equilibrium values n_o and E_o respectively.

Therefore, excess noise will only be observed if there are excess fluctuations Δn, over and above the "normal" flicker noise fluctuations, between contacts a and b. This indicates some kind of carrier injection into the region between the contacts a and b. This injection must come from the bad contact. As long as only <u>one</u> type of carriers contributes, the noise would be generated for one direction of current flow only.

Since some kind of injection must be postulated in order to explain the noise, the simple diode model (i) is excluded, only an "injecting" diode model would be allowed. Models (ii) and (iii) inject carriers naturally. We could have further discriminated

between the models by cooling the device to a sufficiently low temperature so that the diode operation or the injection operation would be tempered by the low temperatures, whereas collisions ionization might be enhanced because of longer free path length. We did not pursue this course, since the contact problem was only a secondary issue in this research.

In the very bad contact excess noise over and above normal flicker noise was generated in both directions of current flow, although there was a difference of a few orders of magnitude in the noise for the two directions. This could be explained by assuming that the bad contact injects electrons when the bad contact is the cathode and holes when the bad contact is the anode. The asymmetry in the noise generation could then be caused by the asymmetry in carrier injection.

The final conclusion of this work is that in order to do meaningful measurements, "bad" contacts should be avoided at all cost. Having extra contacts does not really improve the situation because of the carrier injection effect, and because "good" contacts do not generate excess noise even when carrying current.

CHAPTER VI. GRAIN BOUNDARY EFFECTS ON 1/f NOISE IN (Hg,Cd)Te

In this chapter the effect of grain boundaries on low frequency noise in (Hg,Cd)Te is shown. The correlation between the noises in the case of grain boundary and no grain boundary is also indicated.

6.1 Device Fabrication

Three devices were fabricated for this study from n-type (ρ= 0.05 Ωcm, $n_o \simeq 1.1 \times 10^{16} cm^{-3}$ at 77°K) $Hg_{0.61}Cd_{0.39}Te$ crystal # 91174-P5 which contained a grain boundary. Their final dimensions are shown in Fig. 6.1. The devices were prepared using the same procedures described in Section 2.1. In each device two contacts were made across the grain boundary of the crystal. This was done by photographing the crystal before preparation so that the grain boundary would appear in the photograph. After etching the top side of the slice (step 5, Sec. 2.1), another photograph was taken, and the grain boundary was mapped on it using the first photograph.

6.2 Noise Measurements

Detector # 9743-P5 was tested first. Low frequency noise measurements were carried out using the d.c. technique between the non-current carrying contacts #2 and #3 (no grain boundary) and non-current carrying contacts #3 and #4 (across grain boundary). Fig. 6.2 shows the noise spectra between the non-current carrying contacts #2 and 3 (no grain boundary) while the noise spectra between the non-current carrying contacts #3 and 4 (grain boundary) are shown in Fig. 6.3. In both cases $1/f^{\alpha}$ noise was observed at low frequencies

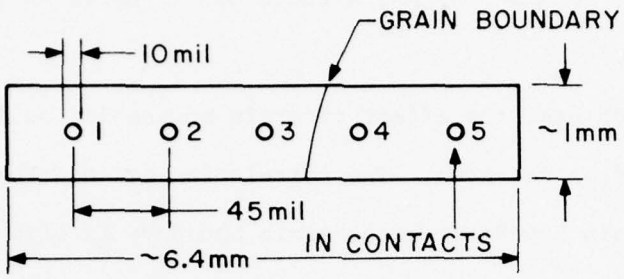

DETECTOR 9743–P5 (THICKNESS ≅ 31μ)

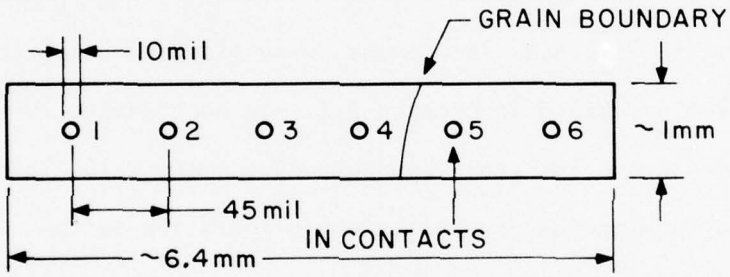

DETECTOR 9745–P5 (THICKNESS ≅ 23μ)

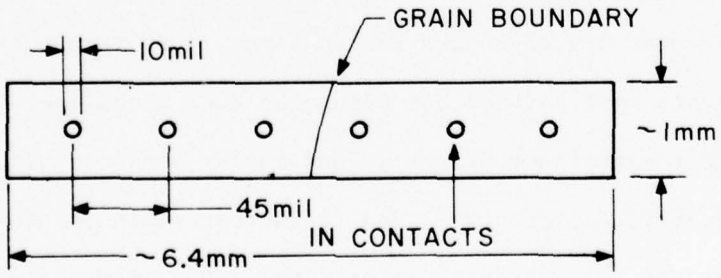

DETECTOR 9742–P5 (THICKNESS ≅ 27μ)

FIG 6.1

FINAL DIMENSIONS OF DETECTORS USED IN GRAIN BOUNDARY STUDIES

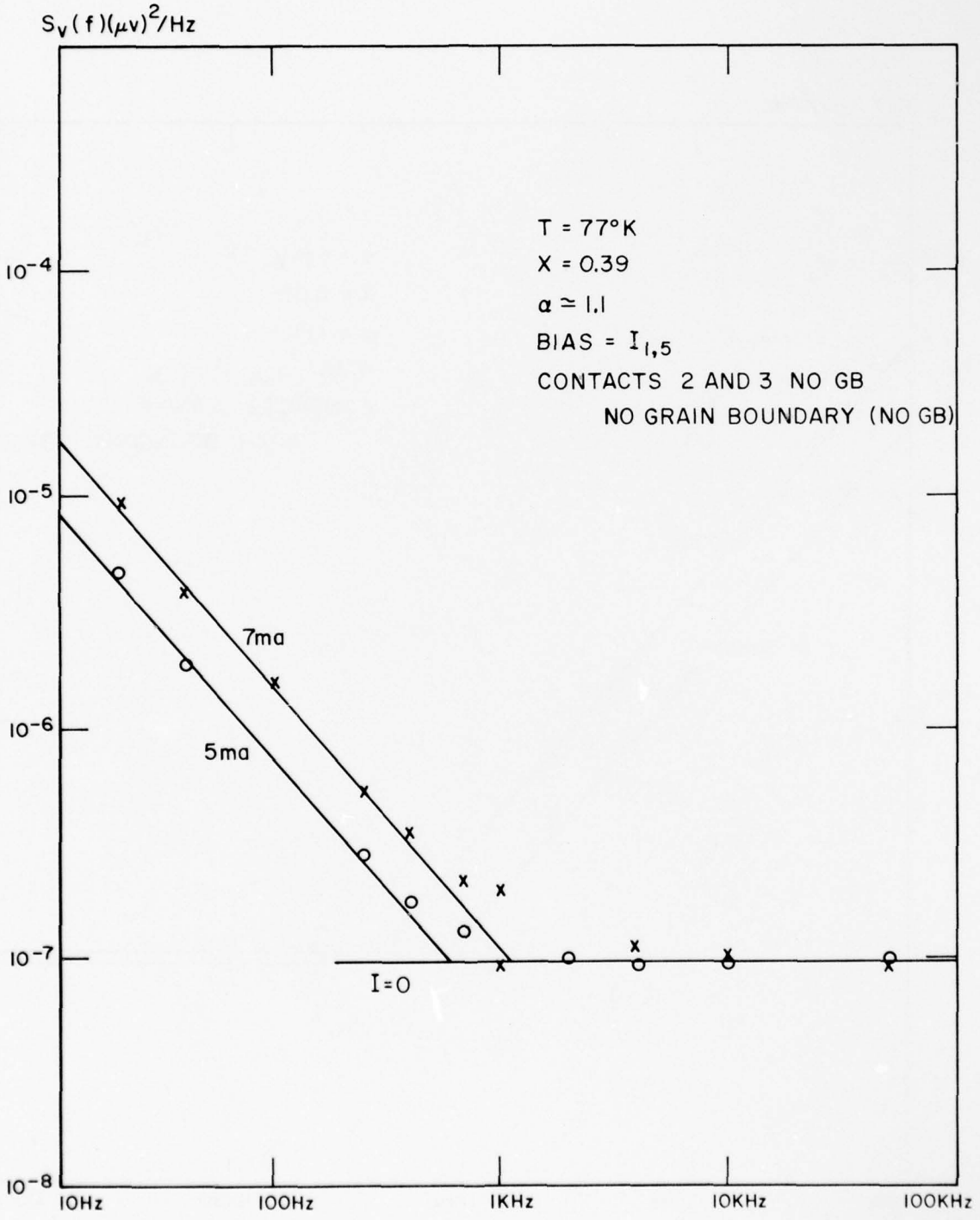

FIG 6.2 LOW FREQUENCY NOISE SPECTRA FOR DETECTOR 9743-P5

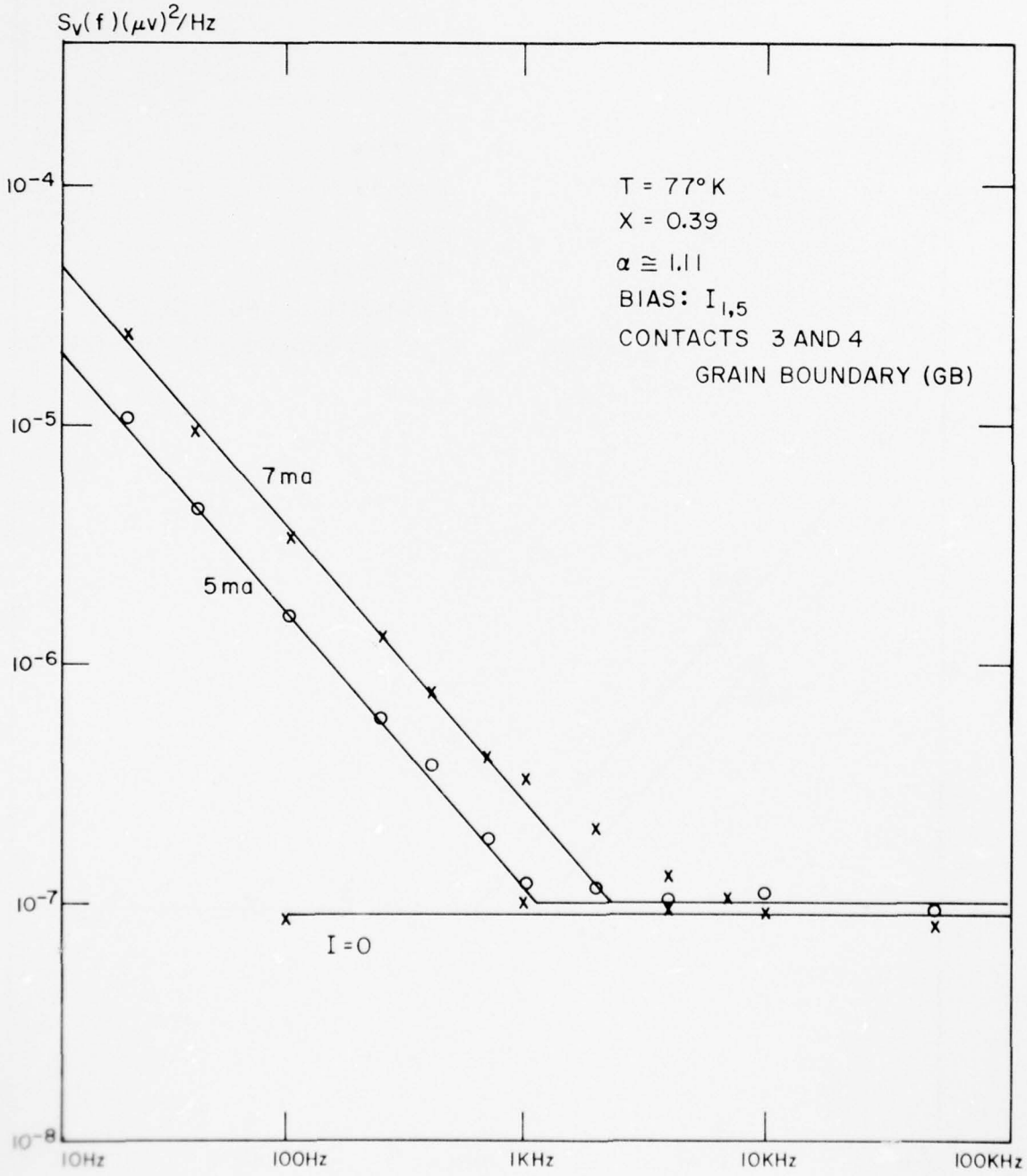

FIG 6.3 LOW FREQUENCY NOISE SPECTRA FOR DETECTOR 9743-P5

where α differed slightly for the two cases. Fig. 6.4 shows flicker noise power spectra versus d.c. current for the grain boundary and no-grain boundary cases. For both cases, the noise increased as the square of the d.c. current in the characteristic way for 1/f noise. For this sample, the low frequency noise in the grain boundary case (contacts 3-4) was about two times larger than the corresponding noise at no-grain boundary (contacts 2-3) as shown in Fig. 6.4.

Detectors # 9742-P5 and 9745-P5 were tested next in the same manner as the first detector. Figs. 6.5 to 6.10 show the results of these experiments. In detector # 9742-P5, the low frequency noise varied slightly between the grain boundary and no-grain boundary cases, while the noise for the grain boundary case for detector # 9745-P5 was about 4.5 times larger than the corresponding noise at no-grain boundary for the same detector.

6.3 Correlation Between Grain Boundary and No-Grain Boundary Noises

In order to find out the correlation between the low frequency noise in the grain boundary case and no-grain boundary case, low frequency noise measurement between the non-current carrying contacts #3 and 5, detector # 9745-P5, were carried out for the biasing current of 8 mA. The results are shown in Fig. 6.11. By adding the two noise spectra at this current (8 mA) obtained from Fig. 6.8 (contacts #3 - 4, no-grain boundary) and Fig. 6.9 (contacts # 4 - 5, grain boundary) we obtained the circles shown in Fig. 6.11. This indeed shows that the two noises are uncorrelated, since

$$S_{V_{3,5}}(f) = S_{V_{3,4}}(f) + S_{V_{4,5}}(f)$$

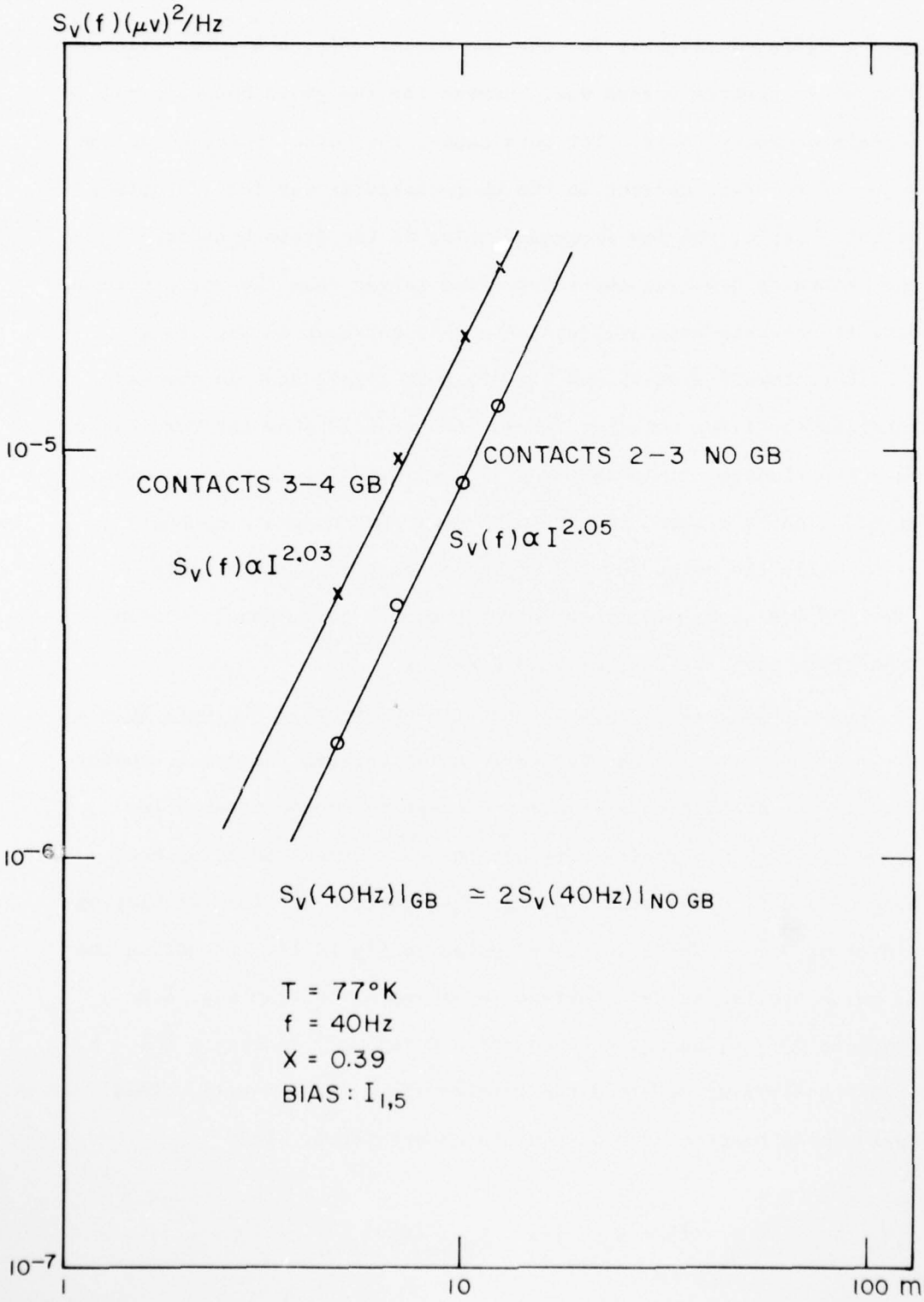

FIG 6.4 I/F NOISE VERSUS DC CURRENT FOR DETECTOR 9743-P5

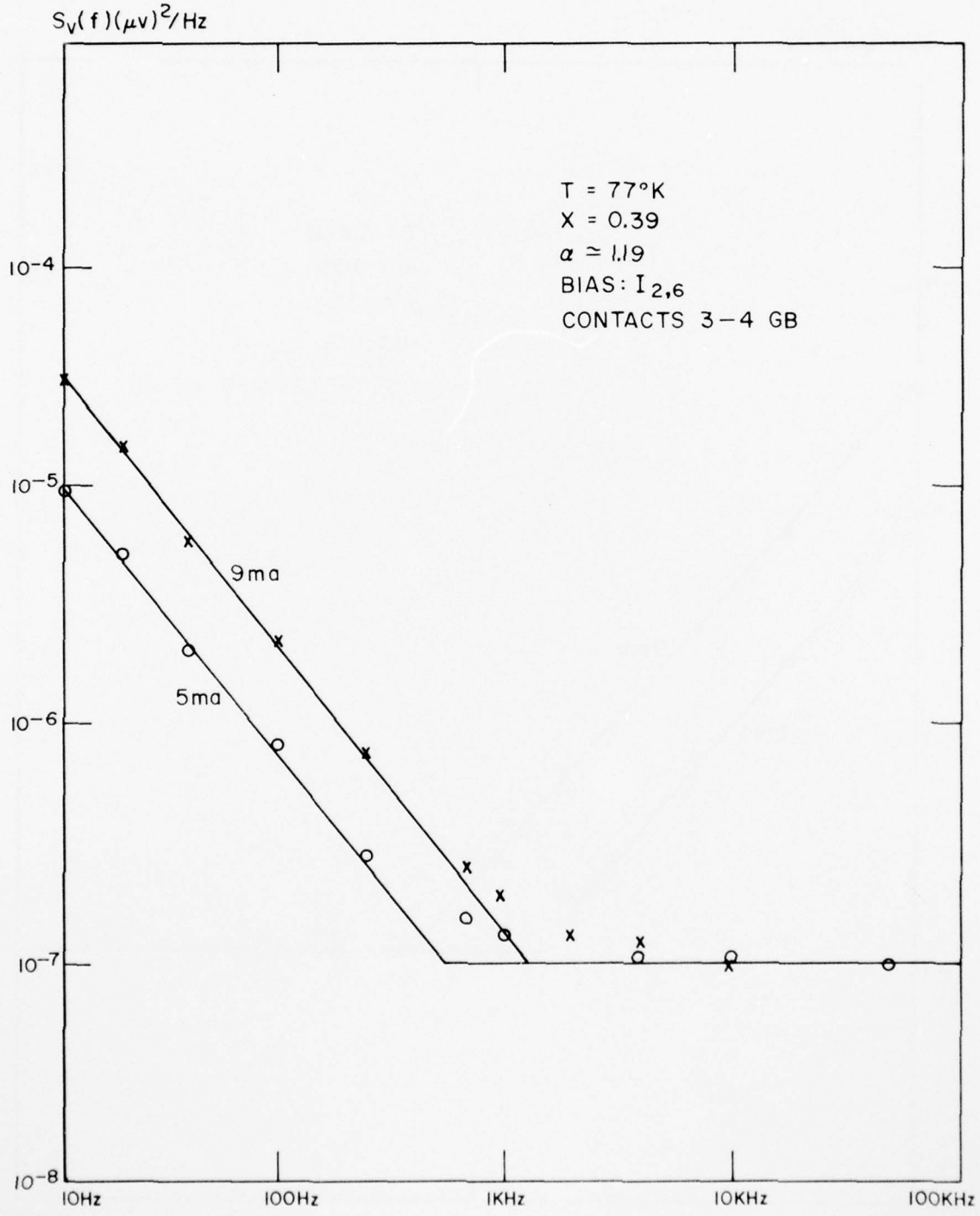

FIG 6.5 LOW FREQUENCY NOISE SPECTRA FOR DETECTOR 9742-P5

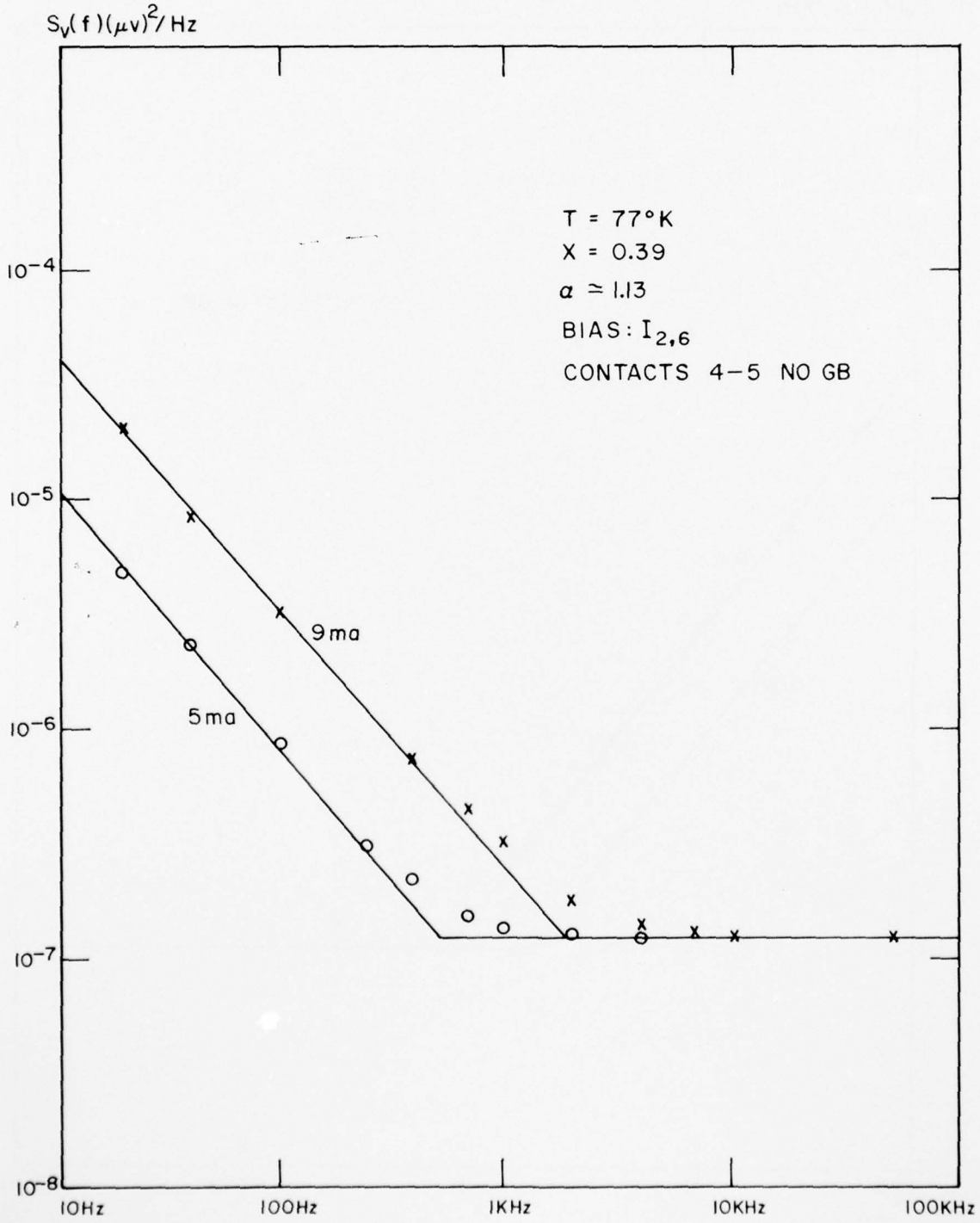

FIG 6.6 LOW FREQUENCY NOISE SPECTRA FOR DETECTOR 9742-P5

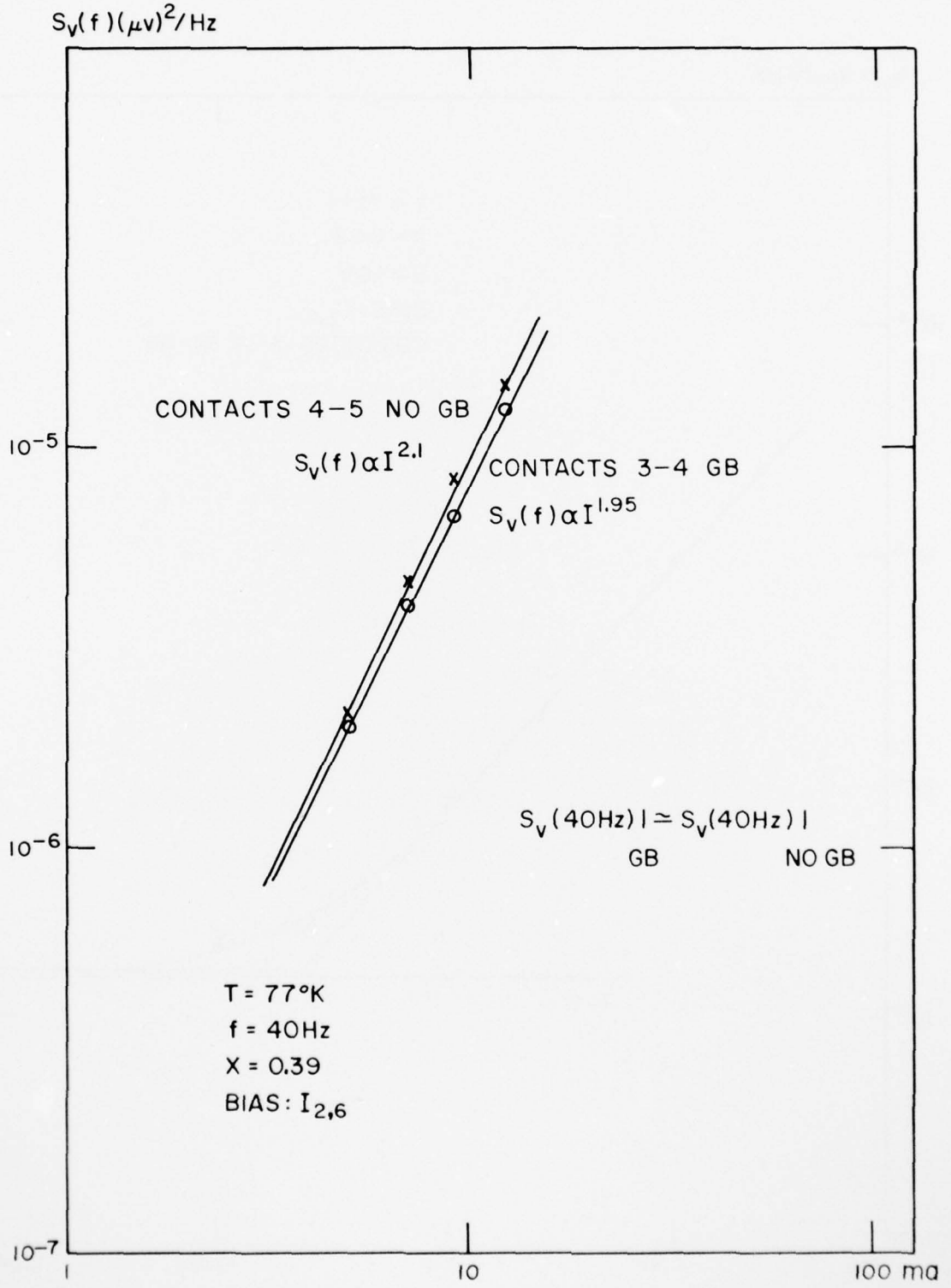

FIG 6.7 I/F NOISE VERSUS DC CURRENT FOR DETECTOR 9742-P5

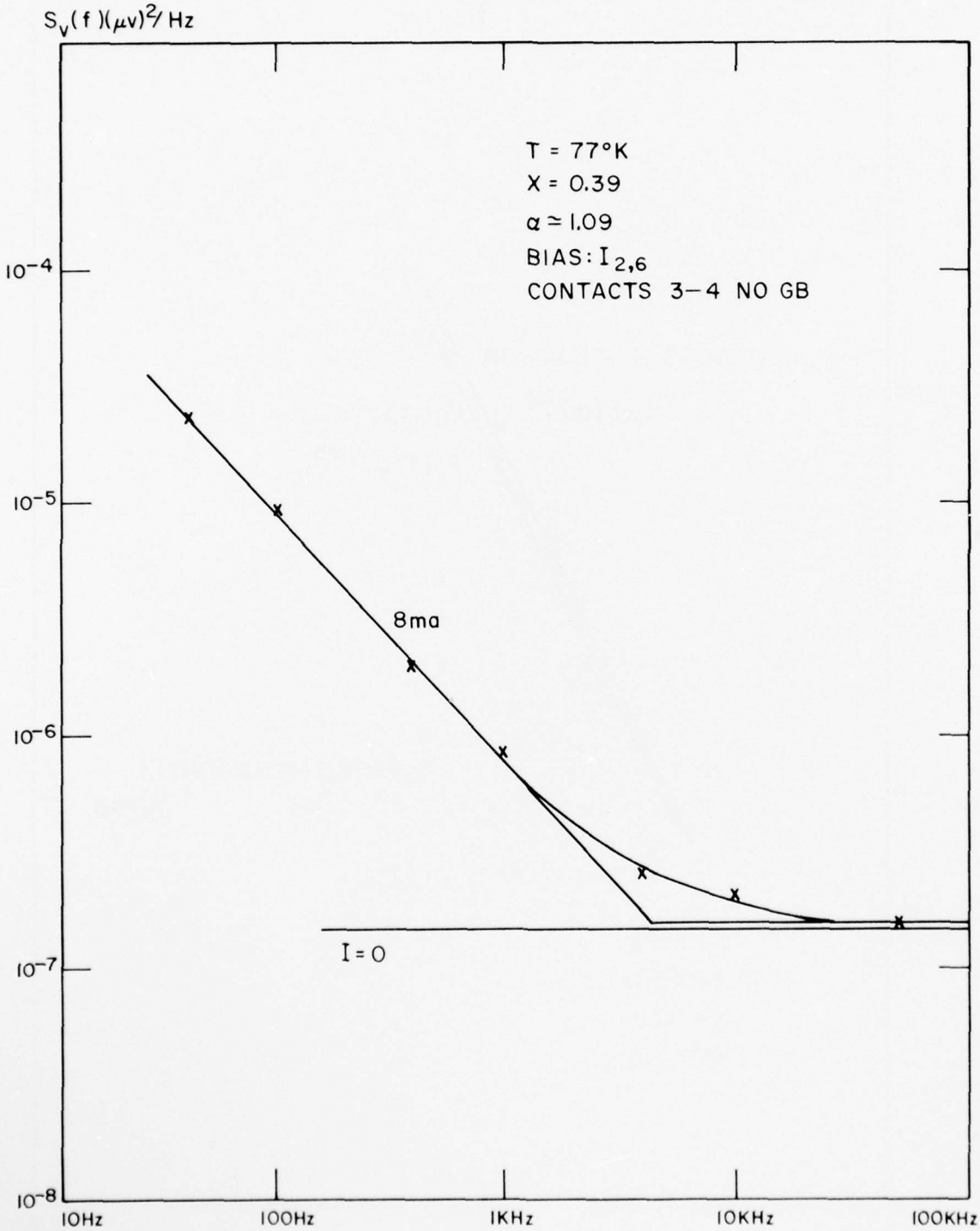

FIG 6.8 LOW FREQUENCY NOISE SPECTRA FOR DETECTOR 9745-P5

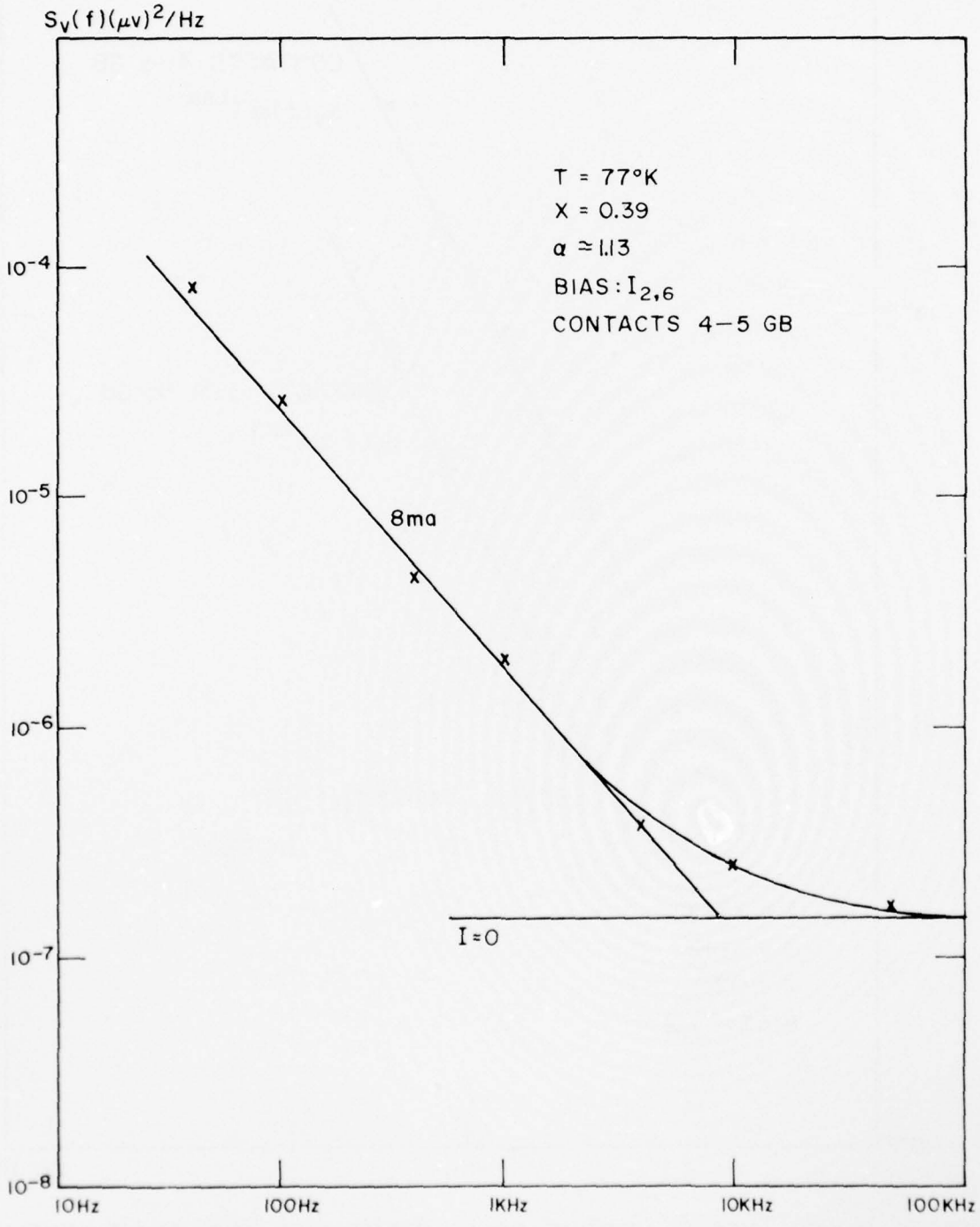

FIG 6.9 LOW FREQUENCY NOISE SPECTRA FOR DETECTOR 9745-P5

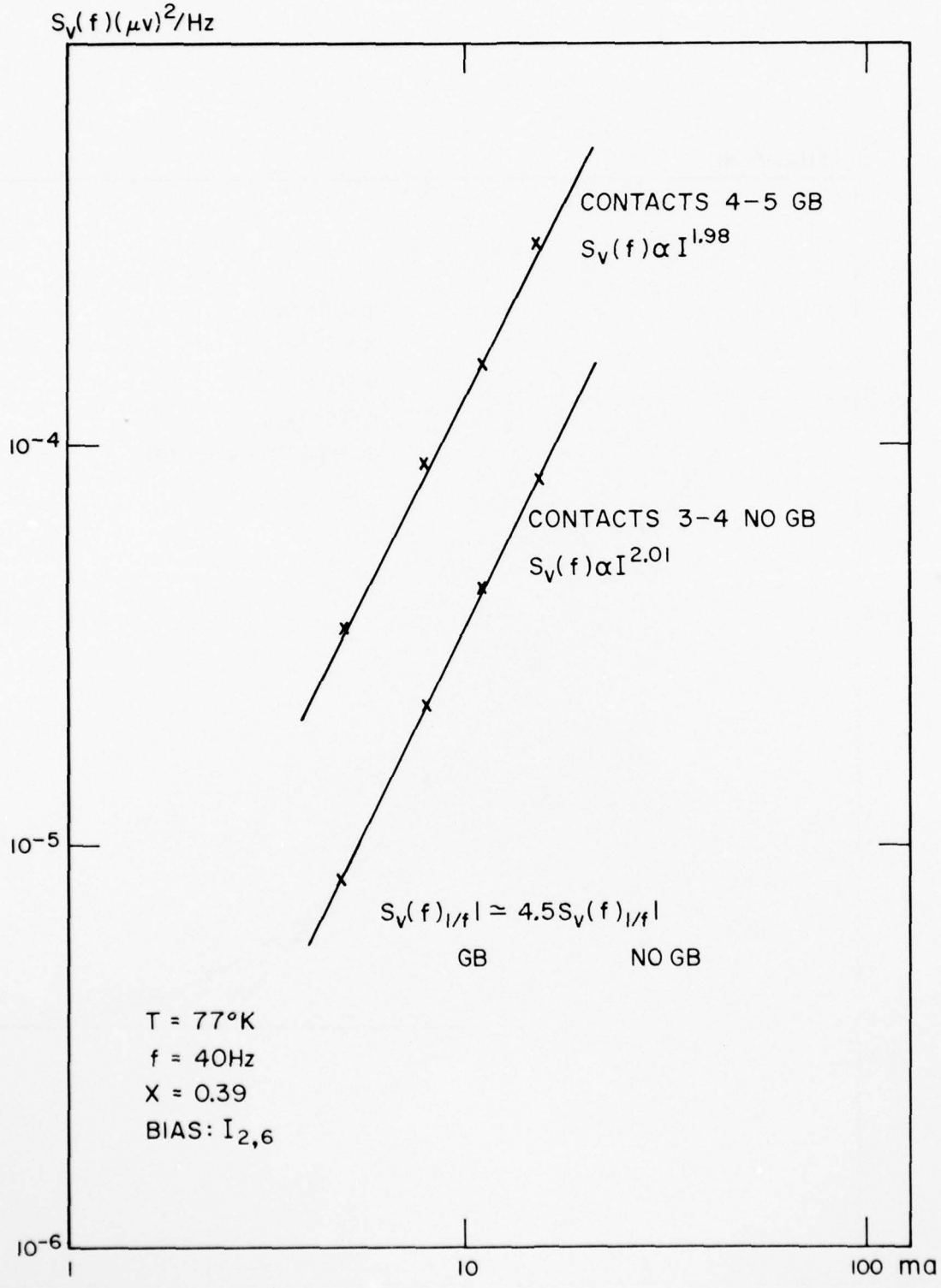

FIG 6.10 I/F NOISE VERSUS DC CURRENT FOR DETECTOR 9745-P5

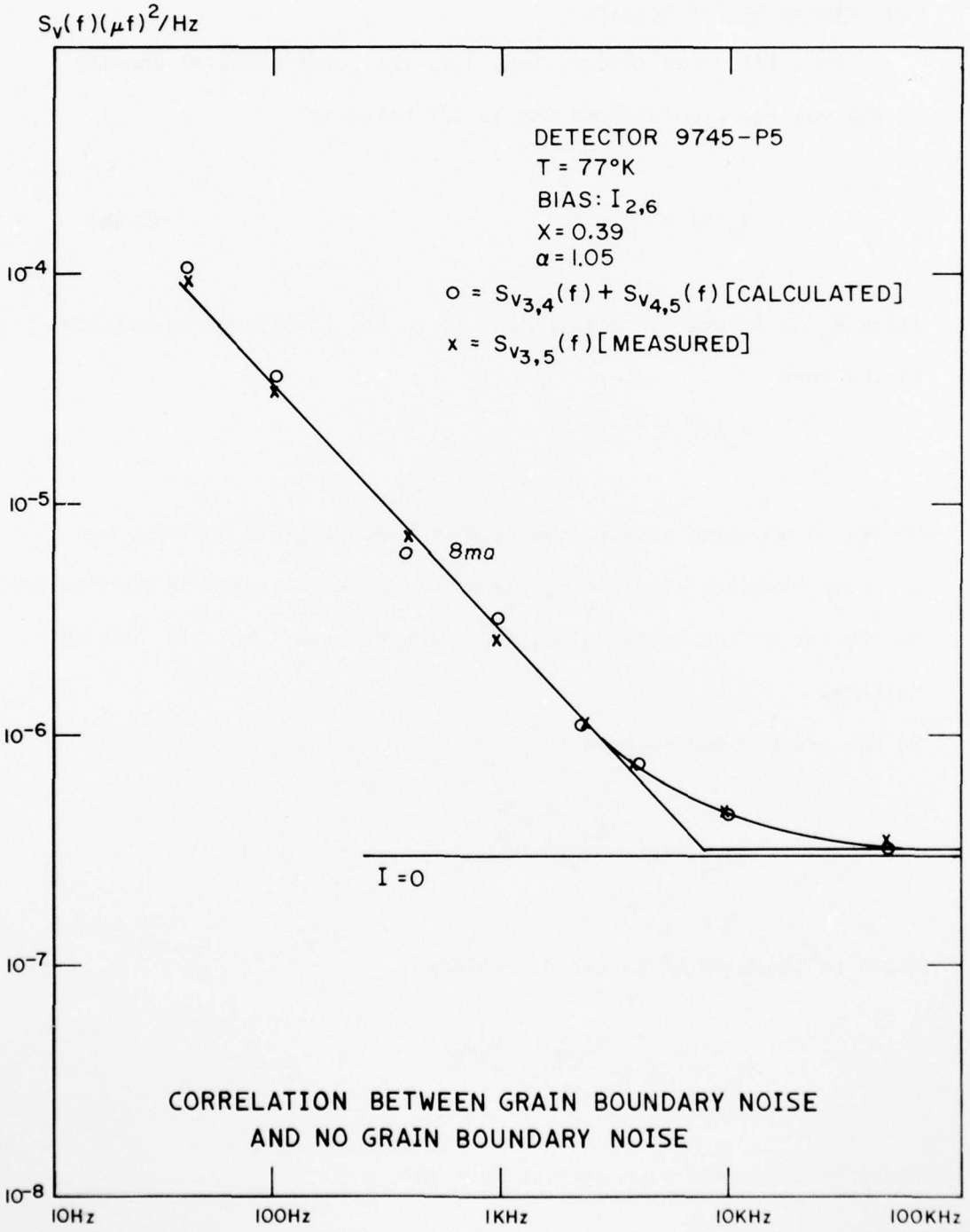

CORRELATION BETWEEN GRAIN BOUNDARY NOISE AND NO GRAIN BOUNDARY NOISE

FIG 6.11

where $S_{V_{3,5}}(f)$, $S_{V_{3,4}}(f)$ and $S_{V_{4,5}}(f)$ are all determined experimentally.

6.4 Discussion of Results

From 1/f noise theory, Sec. 3.3, the power spectral density of the voltage fluctuations due to 1/f noise is

$$S_V(f) = \frac{C\, I^2\, R^2}{N_o\, f} \qquad (5.4a)$$

Since N_o is inversely proportional to R, Eq. (5.4a) may be written in the form

$$S_V(f) = \frac{C'\, I^2\, R^3}{f}$$

Hence, in order to compare the data in case of grain boundary and no-grain boundary eliminating the effect of differences in resistances, the factor C' has to be calculated for each case. This is done as follows.

In the grain boundary case

$$S_{V_{GB}}(f) = \frac{C'_{GB}\, I^2\, R^3_{GB}}{f}$$

while in the case of no-grain boundary

$$S_{V_{NGB}}(f) = \frac{C'_{NGB}\, I^2\, R^3_{NGB}}{f}$$

therefore, for the same current I, we get

$$\frac{S_{v_{GB}}(f)}{S_{v_{NGB}}(f)} = \frac{C'_{GB}}{C'_{NGB}} \times \left(\frac{R_{GB}}{R_{NGB}}\right)^3$$

or

$$\frac{C'_{GB}}{C'_{NGB}} = \frac{S_{v_{GB}}(f)}{S_{v_{NGB}}(f)} \times \left(\frac{R_{NGB}}{R_{GB}}\right)^3$$

Table VI.1 shows the calculated values of (C'_{GB}/C'_{NGB}) for the tested devices. This indicates that the factor C' in case of grain boundary is about four times its value in case of no grain boundary; in other words, for these devices the grain boundary has increased the noise by a factor of 4 over that for the no-grain boundary case. Also, we see that all devices have about the same noise, when corrected for differences in resistance.

The explanation of the effect is straightforward. Grain boundaries are assemblies of dislocations arranged along "dislocation lines". It was shown by Bess[8,9] that dislocations give rise to excess noise over and above the "normal" flicker noise. This should be the case independent of whether the surface or the bulk interpretation of Eq. (5.4a) is adopted.

We notice from our data that the section containing the grain boundary always had a somewhat smaller resistance than the corresponding section containing no grain boundary. We have at present no satisfactory explanation for this behavior.

Table VI.1

DETECTOR #	9743-P5	9742-P5	9745-P5
$S_{V_{GB}}$ (40Hz), at 10mA, V^2/Hz	1.91×10^{-17}	8.6×10^{-18}	1.36×10^{-16}
R_{GB} Ω	$R_{3,4} = 19.5$	$R_{3,4} = 16$	$R_{4,5} = 37$
$S_{V_{GB}} / R_{GB}^3$	2.58×10^{-21}	2.1×10^{-21}	2.685×10^{-21}
$S_{V_{NGB}}$ (40Hz), at 10mA, V^2/Hz	7.92×10^{-18}	9.95×10^{-18}	3.5×10^{-17}
R_{NGB} Ω	$R_{4,3} = 22.8$	$R_{4,5} = 26.5$	$R_{3,4} = 38.5$
$S_{V_{NGB}} / R_{NGB}^3$	6.68×10^{-22}	5.35×10^{-22}	6.133×10^{-22}
C'_{GB} / C'_{NGB}	3.86	3.93	4.38

All measurements were taken at 77°K.

CHAPTER VII. DETERMINATION OF HOOGE'S CONSTANT C

According to Hooge,[2,3] the flicker noise spectrum is

$$S_v(f) = \frac{C\, I^2\, R^2}{N_o\, f} \qquad (7.1)$$

where I is the current, R the resistance, N_o the number of carriers and f the frequency.

This is an empirical formula which sums up all the data that Hooge assembled on a great variety of materials and devices. The dimensionless constant C varies between 10^{-3} and 10^{-2}, is typically 2×10^{-3} and should not differ widely for similar samples. Klaassen[7] and Van der Ziel[6] have shown that under certain conditions a formula of the type (7.1) can be derived for a surface noise mechanism, with the only difference that C now depends on surface state density N_{SS}, (see section 3.3) and may vary more widely. We give the experimental values of C for a large number of (Hg,Cd)Te devices in Table VII.1. All, except devices 50470,S185 and 10770-1, gave values for C between 2.5×10^{-3} and 8×10^{-3}, none of the measurements made on these devices involved a grain boundary. The two exceptions had C values of 0.2×10^{-3} and 0.15×10^{-3}, respectively. This clearly indicates that C can vary widely, even for the same materials; this is better compatible with a surface effect than with a bulk effect, in agreement with Chapter VIII.

Our data does not stand alone; Broudy[13] found a unit that had

AD-A037 185 MINNESOTA UNIV MINNEAPOLIS DEPT OF ELECTRICAL ENGIN--ETC F/G 17/5
LOW-FREQUENCY NOISE IN (HG, CD) TE DETECTORS.(U)
OCT 76 H I HANAFI, A VAN DER ZIEL F33615-74-C-5104
UNCLASSIFIED AFML-TR-76-175 NL

2 OF 2
ADA037185

END
DATE FILMED
4-77

Device # [+]	Contacts	x	L	w	t	T	R	n	α	β	C [*]
			mm	mm	μm	$^{o}_{k}$	ohm	cm^{-3}			$x10^{-3}$
9742-P5	4-5	0.39	1.143	1	27.84	300	85	$1.225x10^{16}$	1.13	2.1	2.46
	4-5	0.39	1.143	1	27.84	77	26.5	$1.116x10^{16}$	1.13	2.1	3.52
9743-P5	2-3	0.39	1.143	1	31	77	22.8	$1.116x10^{16}$	1.1	2.05	3.925
9745-P5	3-4	0.39	1.143	1	23.1	77	38.5	$1.116x10^{16}$	1.09	2.01	3.736
9744-P5	1-2	0.39	1.143	1	38.1	77	15	$1.116x10^{16}$	1.1	1.95	5.297
5667,174	3-4	0.2	1.143	0.84	16.04	300	14	$3.571x10^{16}$	1.0	2.05	7.18
5661	2-3	0.2	0.8	1	3.33	77	72	$2.083x10^{15}$	0.97	1.95	8.074
73V,245	1-2	0.382	0.62	0.44	2.24	77	2.2K	$1.08\ x10^{15}$	1.11	1.88	5.107
73V,247	1-2	0.382	0.6	0.4	2.2	77	2.38K	$1.08\ x10^{15}$	1.1	2.05	6.5
50470,S185	1-2	0.273	0.5	0.5	3.75	300	160.	$1.2\ x10^{16}$	0.95	1.96	0.2
10770-1	1-2	0.26	0.542	0.642	3.84	300	110.	$1.8\ x10^{16}$	1.04	2.0	0.15

All samples are n-type material

* $$C = \frac{S_v(f)_{1/f} \cdot N_{total} \cdot f^{\alpha}}{I^{\beta} \cdot R^{\beta}}$$

$= 2 \times 10^{-3}$ in Hooge's 1/f bulk model

Table VII.1 Calculated values of constant C in Equation (7.1) for different detectors.

a C-value as low as 5×10^{-6}, the lowest ever found by him. The cause of the low C-value is presently unknown. It would be extremely interesting to make such low C-values in a reproducible manner, since flicker noise in (Hg,Cd)Te could then be reduced by more than one order of magnitude. This would require a large-scale comprehensive study far beyond the scope of this thesis.

CHAPTER VIII. SURFACE EFFECTS ON 1/f NOISE IN (Hg,Cd)Te

The objective of this study is to determine the sources of 1/f noise in n-type (Hg,Cd)Te detectors. Utilizing a Metal-Insulator-Semiconductor structure, the effect of depletion and accumulation of the surface on the device noise characteristics is determined. The experimental 1/f noise data are compared to both the bulk and surface models (see Sec. 3.3) to determine whether the low frequency noise in these devices is due to a bulk or to a surface effect.

8.1 Device Fabrication

The experimental devices used to study the effect of depletion and accumulation of the surface on the low frequency noise characteristics of (Hg,Cd)Te devices were Metal-Insulator-Semiconductor (MIS) structures. The structure shown in Fig. 8.1 was fabricated. The (Hg,Cd)Te samples were prepared first as mentioned in Sec. 2.1, steps 1 to 7. Ohmic contacts were made to each detector by evaporating indium; then copper leads were bonded to the contacts using silver epoxy. A zinc sulphide dielectric coating was then evaporated over the whole detector. Aluminum gate electrodes 1000 Å thick were then evaporated over the zinc sulphide after properly masking the contact areas and the edges of each detector. A copper lead was bonded to each gate area using silver epoxy. Each detector was then mounted on a "TO8" IC header using GE varnish. The detector and gate leads were bonded to the IC header pins using In soldering.

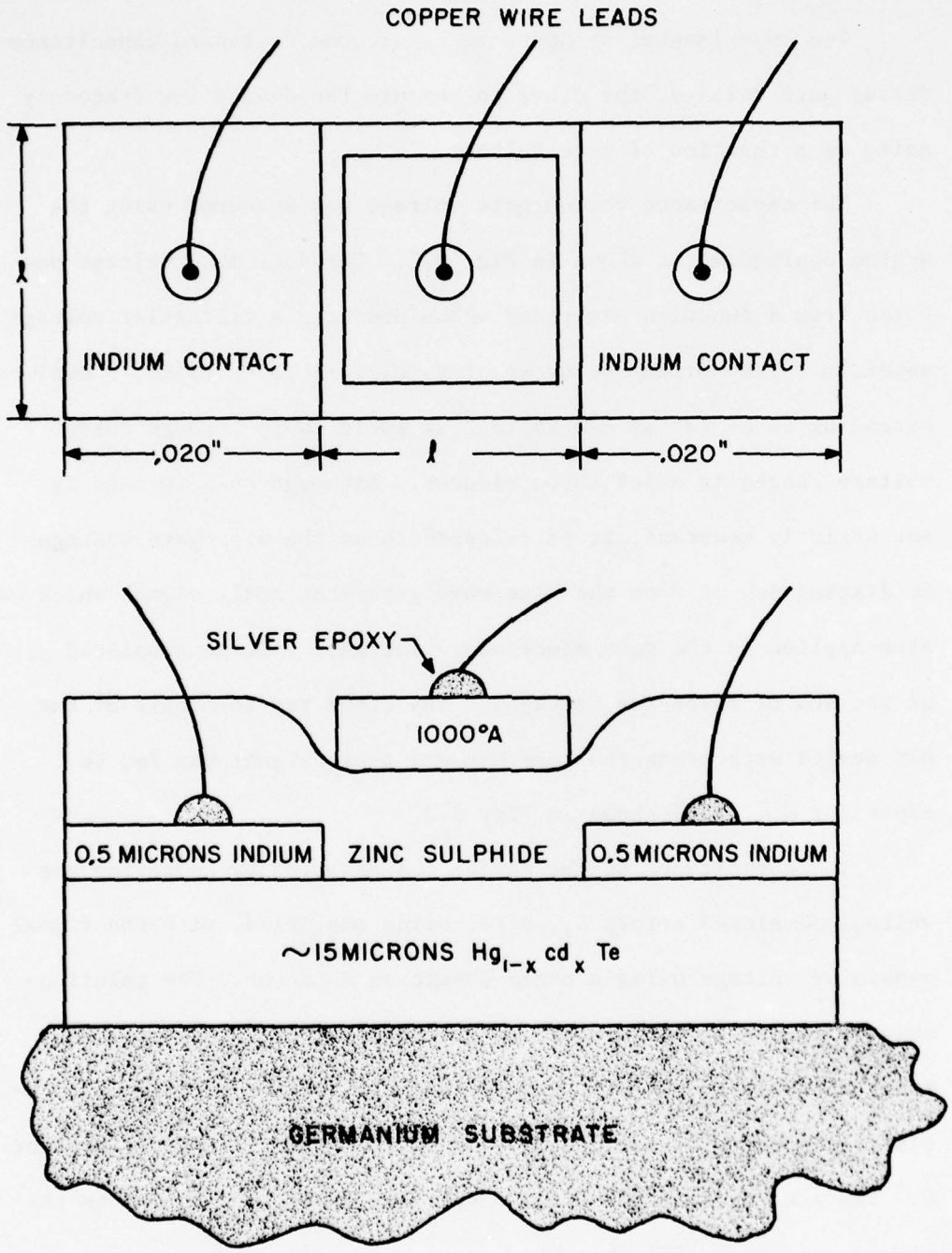

FIG 8.1 MIS STRUCTURE

$l \simeq 40$mil FOR DETECTOR 9744-P5
$\simeq 20$mil FOR DETECTORS 73V,245 AND 73V,247

8.2 Measuring Equipment

Two experimental setups were used; one to record capacitance versus gate voltage, the other to measure the device low frequency noise as a function of gate voltage.

The capacitance versus gate voltage was measured using the system configuration shown in Fig. 8.2. The d.c. gate voltage was taken from a function generator which produced a triangular voltage waveform. The voltage swing was typically +8 to -8 Volts, sometimes extending to as far as -20 Volts. It would sweep through these voltage ranges in about three minutes. Although this voltage is not strictly constant, it is referred to as the d.c. gate voltage to distinguish it from the sine wave generator small signal which was also applied to the gate electrode. The gate voltage consisted of the sum of these two voltages. The other two terminals of the MIS device were connected together and their signal was fed to capacitor C_1(.01μF) shown in Fig. 8.2.

The capacitance of the device was measured by comparing the voltage developed across C_1, after being amplified, with the signal generator voltage using a phase sensitive detector. The relationship is simple to derive. The signal generator voltage will be represented by V_s, and the MIS device as a complex impedance Z consisting of the parallel combination of a resistor R and a capacitor C. The a.c. current flowing through the sample in response to the signal generator will then be

$$I = \frac{V_s}{Z} = \frac{V_s}{R} (1 + j\omega RC)$$

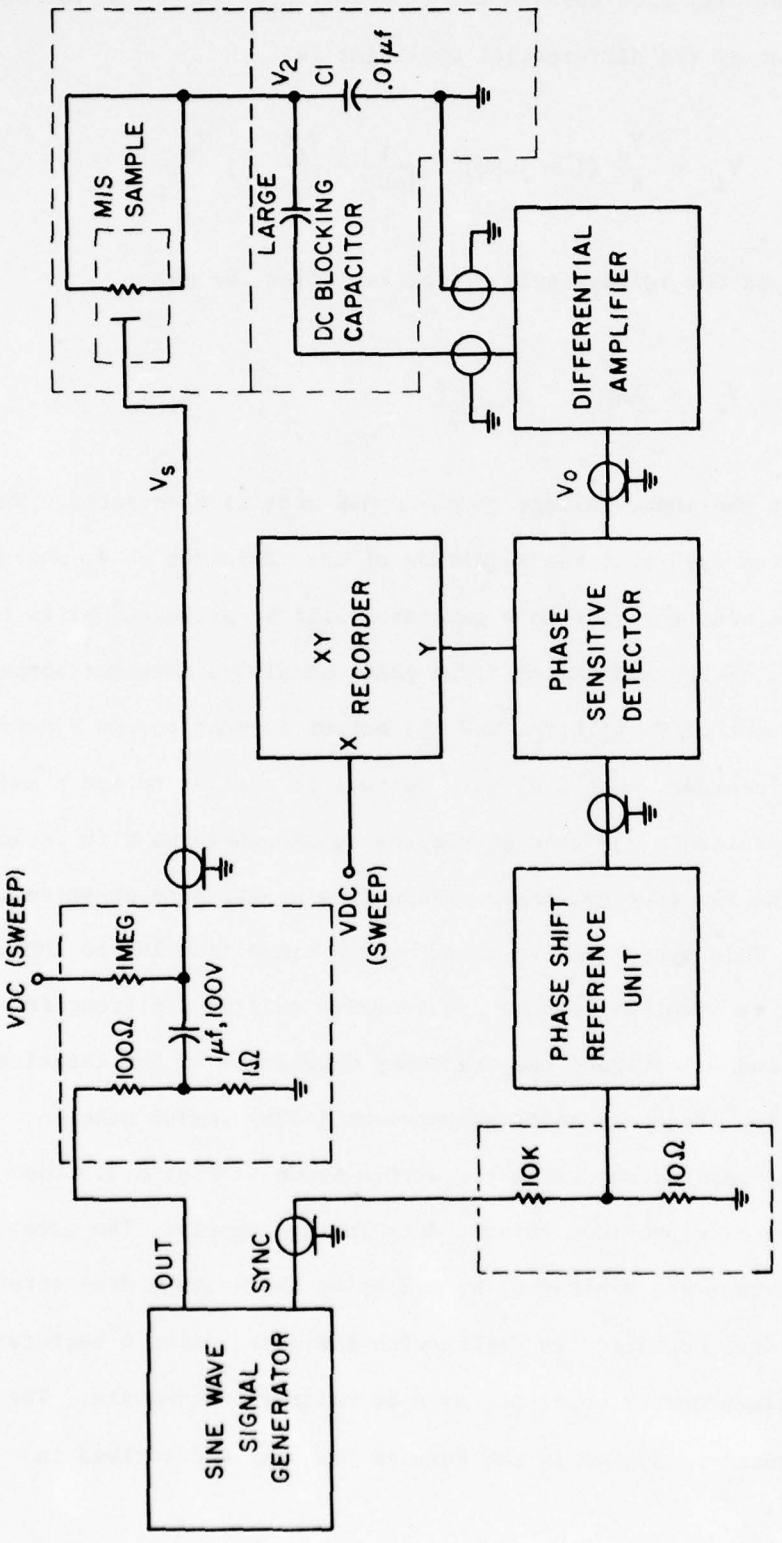

FIG 8.2 IMPEDANCE MEASURMENT EQUIPMENT 1Hz – 1MHz

this current will flow through the capacitor C_1, hence, the voltage at the input of the differential amplifier is

$$V_i = \frac{V_s}{R}(1 + j\omega RC) \cdot \frac{1}{j\omega C_1} = \frac{V_s C}{C_1} - j\frac{V_s}{\omega RC_1}$$

Assuming K is the voltage gain of the amplifier, we get

$$V_o = K\left(\frac{V_s C}{C_1} - j\frac{V_s}{\omega RC_1}\right)$$

where V_o is the input voltage to the phase sensitive detector. The last equation says that the magnitude of the component of V_o which is in phase with the sine wave generator will be proportional to the capacitance of the MIS device. The phase sensitive detector compares this component of V_o with V_s, and the output is sent to the Y axis of an X-Y recorder. The d.c. gate voltage is applied to the X axis, and the capacitance may then be plotted continuously as a function of V_G as the function generator sweeps from positive to negative voltages. This system may be tuned over a range from 1Hz to 1MHz, so that it is possible to make successive runs at different frequencies, and investigate the frequency dependence of the capacitance.

The low frequency noise measurement (40Hz) versus gate voltage was carried out using the system shown in Fig. 8.3. The gate voltage was provided using a d.c. voltage supply. The gate leakage current was monitored, by measuring the voltage drop across a 1MΩ resistor connected in series with the gate, using a battery operated electrometer model 601 made by Keithly Instruments. The noise measurement system is the same as the system described in Sec. 2.2.2.

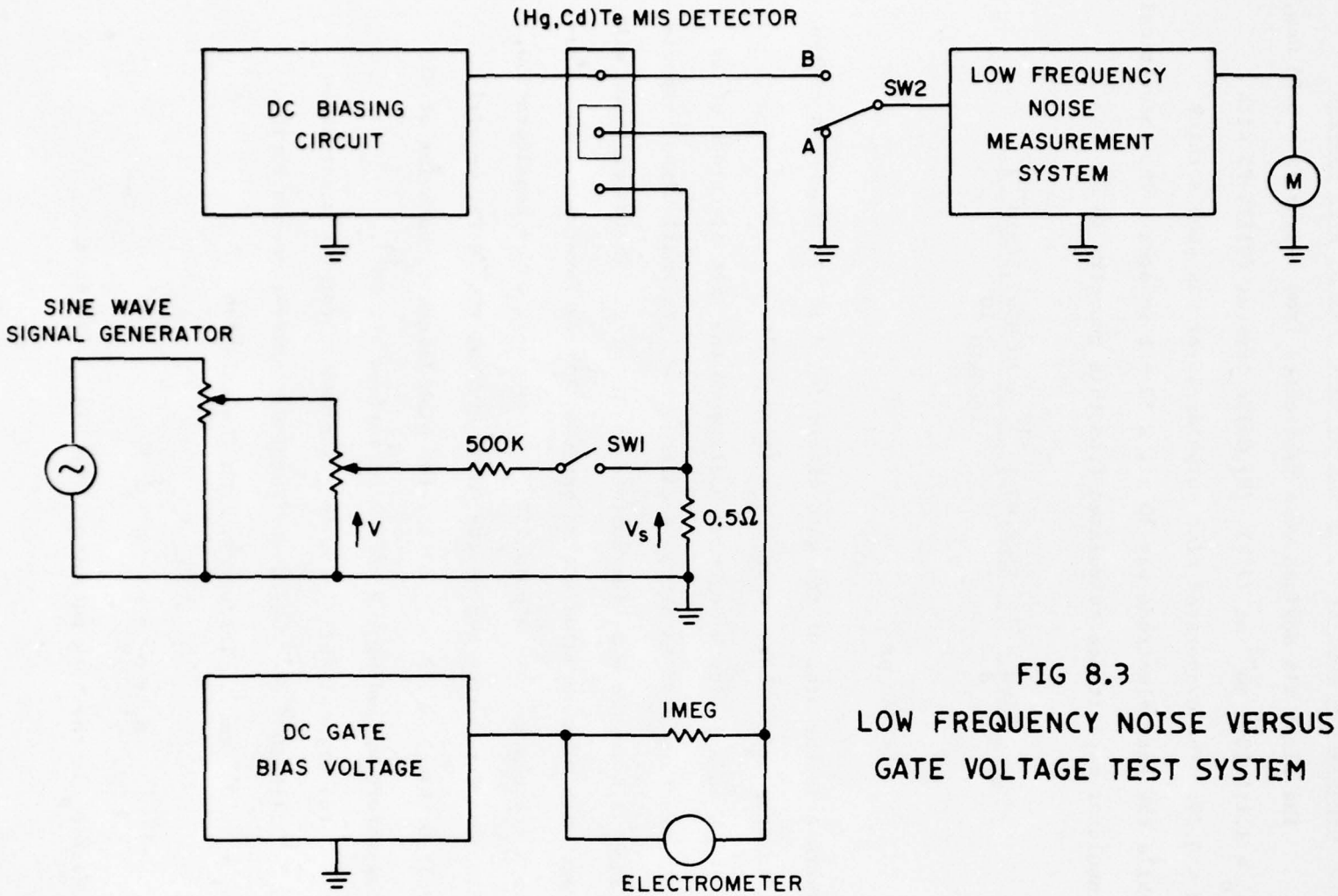

FIG 8.3
LOW FREQUENCY NOISE VERSUS GATE VOLTAGE TEST SYSTEM

8.3 Capacitance and 1/f Noise Versus Gate Voltage Test Results

The first MIS devices were fabricated from n-type (ρ = 0.05 Ωcm, $n_o \simeq 1.116\times10^{16}$ cm^{-3} at 77°K) (Hg,Cd)Te crystal #91174-P5 with $x \simeq 0.39$. The evaporated zinc sulphide layer was 4000 Å thick while the gate electrode was 30 mil x 30 mil in area. The theoretical insulator capacitance calculated from this geometry is

$$C_i = \frac{\varepsilon_{ins}\varepsilon_o A}{d} = \frac{11\times8.85\times10^{-12} \times (0.03\times2.54\times10^{-2})^2}{4000\times10^{-10}}$$

$$\simeq 140 \text{ pF}$$

where A is the area of the gate electrode, d is the thickness of the insulator and we have taken $\varepsilon_{ins} \simeq 11$ at 300°K.

When applying a negative voltage to the gate electrode of an MIS structure with an n-type semiconductor, its small signal capacitance will decrease as the surface is depleted. The capacitance will reach its minimum value at the onset of strong inversion. To calculate the change in the capacitance in the case under consideration, MIS detectors using n-type (Hg,Cd)Te crystal #91174-P5, we will follow the theory developed for the high frequency behavior of MIS capacitors excluding the effect of surface states[14].

For crystal #91174-P5, the extrinsic carrier concentration $n_o \simeq 1.116\times10^{16}$ cm^{-3} while the intrinsic carrier concentration $n_i \simeq 6\times10^{14}$ cm^{-3}. Therefore, from the relation

$$n_i + n_o = n_i \exp\left(\frac{e\phi_B}{KT}\right)$$

where ϕ_B is the bulk potential (see Fig. 3.5), we get

$$\phi_B = \frac{KT}{e} \ln \frac{n_i + n_o}{n_i}$$

$$= \frac{1.38\times10^{-23} \times 300}{1.6\times10^{-19}} \ln \frac{1.176\times10^{16}}{6\times10^{14}}$$

$$= 7.699\times10^{-2} \text{ Volts at } 300°K$$

Now the onset of strong inversion occurs when the bulk potentail ϕ_B equals the surface potential ϕ_s, therefore

$$\phi_s(\text{inv}) = 7.699\times10^{-2} \text{ Volts}$$

at onset of strong inversion. Corresponding to this value of $\phi_s(\text{inv})$, the maximum width of the surface depletion region $X_{d_{max}}$ can be estimated using the depletion approximation which yields

$$X_{d_{max}} = \sqrt{\frac{4\varepsilon_s \varepsilon_o \phi_s(\text{inv})}{e\, n_o}} \qquad (8.3b)$$

where ε_s is the dielectric constant of $Hg_{0.6}Cd_{0.4}Te$ [15] and is taken $\simeq 14$. Hence,

$$X_{d_{max}} = \sqrt{\frac{4\times14\times8.86\times10^{-14} \times 7.699\times10^{-2}}{1.6\times10^{-19} \times 1.116\times10^{16}}}$$

$$= 1.463\times10^{-5} \text{ cm}$$

and the minimum value of the depletion region capacitance is

$$C_{d_{min}} = \frac{\varepsilon_s \varepsilon_o A}{X_{d_{max}}}$$

$$= \frac{14 \times 8.86 \times 10^{-12} \times (0.03 \times 2.54 \times 10^{-2})^2}{1.463 \times 10^{-7}}$$

$$\simeq 490 \text{ pF}$$

Since the capacitance of the MIS structure is given by the series combination of C_i and depletion region capacitance, then the minimum value expected in this case is

$$C_{MIS_{min}} = \frac{C_i C_{d_{min}}}{C_i + C_{d_{min}}} = \frac{140 \times 490}{630} \simeq 109 \text{ pF}$$

Fig. 8.4 shows the measured capacitance versus gate voltage for MIS detector #9744-P5 from crystal #91174-P5. The insulator capicitance and the minimum measured capacitance agrees very well with the theoretical values calculated above. This curve was obtained both at 100KHz and 100Hz indicating that the density of slow surface states is much less than that for the fast surface states. This curve is a typical "low" frequency curve for n-type materials indicating that the generation recombination rates in the inversion layer are fast enough to keep up with the small signal variation at 100KHz (i.e. the fast surface states can interact with the bands fast enough to follow the applied a.c. signal at 100KHz). In this case, the capacitance measured approaches that of the insulator at large negative gate voltage.

Low frequency noise measurements (40Hz) versus gate voltage was

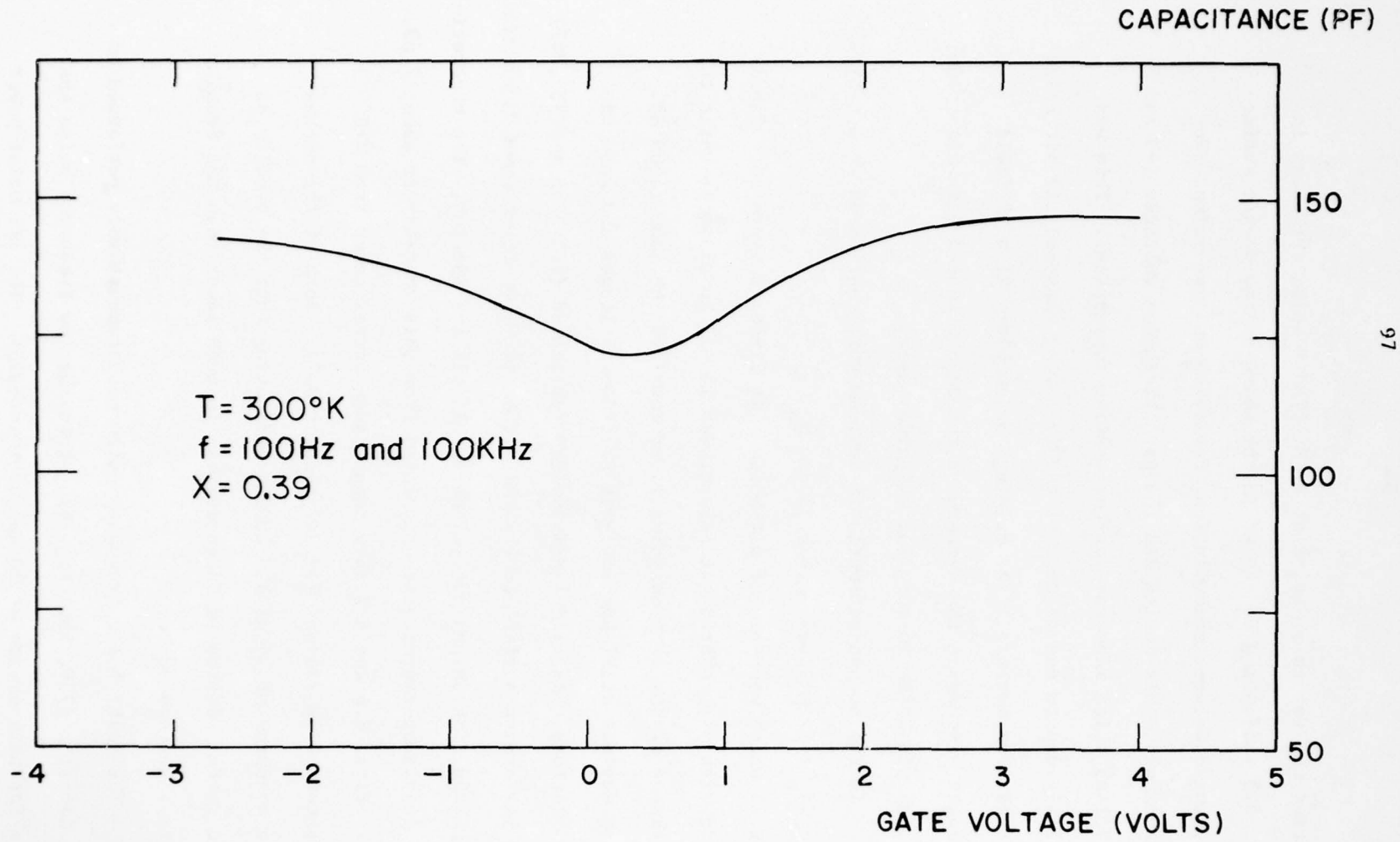

FIG 8.4 CAPACITANCE VERSUS GATE VOLTAGE FOR MIS DETECTOR 9744-P5

carried out for this device at 77°K. The results are shown in Fig. 8.5 indicating no change in the noise as the device surface is changed between accumulation, depletion and inversion. Unfortunately, this device had low gate breakdown voltages (-3 and +4 Volts) which made any further testing impractical. This was possibly due to one or more of the following reasons: 1) pit holes left by free mercury after etching the sample; 2) high field strength existed at the corners of the square shaped gate electrode; and, 3) pin holes in the zinc sulphide layer.

In the second attempt, MIS devices were fabricated from n-type $Hg_{1-x}Cd_xTe$ ($x = 0.382$, $\rho = 0.35\Omega cm$, $n_o \simeq 1.08 \times 10^{15}$ cm^{-3}) crystal #73V,24 which was free of pit holes. At first, devices were fabricated with disk shaped gate electrodes 15 mil in diameter while the thickness of the zinc sulphide layer remained the same (4000 Å). These devices still had low gate breakdown voltages and were unsatisfactory. The final MIS devices fabricated (#73V,245 and 73V,247) and performing satisfactorily had a zinc sulphide layer about 1.5 micron thick and disk shaped gate electrode 15 mil in diameter. The theoretical insulator capacitance calculated from this geometry is about 7 pF.

Figs. 8.6 and 8.7 show capacitance curves taken from MIS detectors #73V,245 and 73V,247 respectively. Both of the curves were measured at 100Hz and 100KHz indicating that the density of slow surface states in these devices is much lower than the density of fast surface states.

The initial low frequency noise measurements were performed on MIS detector #73V,245. Fig. 8.8 shows the low frequency noise spectrum for this device at 30 and 200 microamps. The 1/f noise power

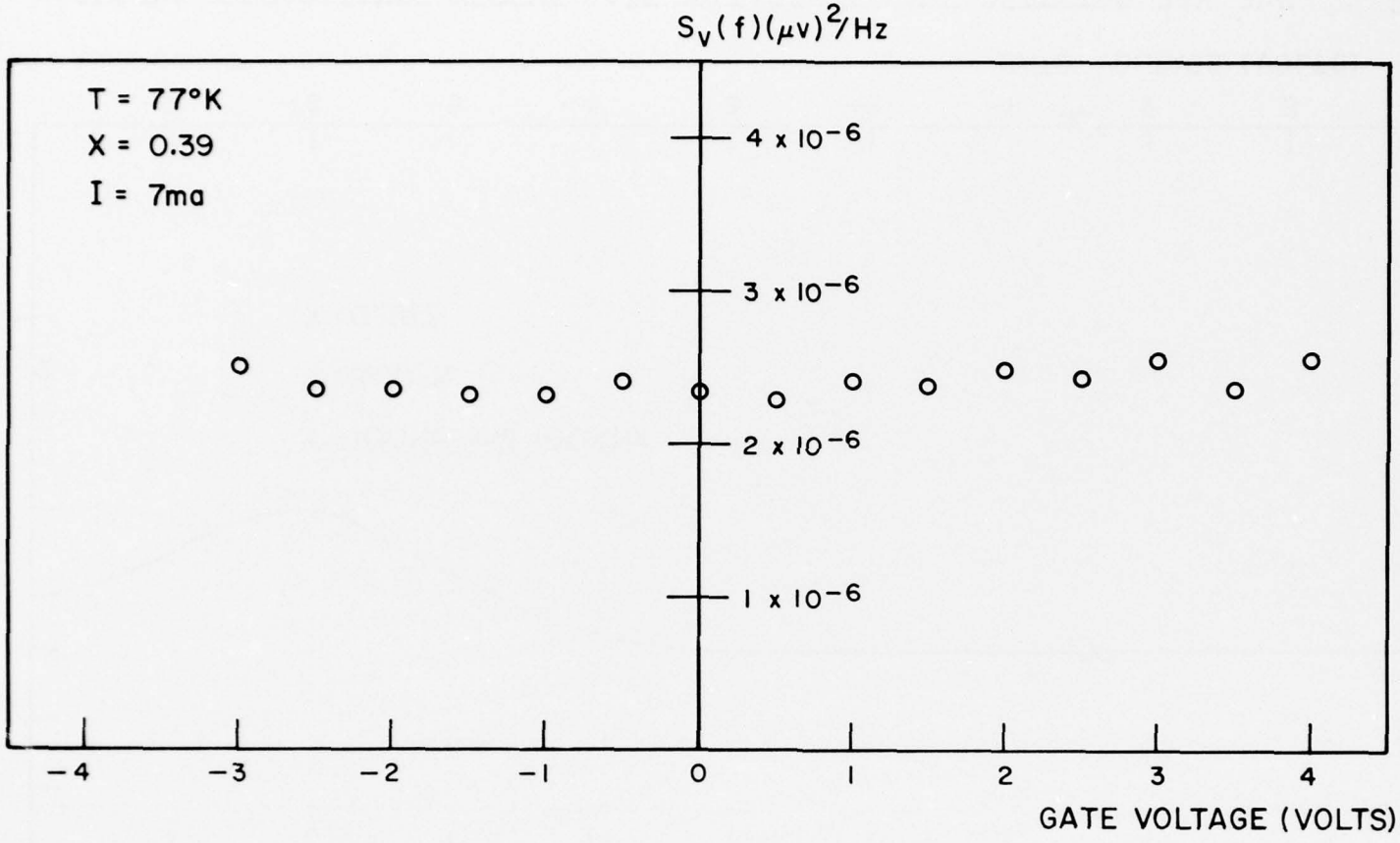

FIG 8.5 LOW FREQUENCY NOISE VERSUS GATE VOLTAGE FOR MIS DETECTOR 9744-P5

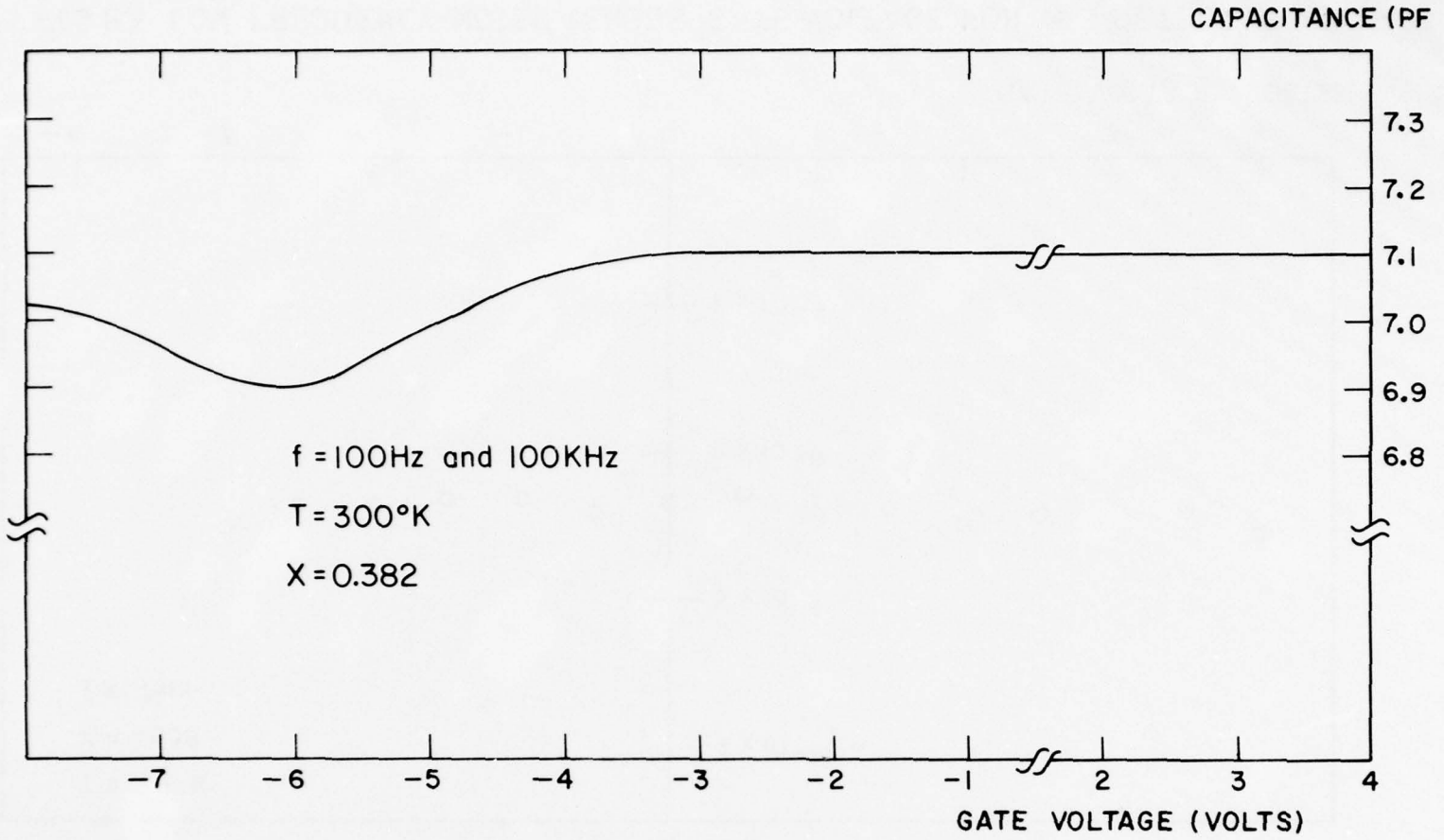

FIG 8.6 CAPACITANCE VERSUS GATE VOLTAGE FOR MIS DETECTOR 73V, 245

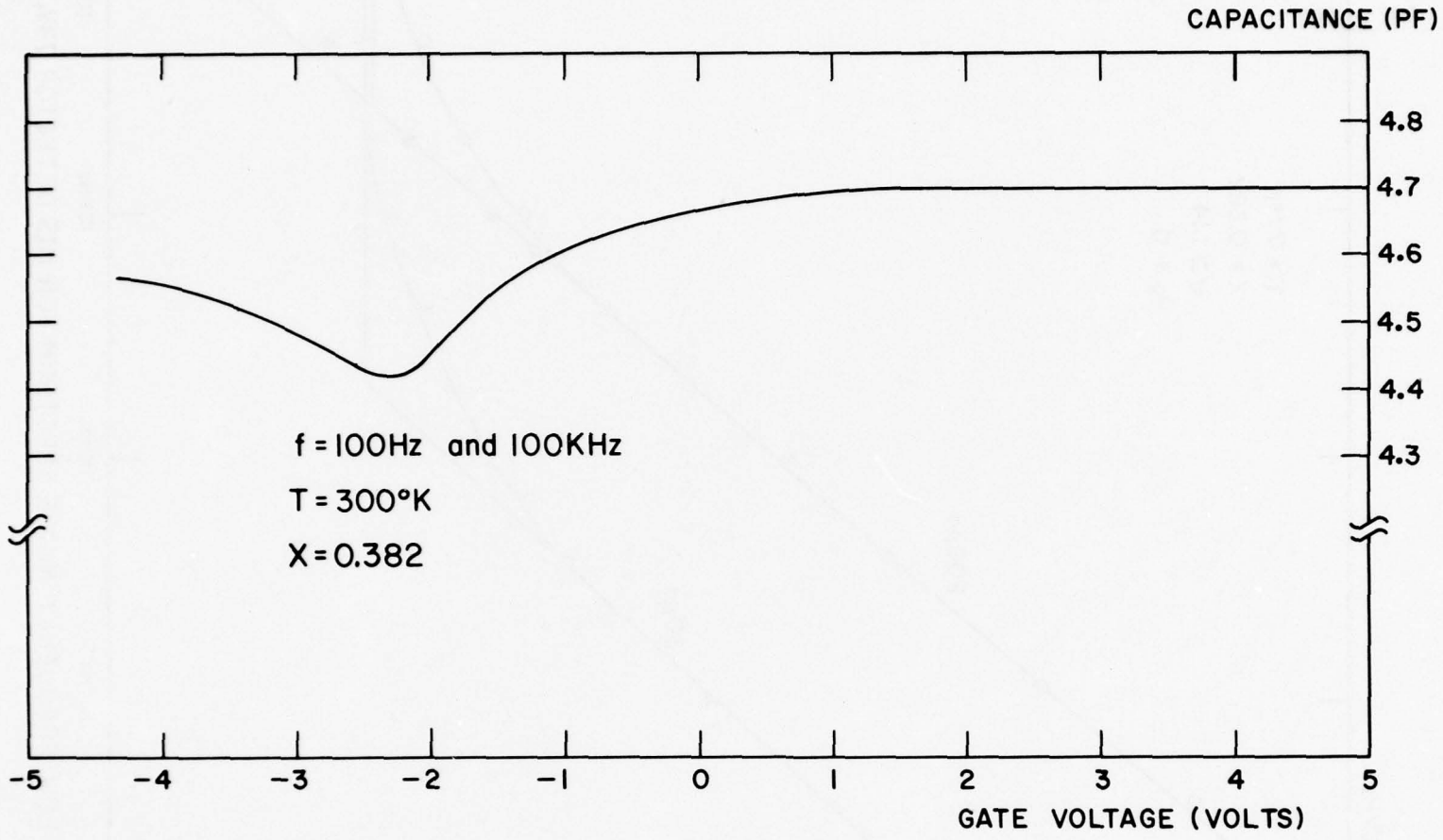

FIG 8.7 CAPACITANCE VERSUS GATE VOLTAGE FOR MIS DETECTOR 73V, 247

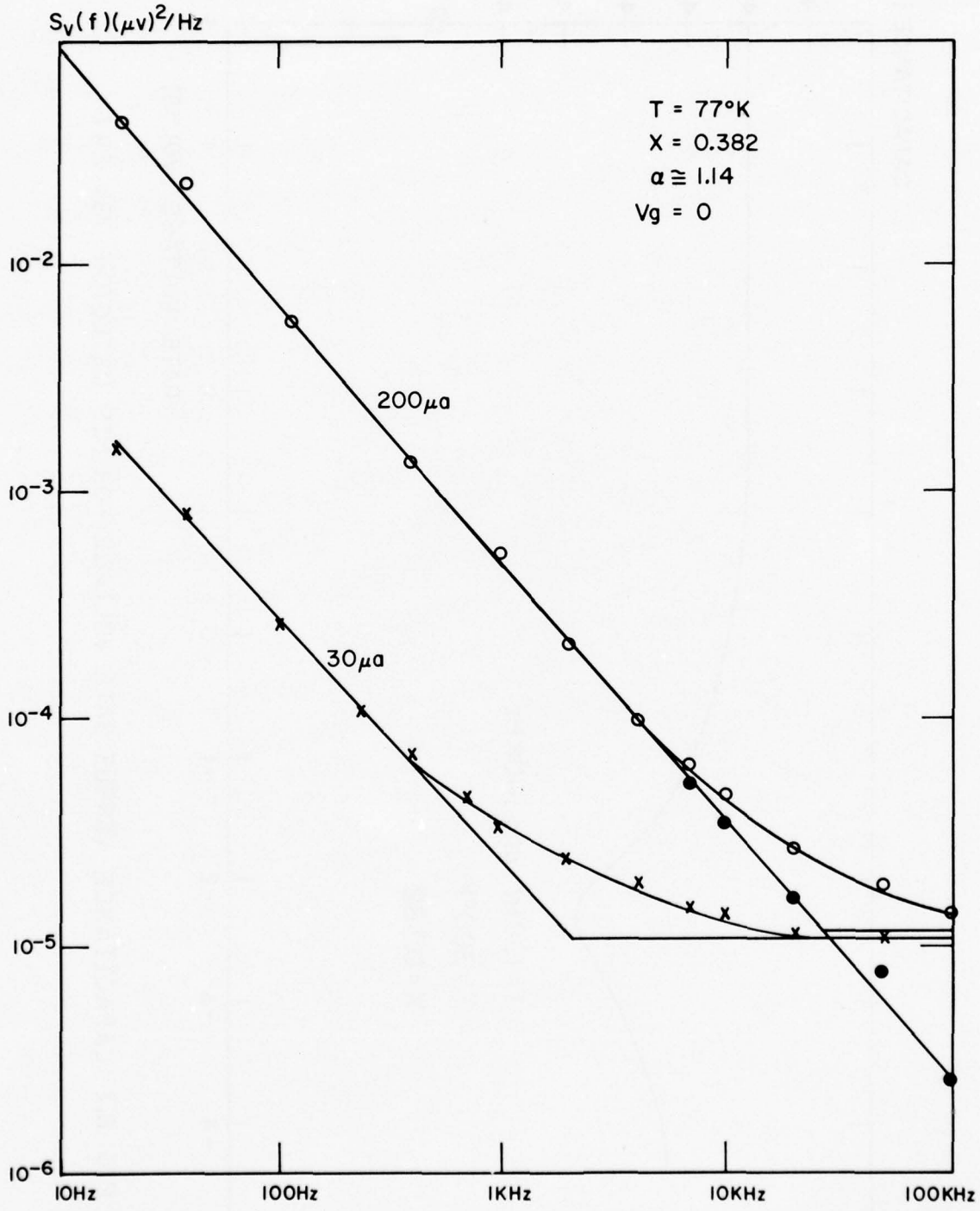

FIG 8.8 LOW FREQUENCY NOISE SPECTRUM FOR MIS DETECTOR 73V,245

spectral density at 40Hz increased approximately with the square of the d.c. current as shown in Fig. 8.9. Low frequency noise measurements versus gate voltage were performed at 40Hz and at 30μA. The results which are shown in Fig. 8.10 indicate no change in the measured noise as the surface changed from accumulation to strong inversion. Noise measurements versus gate voltage were also performed at 100KHz and at 200μA. The results shown in Fig. 8.11 indicate that the noise increases slowly as the surface changed from accumulation to depletion. At the onset of strong inversion, the noise increased much more rapidly and then levelled off as the device went into deep inversion. Unfortunately, we were not able to perform thermal noise versus gate voltage measurements for this device (#73V,245) due to damage of the gate insulator caused by accidentally applied high voltage.

Device #73V,247 was tested next. The low frequency noise spectral density of this device obeyed a 1/f law as shown in Fig. 8.12 while it increased with the square of the d.c. current in the characteristic way for 1/f noise (Fig. 8.13). The low frequency noise measured at 40Hz did not change as we decreased the gate voltage and inverted the surface. This is shown in Fig. 8.14. Finally, the device thermal noise was measured versus gate voltage and the results are indicated in Fig. 8.15. The thermal noise, i.e. the device resistance, increased gradually and levelled off as the device went into deep inversion. This could be explained simply by considering two resistors in parallel. In the accumulation region, we have a strongly conducting n-type skin on the material which shunts the bulk resistance. As the accumulation at the surface decreases, we

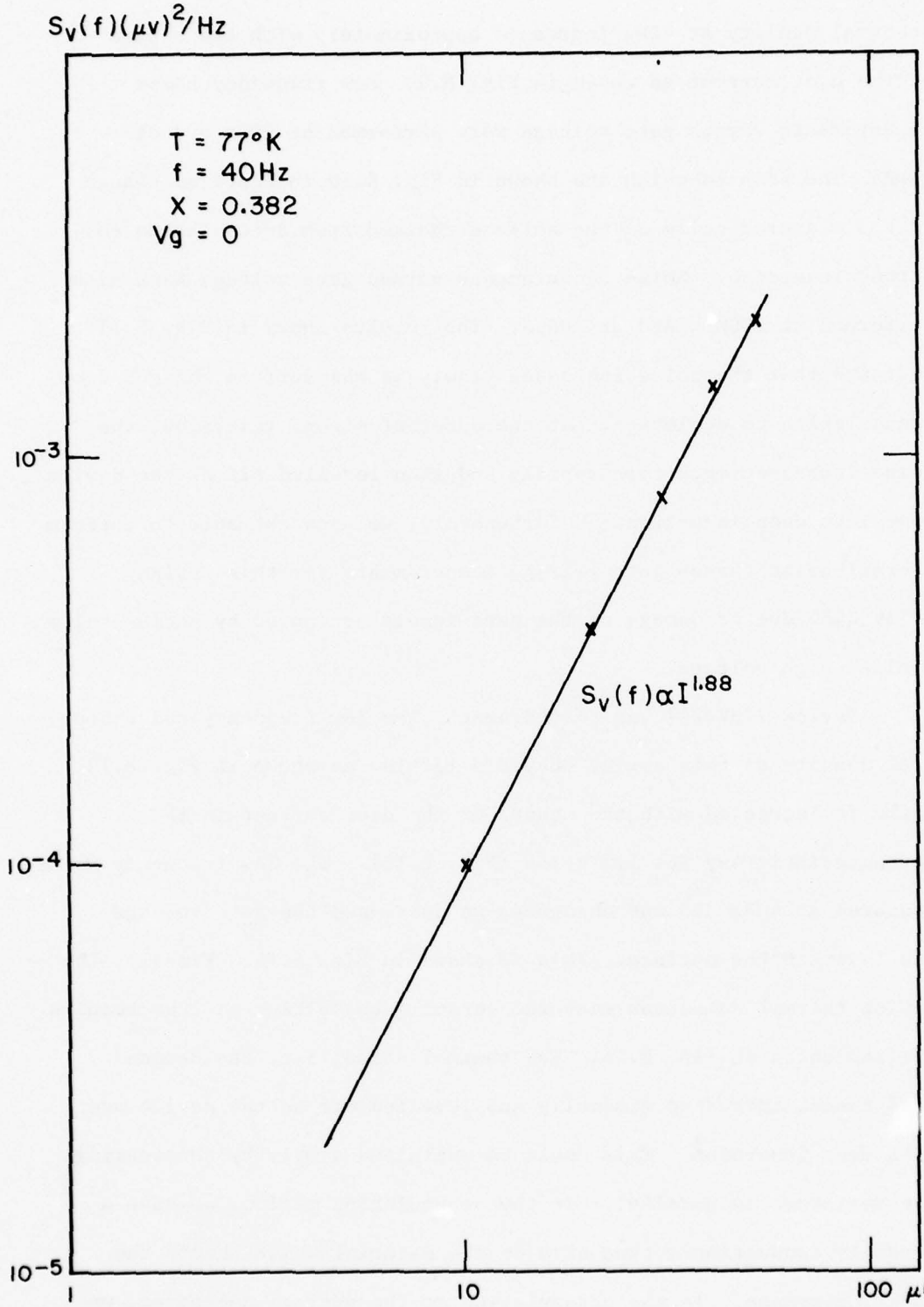

FIG 8.9 I/F NOISE VERSUS DC CURRENT FOR MIS DETECTOR 73V, 245

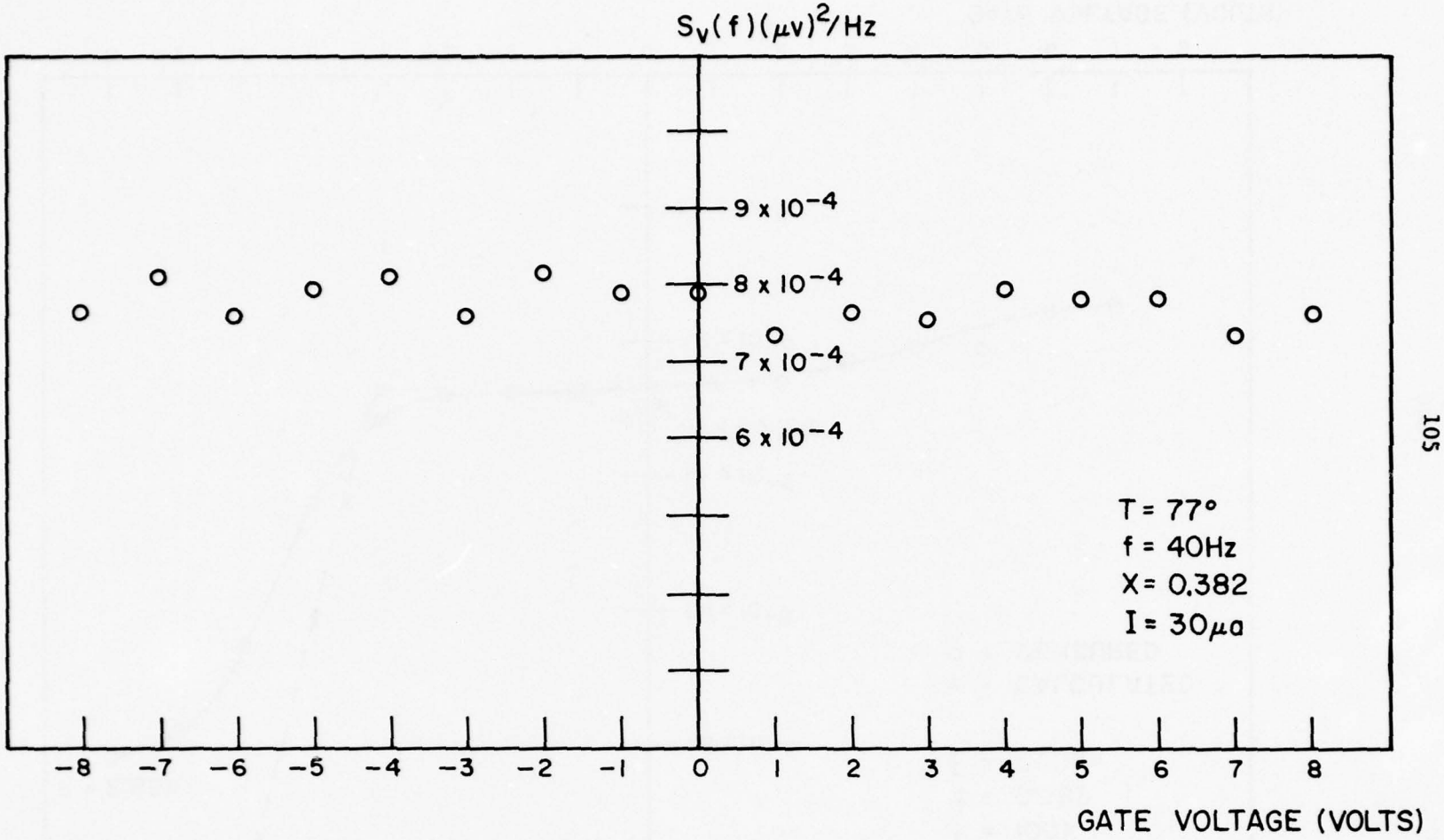

FIG 8.10 LOW FREQUENCY NOISE VERSUS GATE VOLTAGE FOR MIS DETECTOR 73V, 245

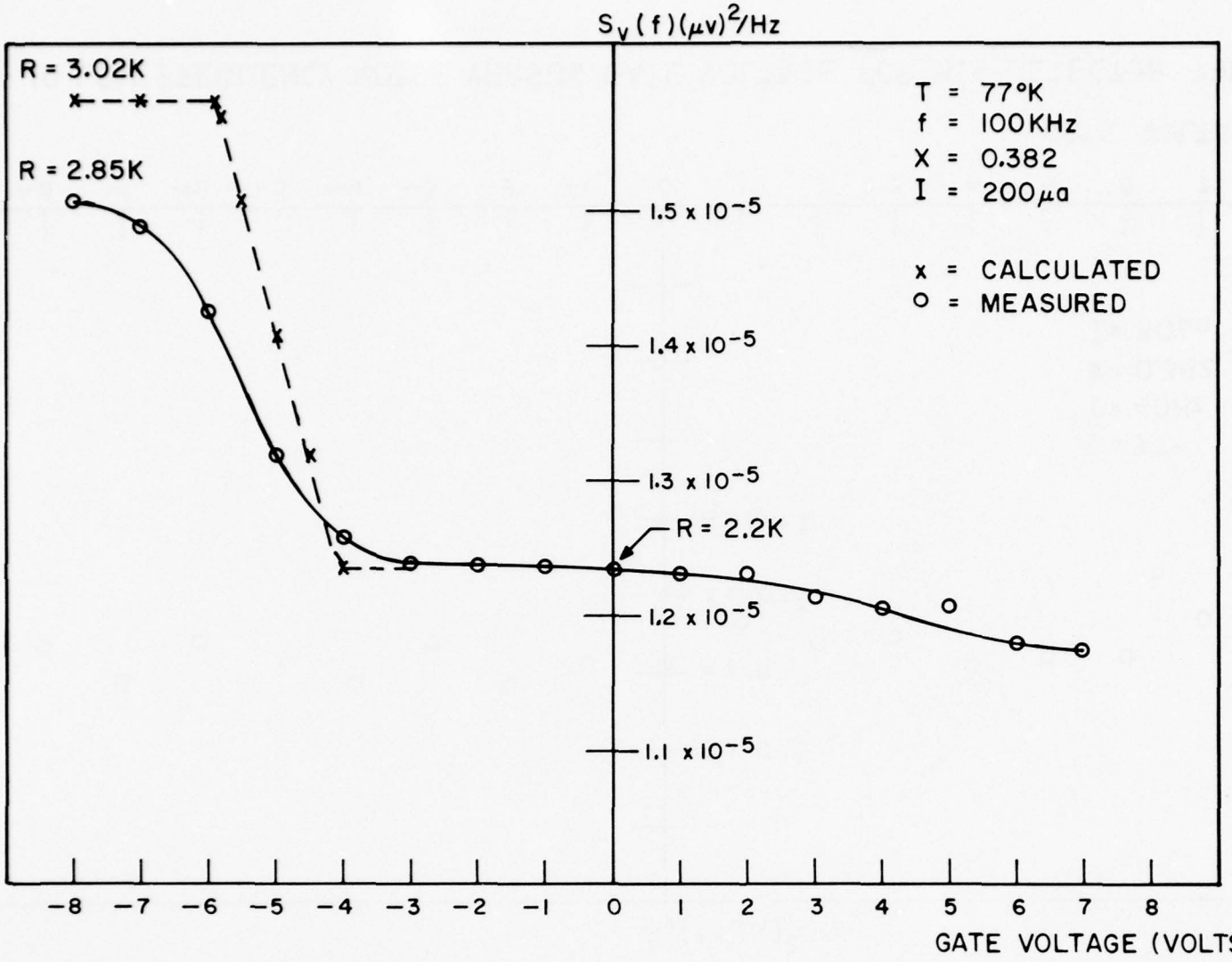

FIG 8.11 MEASURED NOISE AT 100KHz VERSUS GATE VOLTAGE FOR MIS DETECTOR 73V, 245

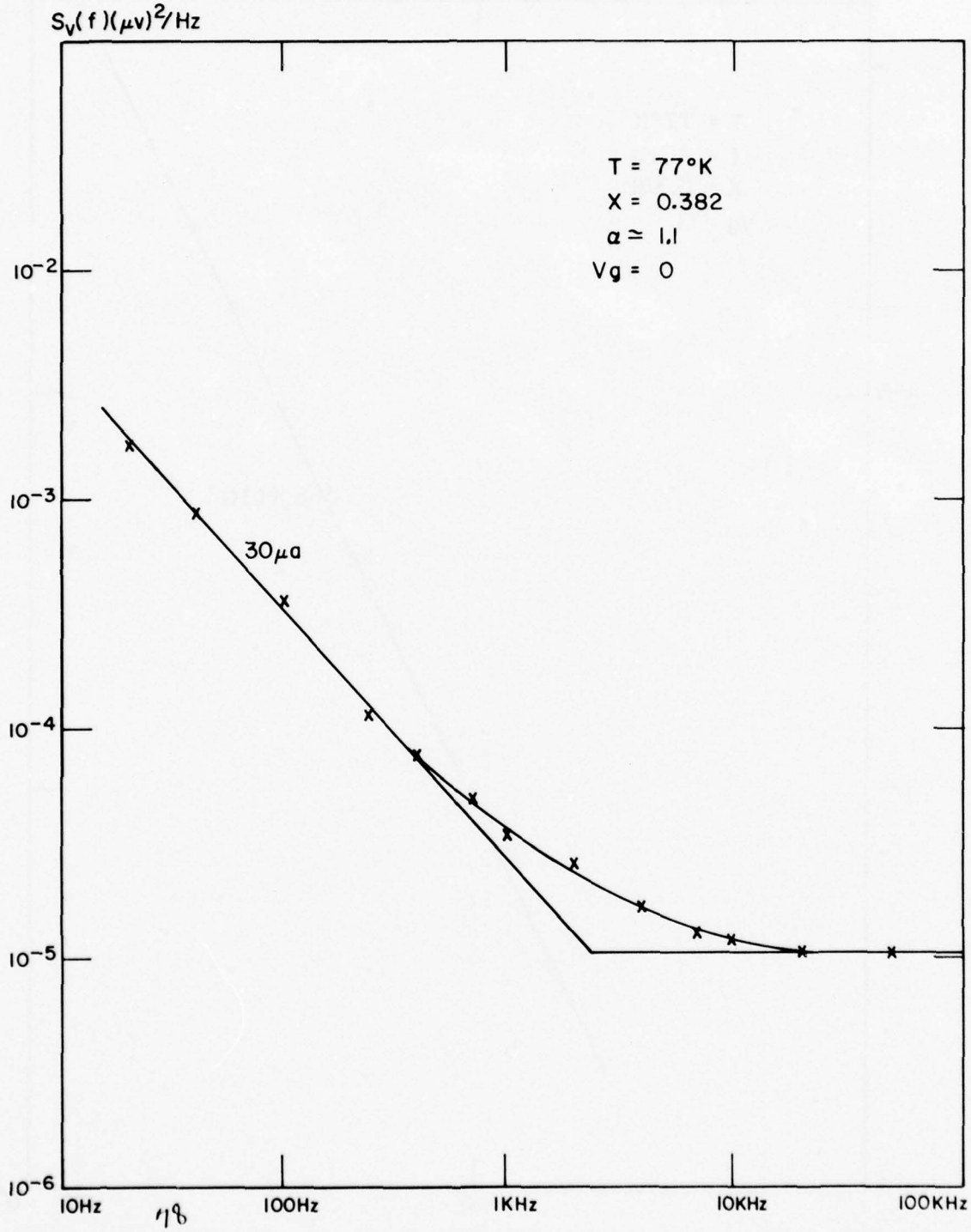

FIG 8.12 LOW FREQUENCY NOISE SPECTRUM FOR MIS DETECTOR 73V, 247

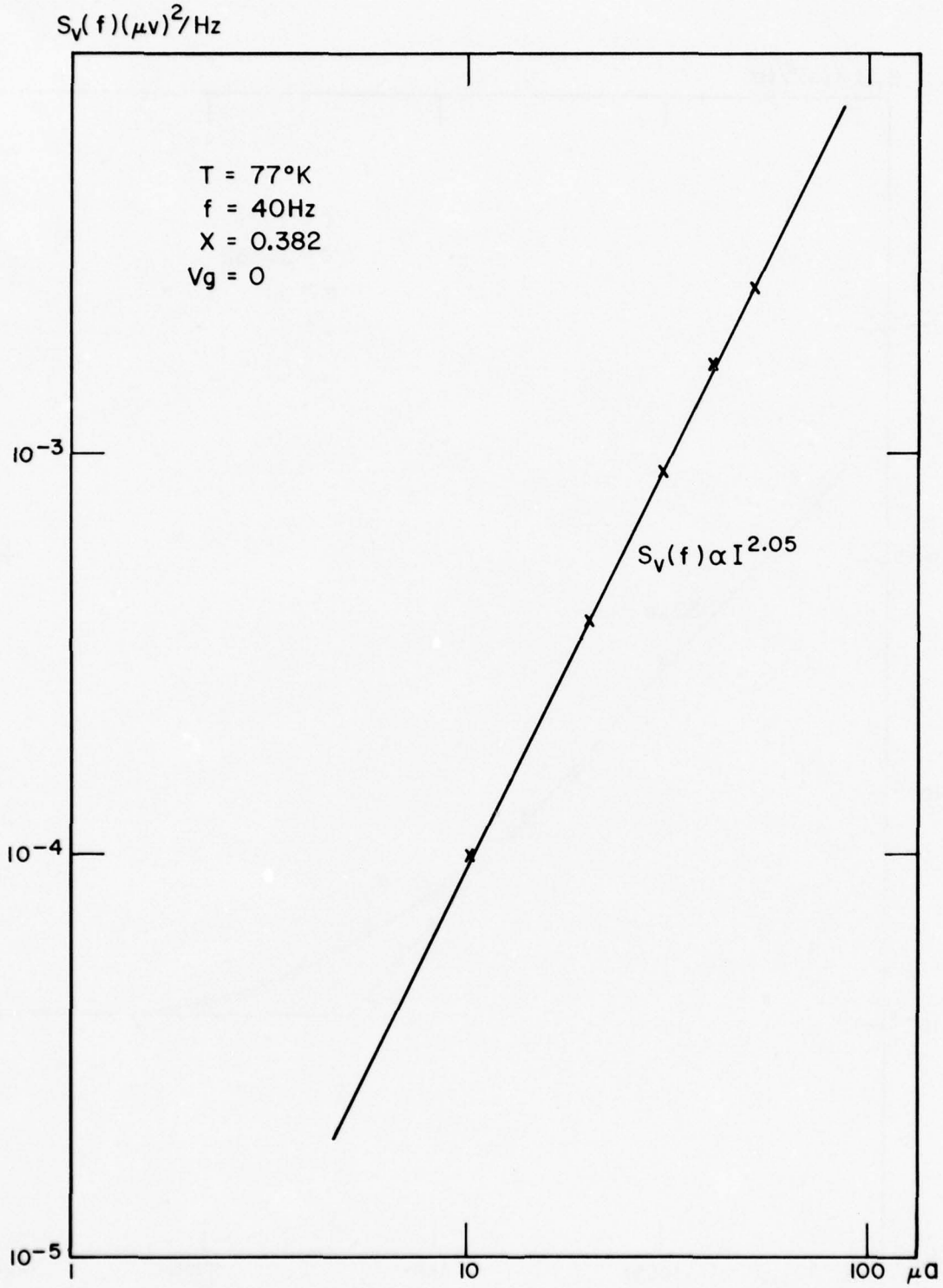

FIG 8.13 I/F NOISE VERSUS DC CURRENT FOR MIS DETECTOR 73V,247

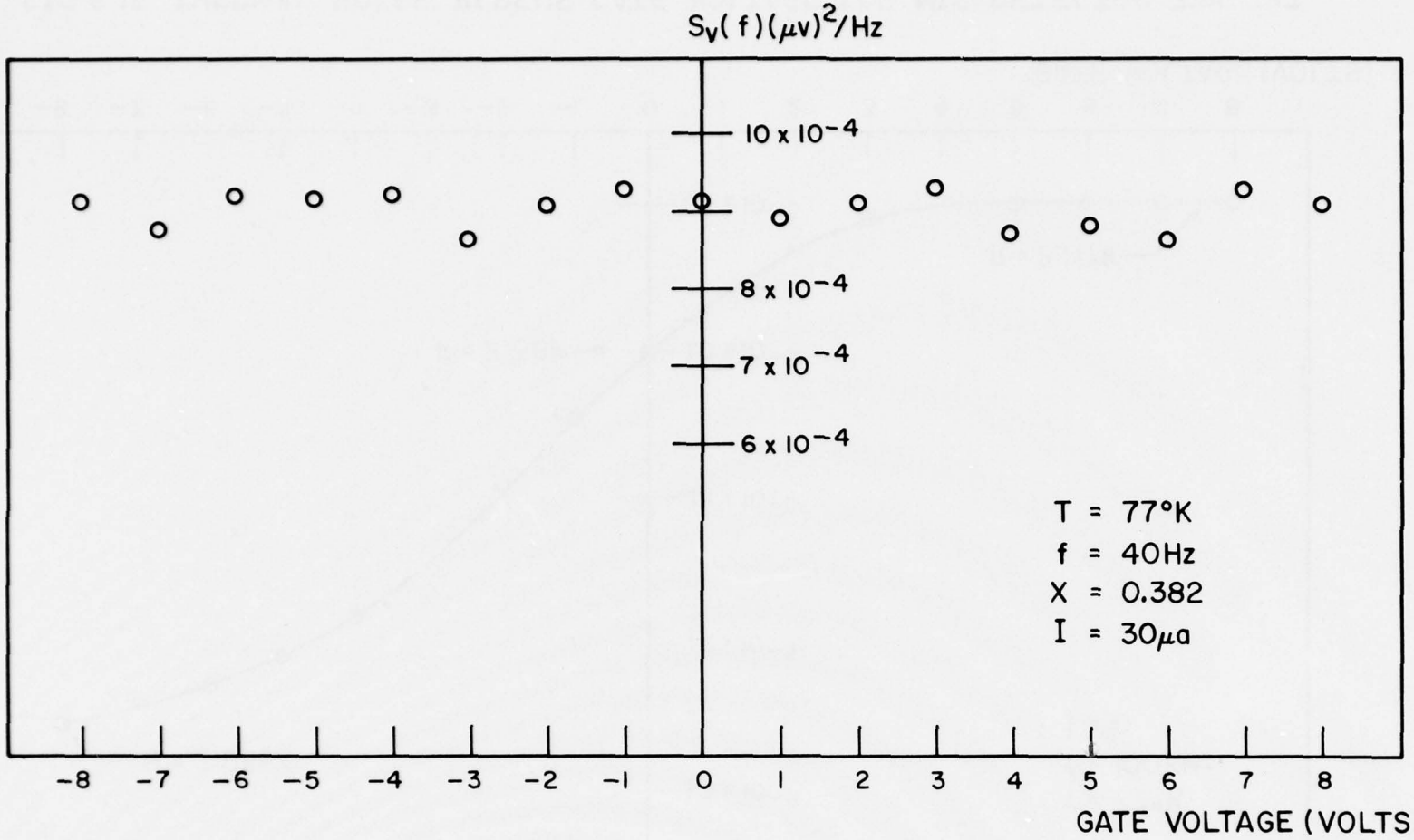

FIG 8.14 LOW FREQUENCY NOISE VERSUS GATE VOLTAGE FOR MIS DETECTOR 73V, 247

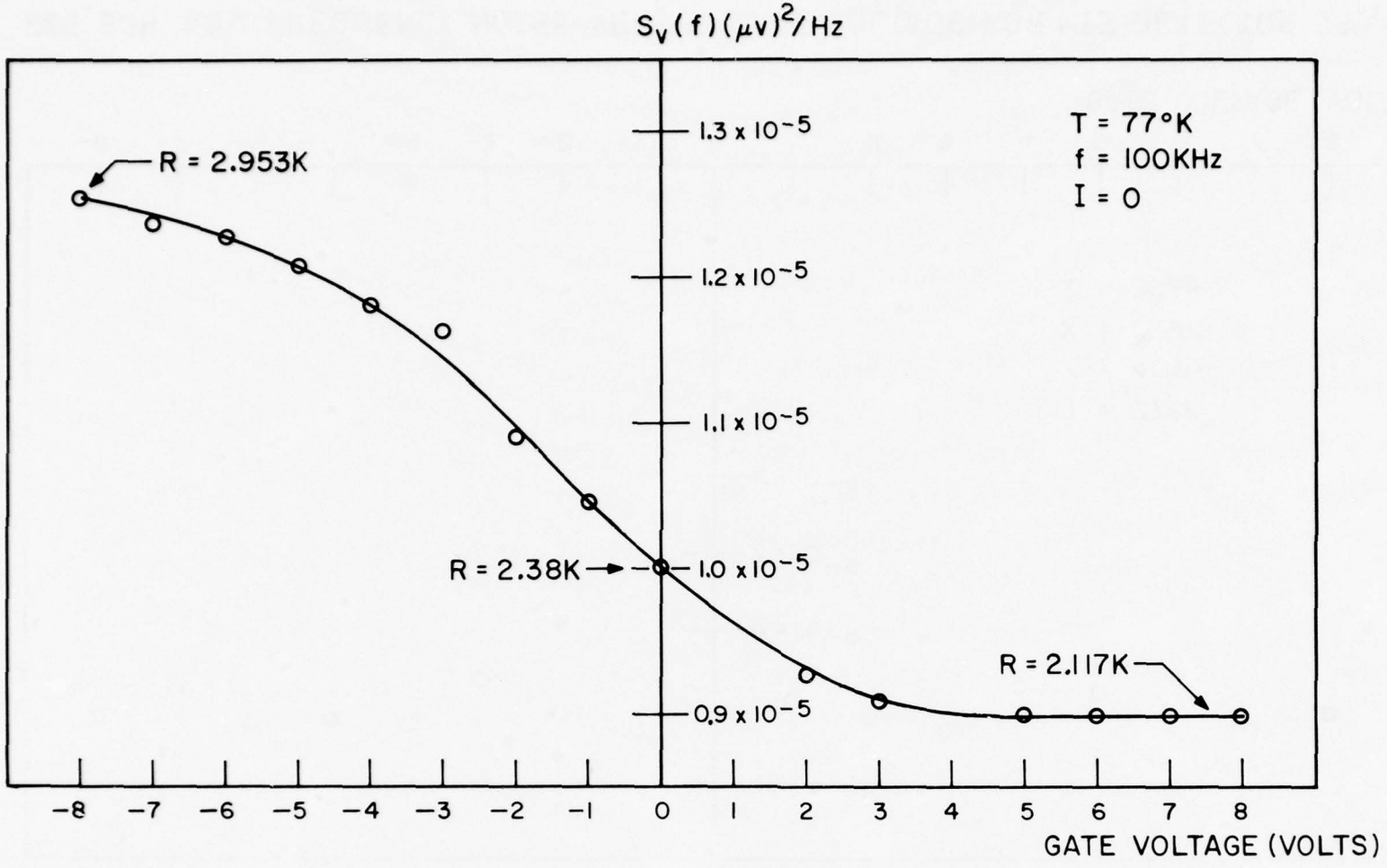

FIG 8.15 THERMAL NOISE VERSUS GATE VOLTAGE FOR MIS DETECTOR 73V, 247

decrease the conductivity of the n-type skin, and the net device resistance increases. By depleting the surface, we drive electrons away from the surface. The skin resistance is now high, and the depletion region is "squeezing" the bulk, so that we are effectively decreasing the width of the sample. This means that again the resistance will increase as we go through the depletion region. As we go into inversion, the holes at the surface will not significantly change the sample resistance. This is because in (Hg,Cd)Te with x = 0.382, the hole mobility is about 100 times smaller than the electron mobility, so that the bulk electrons will determine the resistance behavior of the device. Since the depletion region does not increase very much once we are in the inversion region, we would expect the resistance (and hence the thermal noise) to level off to a constant value, as it did for MIS detector #73V,247.

8.4 Discussion of results

First we will determine whether the variation in the measured noise at 100KHz as we decreased the gate voltage and inverted the surface of device #73V,245 is due to an increase in g-r noise, 1/f noise and/or thermal noise (Fig. 8.11). The material used for fabricating this device has an x-value of 0.382. For this material the excess carrier lifetime at 77°K and zero field of view (all the experiments conducted in this research, except for those using the a.c. modulation technique, were at zero field of view) is in the order of milliseconds. This results in a roll off frequency for the g-r noise less than 200Hz. Therefore, at normal device biasing currents, the g-r noise will be much smaller than the thermal noise at high frequencies (above 200Hz) and any excess noise measured will

be due to 1/f noise. Now, for the noise increase observed for device #73V,245 when the gate voltage was decreased (Fig. 8.11) to be due to g-r noise, the excess carrier lifetime should decrease from milliseconds to microseconds as the surface is depleted, an improbable condition. For that reason the g-r noise will be excluded in the following calculations which will be fully justified as we proceed.

8.4.1 Calculations

1. Measured resistance for device #73V,245 at zero bias and 77°K is 2.2KΩ; hence, the device thermal noise

$$= 4KTR$$

$$= 4 \times 1.38 \times 10^{-23} \times 77 \times 2.2 \times 10^{3}$$

$$= 0.935 \times 10^{-17} \quad V^2/Hz$$

2. Measured noise at 100KHz, 200μA and zero bias (Fig. 8.11)

$$= 1.238 \times 10^{-17} \quad V^2/Hz$$

Calculated thermal noise at 77°K

$$= 0.935 \times 10^{-17} \quad V^2/Hz$$

Therefore, flicker noise measured

$$= (1.238 - 0.935) \times 10^{-17}$$

$$= 0.303 \times 10^{-17} \quad V^2/Hz$$

3. Calculations of α in spectrum $S_v(f) = \text{Const.} \times (1/f^{\alpha})$:

From Fig. 8.8, we get (at 200μA)

$$S_v(10\text{Hz}) \quad \text{(extrapolated)} = 9.5\times10^{-14} \quad V^2/\text{Hz}$$

$$S_v(10\text{KHz}) \quad \text{(extrapolated)} = 3.5\times10^{-17} \quad V^2/\text{Hz}$$

therefore, we have

$$\left(\frac{10000}{10}\right)^{\alpha} = \frac{9.5\times10^{-14}}{3.5\times10^{-17}} = 2714$$

which yields $\alpha = 1.144$

Similarly, repeating the same calculations using different points

$$S_v(10\text{Hz}) \quad \text{(extrapolated)} = 9.5\times10^{-14} \quad V^2/\text{Hz}$$

$$S_v(1\text{KHz}) = 4.9\times10^{-16} \quad V^2/\text{Hz}$$

hence, $$\left(\frac{1000}{10}\right)^{\alpha} = \frac{9.5\times10^{-14}}{4.9\times10^{-16}} = 193.8$$

which yields $\alpha = 1.143$

This value of α fits excellently with the measured value shown in Fig. 8.8.

4. Estimated flicker noise at 100KHz and at 200μA:

Measured flicker noise at 40Hz (Fig. 8.8)

$$= 1.95\times10^{-14} \quad V^2/\text{Hz}$$

Since $\alpha = 1.144$ hence, the estimated flicker noise at 100KHz

$$= \frac{1.95\times10^{-14}}{(2500)^{1.144}}$$

$$= \frac{1.95\times10^{-14}}{7713}$$

$$= 0.253\times10^{-17} \quad V^2/Hz$$

Flicker noise measured at 100KHz $= 0.303\times10^{-17} \quad V^2/Hz$

This is an excellent agreement if we take into account two items.

i) The resistor might have a few °K higher temperature than the 77°K assumed in the calculation because of heating.

ii) The calculations are somewhat sensitive to the value of α .

5. Noise measured at depletion (from Fig. 8.11), V_G = -8 Volts,

200μA and 77°K $= 1.508\times10^{-17} \quad V^2/Hz$

Flicker noise (assumed to be the same) $= 0.303\times10^{-17} \quad V^2/Hz$

Therefore, thermal noise at depletion $= (1.508-0.303) \times 10^{-17}$

$$= 1.205\times10^{-17} \quad V^2/Hz$$

Now, $\frac{\text{Thermal Noise at depletion}}{\text{Thermal Noise at Zero bias}} = \frac{1.205\times10^{-17}}{0.935\times10^{-17}}$

$$= 1.289$$

This corresponds to a maximum device resistance at depletion

(V_G = -8 Volts) of $1.289\times2.2K\,\Omega = 2.84K\Omega$

6. Calculation of device resistance versus gate voltage from depletion approximation model:

For n-type $Hg_{0.618}\ Cd_{0.382}\ Te$ with 10^{15} free electrons $/cm^3$ added to the conduction band and at 77°K we have[16]

$$\text{Fermi energy } E_f = -0.0166 \quad \text{eV}$$

and $$\text{Intrinsic Fermi energy } E_i = -0.145 \quad \text{eV}$$

where both are measured from the bottom of the conduction band. Hence, surface potential ϕ_s at onset of strong inversion

$$= 0.145 - 0.0166$$

$$= 0.1284 \quad \text{Volts}$$

From Eq. (8.3b), the maximum width of the surface depletion region $X_{d_{max}}$ for device #73V,245 is

$$X_{d_{max}} = \sqrt{\frac{4 \times 14 \times 8.86 \times 10^{-14} \times 0.1284}{1.6 \times 10^{-19} \times 1.08 \times 10^{15}}}$$

$$= 6.072 \times 10^{-5} \quad \text{cm}$$

Now, assuming that the depletion region is "squeezing" the bulk, so that we are effectively decreasing the width of the sample, the <u>maximum</u> device resistance (see Sec. 8.3) is

$$R_{max} = \frac{\text{Sample thickness at zero bias}}{\text{effective sample thickness at depletion}} \times 2.2K\Omega$$

$$= \frac{2.24}{(2.24 - 0.607)} \times 2.2K\Omega$$

$$= 3.02K\Omega$$

Now, we calculate the variation of the device resistance as a function of gate voltage using the depletion model. When the semiconductor is depleted, the charge Q_s per unit area within the semiconductor is given by

$$Q_s = e\, n_o\, X_d \tag{8.4.1a}$$

where X_d is the width of the surface depletion region. Now, integration of Poisson's equation yields the surface potential ϕ_s as

$$\phi_s \approx \frac{e\, n_o\, X_d^2}{4\, \varepsilon_s\, \varepsilon_o} \tag{8.4.1b}$$

where ϕ_s is defined in Fig. 3.5.

If the flat band voltage $V_{FB} = 0$, any applied gate voltage V_G will partly appear across the insulator V_i and partly across the sample. Thus,

$$V_G = V_i + 2\phi_s \tag{8.4.1c}$$

If there are no charges present within the insulator, V_i is given by

$$V_i = \frac{Q_s}{C_{ins}} \tag{8.4.1d}$$

where $C_{ins} = \frac{\varepsilon_{ins}\, \varepsilon_o}{d}$ is the capacitance per unit area of the insulator layer and d is the insulator layer thickness.

Equations (8.4.1a, b, c and d) yield

$$V_G = \frac{e\, n_o\, X_d\, d}{\varepsilon_{ins}\, \varepsilon_o} + \frac{e\, n_o\, X_d^2}{2\, \varepsilon_s\, \varepsilon_o} \qquad (8.4.1e)$$

when $V_{FB} \neq 0$, equation (8.4.1e) is replaced by

$$|V_G - V_{FB}| = \frac{e\, n_o\, X_d\, d}{\varepsilon_{ins}\, \varepsilon_o} + \frac{e\, n_o\, X_d^2}{2\varepsilon_s\, \varepsilon_o} \qquad (8.4.1f)$$

which yields

$$\left(\frac{e\, n_o}{2\varepsilon_s\, \varepsilon_o}\right) X_d^2 + \left(\frac{e\, n_o\, d}{\varepsilon_{ins}\, \varepsilon_o}\right) X_d - |V_G - V_{FB}| = 0 \qquad (8.4.1g)$$

Substituting numerical values for the coefficients we get

$$(6.965 \times 10^7)\, X_d^2 + (2.66 \times 10^4)\, X_d - |V_G - V_{FB}| = 0$$

which has the solution

$$X_d = \frac{-(2.66\times10^4) + \sqrt{(7.073\times10^8) + (2.786\times10^8)\,|V_G - V_{FB}|}}{1.393\times10^8} \qquad (8.4.1h)$$

hence, the sample resistance at gate voltage V_G, where $X_{d_{max}} = 6.072\times10^{-5}$ cm, will be given by

$$R(V_G) = \frac{2.24}{(2.24 - X_d)} \times 2.2K\Omega$$

for $|V_G| \geq |V_{FB}|$ and $X_d \leq X_{d_{max}}$ (8.4.1i)

Equations (8.4.1h and i) were used to calculate the device thermal noise as a function of the gate voltage for gate voltages below -4 Volts ($\equiv V_{FB}$ for device #73V,245, Fig. 8.6). The results are shown in Fig. 8.11. The calculated noise in this figure is obtained by adding the measured excess noise at zero bias (= 0.303×10^{-17} V^2/Hz) to the calculated thermal noise. Both the calculated and measured noises agree within 10%. This is due to the fact that the depletion model gives resistance values slightly too large because the width of the depletion region is somewhat smaller than the depletion model indicates.

7. Up to here everything is consistent. We thus have

   i) The calculated device (#73V,245) resistance after depletion is = 3.02KΩ.

   ii) The measured resistance from thermal noise at 77°K = 2.84KΩ (assuming constant flicker noise).

   iii) The difference is less than 6%, well within accuracy of the depletion model.

   iv) Since flicker noise at 40Hz is independent of gate bias, it was reasonable to assume that the same is true at 100KHz.

   v) Thus the measurements at 100KHz give mainly thermal noise, contaminated by a small amount of flicker noise.

   vi) Conversely, if we take the 3.02KΩ to be correct, we have

$$\text{thermal noise at depletion} = \frac{3.02}{2.2} \times 0.935 \times 10^{-17}$$

$$= 1.284 \times 10^{-17} \quad V^2/Hz$$

measured noise at depletion (Fig. 8.11)

$$= 1.508 \times 10^{-17} \quad V^2/Hz$$

hence, the calculated flicker noise at depletion

$$= (1.508 - 1.284) \times 10^{-17}$$

$$= 0.224 \times 10^{-17} \quad V^2/Hz$$

so the flicker noise at depletion would be even lower than at zero bias.

vii) But we know that 3.02KΩ is an overestimation, so 2.84KΩ looks much better and then flicker noise is assumed to be constant.

From the above argument, we conclude that the variation in the measured noise at 100KHz when the device gate voltage was decreased (Fig. 8.11) is due to variation in the device thermal noise, i.e. its resistance.

8.4.2 Origin of 1/f Noise in MIS Detectors #73V,245 and #73V,247

As indicated in Sec. 3.3, the flicker noise spectrum is given by

$$S_v(f) = \frac{C R^2 I^2}{N_o f} \qquad (8.4.2a)$$

where I is the current, R the device resistance and N_o is the number of carriers. This relation is true for: a) Hooge's mechanism (bulk model); and b) McWhorter's mechanism (surface model) as shown by van der Ziel[6].

Case (a): The noise is a bulk phenomenon. Therefore, C is independent of conductor volume and should not change when a

(depletion) space charge region is formed. Now, according to our calculations for device #73V,245 and our measurements for device #73V,247, the device resistance changes by a factor $\frac{2.84}{2.2} = 1.291$ for device #73V,245 and by a factor $\frac{2.953}{2.38} = 1.241$ for device #73V,247 (see Fig. 8.15) when going from zero bias to depletion. Since R varies as $1/N_o$, so R^2/N_o varies as $R^3 \equiv (1.291)^3 = 2.15$ for device #73V,245 and $\equiv (1.241)^3 = 1.91$ for device #73V,247. Therefore, flicker noise should change by a factor of 2.15 (device #73V,245) and by a factor of 1.91 (device #73V,247). Best measurements indicate that $S_v(f)$ at 40Hz does not change for either of these devices by more than $\pm$ 10% (see Figs. 8.10 and 8.14). Therefore case (a) must be incorrect and Hooge's model cannot explain our data.

Case (b): The formula for $S_v(f)$ is still valid, but the effect is now a surface effect. Equation (8.4.2a) is derived under the assumption that the surface has constant area. But in fact the depleted surface can no longer contribute to flicker noise. So by going to depletion C should decrease by a factor 2, because the effective surface area is halved, and therefore the flicker noise should increase by a factor $= \frac{2.15}{2.0} = 1.075$ for device #73V,245 or change by a factor $= \frac{1.91}{2.0} = 0.96$ for device #73V,247. These factors are too small to measure at 40Hz.

Up to here we have only compared the end points of the transition: accumulation - depletion and strong inversion. This does not exclude a priori that there could be a variation (e.g. a peak) at the transition point. But our data does not give such a variation, and so there is no need to say anymore about it.

8.5 The Gate Voltage Hysteresis Effects

It was noted that the recorded C-V curves on the X-Y plotter would vary significantly depending on whether the gate voltage was increasing or decreasing while recording, and they would depend on the rate of change of gate voltage. In order to be able to correlate C-V plots from one run to the next, all data on the X-Y recorder was taken at the same rate of change of the gate voltage. This rate was chosen to be much smaller than the frequency of the applied a.c. signal to avoid any transient effects.

We can get an idea of the hystersis effect from Figs. 8.16, 8.17 and 8.18. In obtaining each curve, the gate voltage wave form was triangular, so that it swept at the same rate whether it was increasing or decreasing. The gate voltage sweeping rate used was 0.1 Volts/sec. Each curve was retraced by the X-Y plotter several times so that the data was reproducible in that sense. Fig. 8.16 is the C-V plot for MIS detector #9744-P5 taken both at 100Hz and 100KHz. The curve on the right was swept out while the gate voltage was decreasing and the one on the left while it was increasing. The same explanation could be applied to both Figs. 8.17 and 8.18. We notice also from these curves that the increasing and decreasing C-V curves need not be symmetric. The extreme case is shown in Fig. 8.18. The decreasing curve was much broader than the other, although they both had about the same minimum value.

The mechanism which could be responsible for the observed hysteresis effect is that there could be slow surface states in the zinc sulphide insulator. These are surface states with time constants on the order of seconds or even minutes. Since they

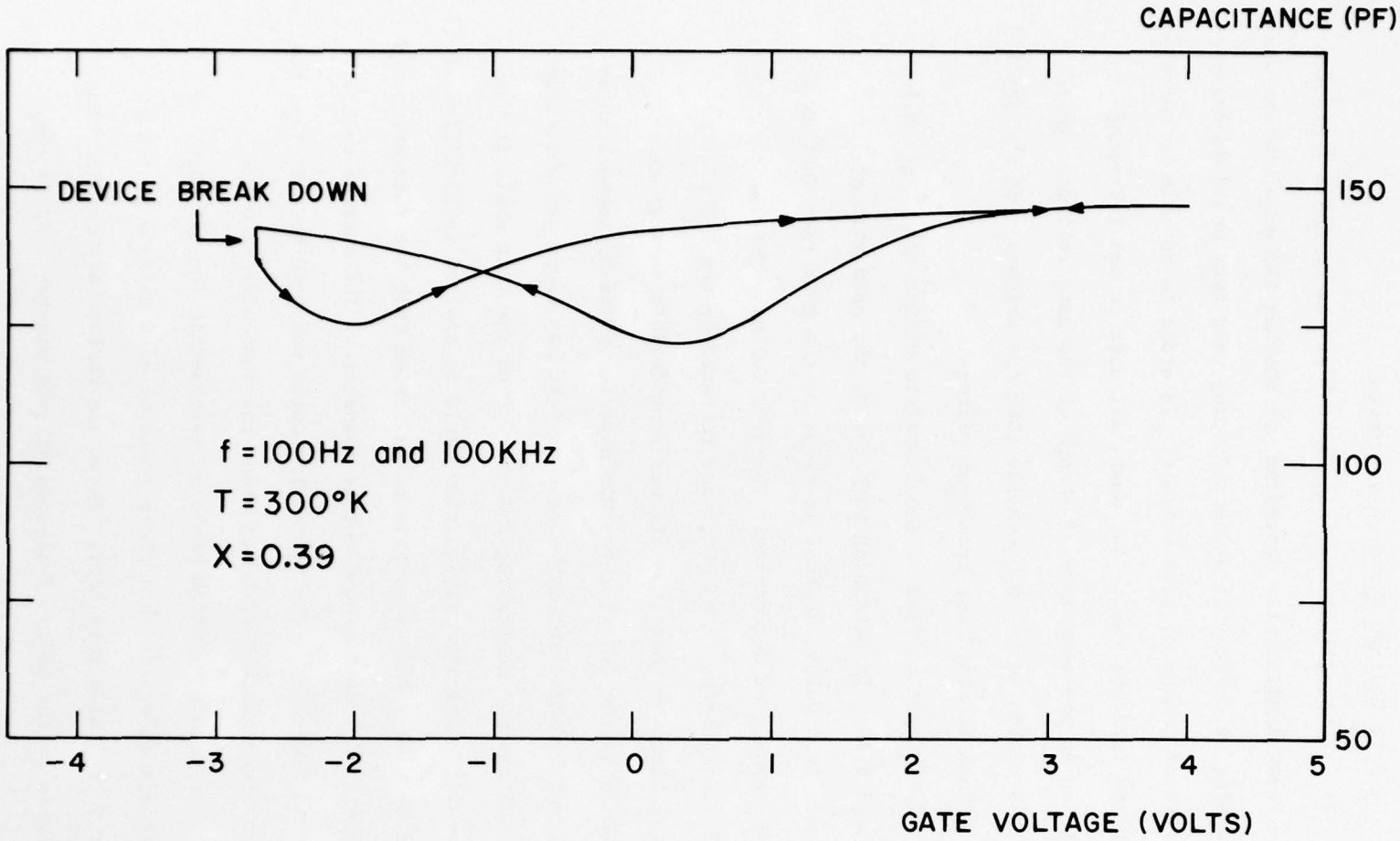

FIG 8.16 CAPACITANCE VERSUS GATE VOLTAGE FOR MIS DETECTOR 9744-P5 SHOWING HYSTERESIS EFFECTS

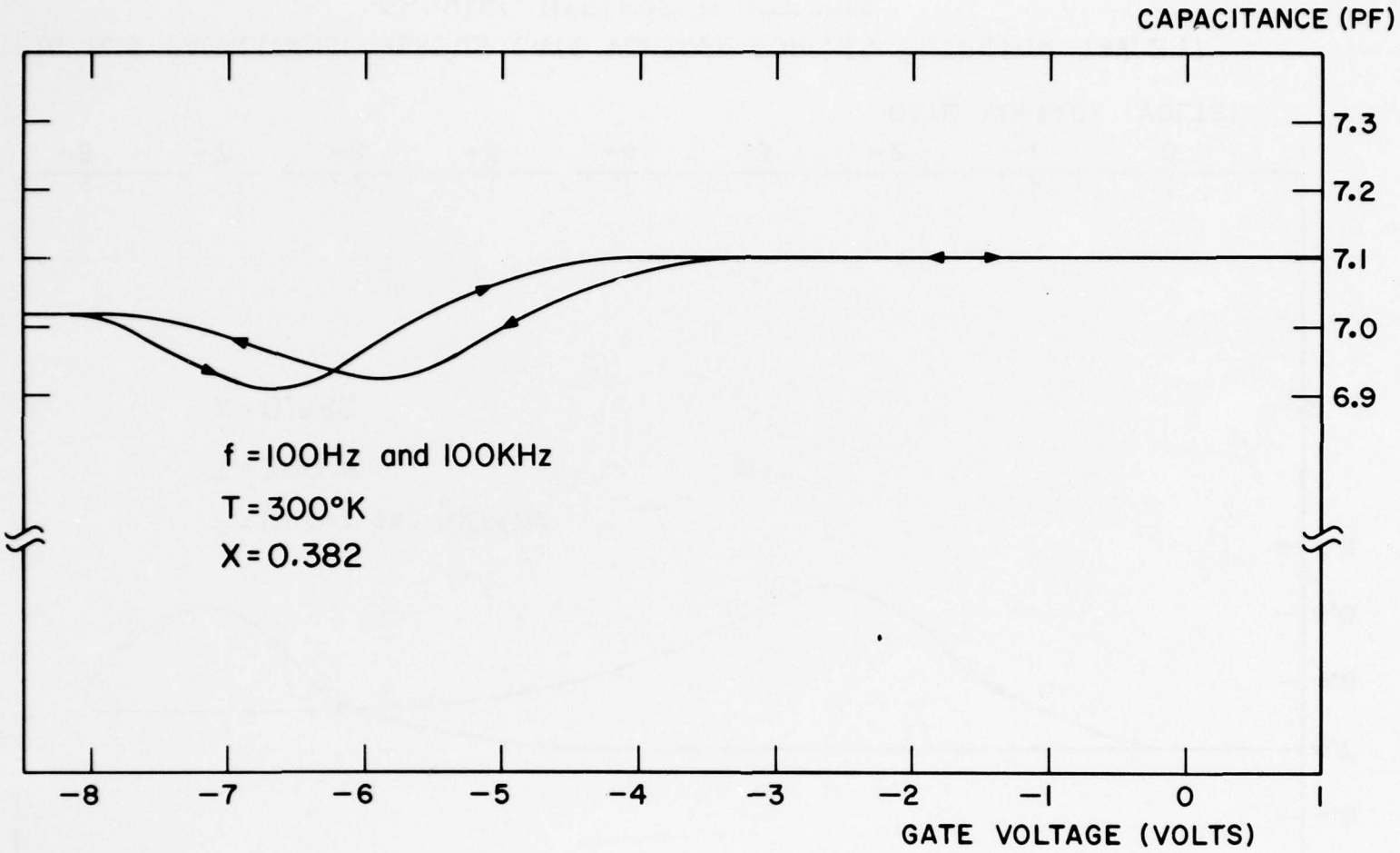

FIG 8.17 CAPACITANCE VERSUS GATE VOLTAGE FOR MIS DETECTOR 73V, 245 SHOWING HYSTERESIS EFFECTS

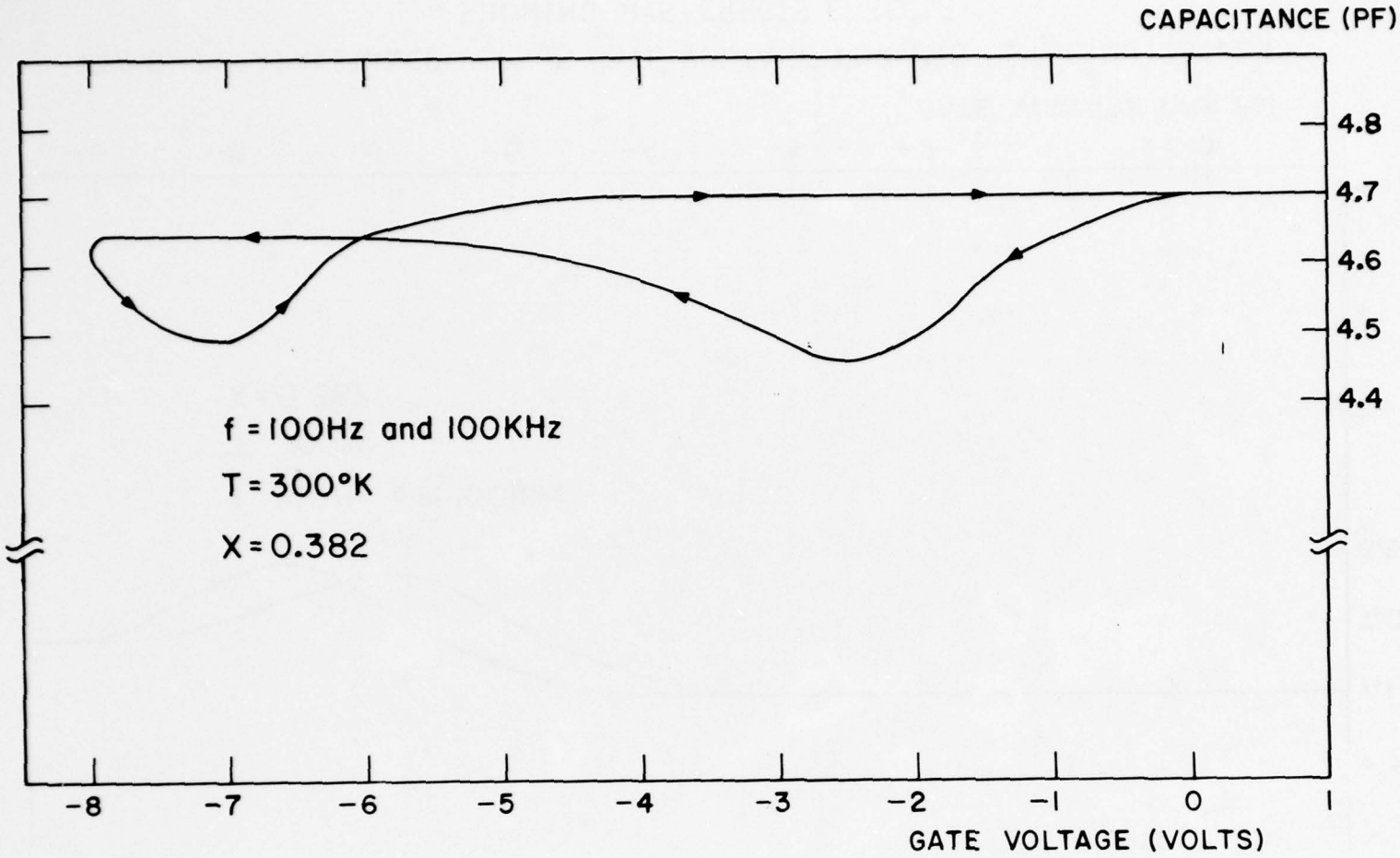

FIG 8.18 CAPACITANCE VERSUS GATE VOLTAGE FOR MIS DETECTOR 73V, 247 SHOWING HYSTERESIS EFFECTS

interact with the valence band so slowly, we must wait a long time for them to reach equilibrium. Their population as a function of time, and thus also their effects on the surface properties, would depend on the "history" of the gate voltage.

We did not have this problem when we did the noise measurements, since we measured point by point and operated at equilibrium at each point.

CHAPTER IX. CONCLUSIONS AND RECOMMENDATIONS

9.1 Conclusions

1. The measuring system based on a modulation technique works perfectly and can be used to discriminate between noise sources.

2. Some contacts to the photoconductive devices showed excess noise over and above the normal flicker noise (1/f noise) when carrying current. The amount of excess noise produced depends on the polarity of the current. We traced this to carrier injection at the "bad" contact.

3. We observed that photoconductive devices with a grain boundary showed higher flicker noise than devices without grain boundary. Correlation measurements of the noise of two adjacent devices on the same chip carrying the same current showed that the noises were uncorrelated. When normalized to the same resistance values, the difference in noise was about a factor of 4 in our geometry.

4. When the flicker noise was expressed in terms of Hooge's constant C, which should typically be between $1x10^{-3}$ - $10x10^{-3}$ we found that it varied between $0.15x10^{-3}$ and $8.0x10^{-3}$. It is somewhat doubtful whether such a large variation in C can be attributed to a bulk effect.

5. We manufactured n-type (Hg,Cd)Te MIS devices with a gate electrode to modulate any surface-generated noise and so discriminate between bulk noise and surface noise. The devices gave C-V plots

that showed a transition from accumulation to depletion (inversion). The resistance of the devices increased by about 30% when going from zero bias to depletion. However, the flicker noise did not change when going from accumulation to depletion. This could be explained by a surface effect, since the depleted surface can no longer interact with the electrons of the (Hg,Cd)Te. The bulk theory would require an increase in flicker noise by about a factor 2 due to the increase in the device resistance; in the surface model this factor 2 is just compensated by the decrease in effective surface area by about the same factor.

6. The fact that flicker noise has been shown to be a surface effect indicates that significant improvement in the flicker noise of (Hg,Cd)Te photoconductors should be possible by proper manufacturing and/or by proper surface treatment.

9.2 Recommendations

1. It is recommended to study the contact problem in greater detail to understand what is going on in "poor" contacts. This is not an urgent practical problem, since it is not difficult to make "good" contacts consistently, but it would be of theoretical interest to understand the mechanism of noise generation in "poor" contacts better.

2. It is recommended that (Hg,Cd)Te photodetectors be so constructed that no grain boundary is included in the device. For the relatively small devices presently in use this is not difficult to achieve.

3. Now that the flicker noise problem in (Hg,Cd)Te has been demonstrated to be surface phenomenon, it would be worthwhile to

design the manufacturing process, and/or the surface treatment in such a way that the flicker noise is minimized.

APPENDIX A

We give here a detailed description of all detectors used in this research. The detectors were fabricated from n-type $Hg_{1-x}Cd_xTe$ crystals with x either ≃0.2 or ≃0.4. All crystals were obtained from Honeywell Research Center, Bloomington, Minnesota as slices of about 2mm in thickness and 10x10 mm in area. Crystal #91174-P5 contained grain boundary and was used to fabricate detectors for grain boundary studies. MIS detectors were fabricated from crystal # 73V,21 since it contained no pit holes (see Sec. 8.3). Detectors # 10770-1 and #50470,S185 were also obtained from Honeywell Research Center, Bloomington, Minnesota for measuring their C values (see Chapter VII).

Tabulation of (Hg,Cd)Te detectors used in this research is given in Table A.1. All data was obtained at 77°K except otherwise specified.

Table A.1

Crystal #	Detector #	x	λ_{co} μm	ρ Ωcm	n_o cm^{-3}	Number of Contacts	L bet. Contacts mm	w mm	t μm
91174-P5	9742-P5	0.39	~3.1	0.05	1.116×10^{16}	6	~1.143	~1	~28
	9743-P5					6	~1.143	~1	~28
	9744-P5					2	1.143	1	38.1
	9745-P5					6	~1.143	~1	~23
	9746-P5					7	~1.143	~1	~23
	9747-P5					7	~1.143	~1	~23
	9748-P5					7	~1.143	~1	~23
50466,174	5667,174	0.2	~13.8	0.033	3.571×10^{16}	7	~1.143	~1	~16
51166	5661	0.2	~13.8	0.033	2.083×10^{15}	4	~0.8	~1	~ 3
	5663					4	~0.8	~1	~ 3
73V,24	73V,245	0.382	~ 3.2	0.35	1.08×10^{15}	2	0.62	0.44	2.24
	73V,247					2	0.6	0.4	2.2
	50470,S185*	0.273	~ 4.8	0.06	$n_i=1.2 \times 10^{16}$	2	0.5	0.5	3.75
10770,153	10770-1*	0.26	~ 5.3	0.05	$n_i=1.8 \times 10^{16}$	2	0.542	0.642	3.84

*Detector data was taken at 300°K.

APPENDIX B

We give here the proof of Eq. (4.2a). Consider a semiconductor material having an equilibrium electron concentration n_o and an equilibrium hole concentration p_o when not irradiated by light. If the electron and hole mobilities are μ_n and μ_p respectively, then the dark conductivity σ_o of the sample is

$$\sigma_o = e(n_o\mu_n + p_o\mu_p) \tag{B.1}$$

Now, let the sample be irradiated uniformly by P watts of light consisting of quanta $h\nu$. Let r be the power reflection coefficient of the surface and η the quantum efficiency of the hole-electron pair production process. Then the number of hole-electron pairs produced per second is

$$Q = \eta \frac{P(1-r)}{h\nu} \tag{B.2}$$

If the electrons and holes thus created have lifetimes τ_n and τ_p, respectively, then the steady-state added numbers of carriers are

$$\Delta N = Q\tau_n \qquad \Delta P = Q\tau_p \tag{B.3}$$

where ΔN is the number of added electrons and ΔP the number of added

holes. These numbers of carriers are added to the "dark" numbers $N_o = n_o AL$ and $P_o = p_o AL$, where A is the cross section of the sample and L its length.

Now, the dark conductance of the sample G_o is given by

$$G_o = \sigma_o \frac{A}{L} = e\left(\frac{N_o}{AL}\mu_n + \frac{P_o}{AL}\mu_p\right)\frac{A}{L}$$

$$= e\,\frac{(N_o\mu_n + P_o\mu_p)}{L^2} \qquad (B.4)$$

hence, the change in conductance due to the light is

$$\Delta G = \frac{e(\Delta N\,\mu_n + \Delta P\,\mu_p)}{L^2}$$

$$= \frac{eQ(\mu_n\tau_n + \mu_p\tau_p)}{L^2} \qquad (B.5)$$

If the light radiant power P consists of a steady part P_{lo} and a time dependent part $P_1 \sin\omega_1 t$, and considering only the time-dependent part, Eq. (B.5) gives,

$$\Delta G = \frac{e\eta(1-r)}{L^2 h\nu}(\mu_n\tau_n + \mu_p\tau_p)\,P_1 \sin\omega_1 t \qquad (B.6)$$

where we have substituted Eq. (B.2) for Q.

For small changes in the sample conductance, we have

$$\frac{\Delta R}{R_o} = -\frac{\Delta G}{G_o}$$

where R_o is the dark "resistance" of the sample, hence Eq. (B.6)

yields

$$\Delta R = - \frac{e\eta(1-r)R_o^2}{L^2 h\nu} (\mu_n\tau_n + \mu_p\tau_p) P_1 \sin\omega_1 t \qquad (B.7)$$

and

$$\overline{\Delta R^2} = \frac{\eta^2(1-r)^2 L^4}{2(h\nu)^2 e^2} \frac{(\mu_n\tau_n + \mu_p\tau_p)^2}{(N_o\mu_n + P_o\mu_p)^4} P_1^2 \qquad (B.8)$$

where we have substituted Eq. (B.4) for G_o ($= \frac{1}{R_o}$) in the last equation.

Therefore, the spectral density $S_R(f)$ of the resistance fluctuations of the sample due to the modulating light $P_1 \sin\omega_1 t$ is

$$S_R(f) = \frac{\overline{\Delta R^2}}{B}$$

$$= \frac{1}{2} \frac{K^2 L^4}{(h\nu)^2 e^2} \frac{(\mu_n\tau_n + \mu_p\tau_p)^2}{(N_o\mu_n + P_o\mu_p)^4} \frac{P_1^2}{B}$$

where $K = \eta(1-r)$ and B is the system bandwidth. This proves Eq. (4.2a)

LIST OF REFERENCES

1. McWhorter, A.L., "1/f Noise and Related Surface Effects in Germanium," M.I.T. Lincoln Lab. Report No. 80, May 1955.

2. Hooge, F.N., Physics Letters, Vol. 29A (1969), p. 139.

3. Hooge, F.N., Physica, Vol. 60 (1972), p. 130.

4. Kleinpenning, T.G.M., Physica, Vol. 77 (1974), p. 78.

5. Kleinpenning, T.G.M., Physica, Vol. 81B (1976), p. 301.

6. Van der Ziel, A., Solid State Electronics, Vol. 17 (1974), p. 110.

7. Klaassen, F.M., IEEE Trans. Electron Devices, ED18 (1971), p. 887.

8. Bess, L., Physics Review, Vol. 91 (1953), p. 1569.

9. Bess, L., ibid., Vol. 103 (1956), p. 72.

10. Khintchine, A., Math. Annalen, Vol. 109 (1934), p. 604.

11. Van der Ziel, A., Fluctuation Phenomena in Semiconductors, Butterworths, London, 1959, pp. 26-28.

12. Van der Ziel, A., Fluctuation Phenomena in Semiconductors, Butterworths, London, 1959, p. 19.

13. Broudy, R.M., Study to Improve the Low Frequency Noise Characteristics of (Hg,Cd)Te Detectors, Honeywell Radiation Center, Lexington, Massachusetts, Final Technical Report on Contract NASA CR-132512 (1973).

14. Grove, A.S., Physics and Technology of Semiconductor Devices, John Wiley and Sons, Inc., New York, 1967, Chapter 9.

15. Long, D. and Schmit, J.L., Semiconductors and Semimetals, Beer, A.C. and Willardson, R.K. (Eds.), Academic Press Inc., New York, Vol. 5 (1970), p. 190.

16. Schmit, J.L., Journal of Applied Physics, Vol. 41, No. 7 (1970), p. 2876.

General References

17. Van der Ziel, A., Fluctuation Phenomena in Semiconductors, Butterworths, London, 1959, Chapter 5.

18. Van der Ziel, A., Noise; Sources, Characterization, Measurement, Prentice-Hall, Inc., Englewood Cliffs, NJ, 1970.

19. Fu, H.S. and Sah, C.T., IEEE Trans. Electron Devices, ED-19, No. 2 (1972), p. 273.

20. Sah, C.T. and Hielscher, F.H., Phys. Rev. Lett., Vol. 17 (1966), p. 956.

21. Van der Ziel, A., Solid State Physical Electronics, Prentice-Hall, Inc., Englewood Cliffs, N.J., 1968, Chapter 11.

22. Long, D. and Schmit, J.L., Semiconductors and Semimetals, Beer, A.C. and Willardson, R.K. (Eds.), Academic Press Inc., New York, Vol. 5 (1970), Chapter 5.

☆ U. S. GOVERNMENT PRINTING OFFICE: 1977 — 757-001/205